Intrinsic vibrational angular momentum driven by non-adiabatic effects in non-collinear magnetic systems

Oliviero Bistoni

Intrinsic vibrational angular momentum driven by non-adiabatic effects in non-collinear magnetic systems

A thesis presented for the degree of Doctor of Philosophy in physics in compliance with the co-tutelle agreement between

Sorbonne Université *and* Università di Trento

Institut de Nanosciences de Paris
École doctorale n° 564: Physique en Île-de-France

Dipartimento di fisica dell'Università di Trento
Corso di Dottorato in Fisica – XXXIV Ciclo

Candidate
Oliviero Bistoni
ID number 3877248

Supervisors
Prof. Matteo Calandra
Prof. Tristan Cren

January 2022

Thesis defended on 27 January 2022 in front of a Board of Examiners composed by

Reviewer	Prof. Francesca Baletto	Università degli Studi di Milano
Reviewer	Prof. Ivo Souza	Universidad del País Vasco
Examiner	Prof. Daniela Ascenzi	Università di Trento
Examiner	Prof. Jean-Noël Fuchs	Sorbonne Université
Supervisor	Prof. Matteo Calandra	Università di Trento
Supervisor	Prof. Tristan Cren	Sorbonne Université

Intrinsic vibrational angular momentum driven by non-adiabatic effects in non-collinear magnetic systems

Doctoral thesis. Sorbonne University, University of Trento.

This thesis has been typeset by LaTeX.

Author's email: oliviero.bistoni@insp.upmc.fr, oliviero.bistoni@unitn.it

Perfect is the enemy of good.

To my uncle Sandro.

Abstract

In absence of external fields, vibrational modes of periodic systems are usually considered as linearly polarized and, as such, they do not carry angular momentum. Our work proves that non-adiabatic effects due to the electron-phonon coupling are time-reversal symmetry breaking interactions for the vibrational field in systems with non-collinear magnetism and large spin-orbit coupling. Since in these systems the deformation potential matrix elements are necessarily complex, a nonzero synthetic gauge field (Berry curvature) arises in the dynamic equations of the ionic motion. As a result, phonon modes are elliptically polarized in the non-adiabatic framework and intrinsic vibrational angular momenta occur even for non-degenerate modes and without external probes. These results are validated by performing fully relativistic *ab-initio* calculations on two insulating platinum clusters and a metallic manganese compound, with non-collinear magnetism. In both cases, non-adiabatic vibrational modes carry sizeable angular momenta comparable to the orbital electronic ones in itinerant ferromagnets.

Keywords: *non-adiabatic effects, phonon angular momentum, Berry curvature, non-collinear magnetism, electron-phonon coupling, time-reversal symmetry*

Abstrait

En l'absence de champs externes, les modes vibrationnels des systèmes périodiques sont généralement considérés comme linéairement polarisés et, en tant que tels, ils ne portent pas de moment cinétique. Notre travail prouve que les effets non adiabatiques dus au couplage électron-phonon sont des interactions de rupture de symétrie par inversion du temps pour le champ vibrationnel dans des systèmes à magnétisme non colinéaire et à grand couplage spin-orbite. Comme dans ces systèmes les éléments de matrice de potentiel de déformation sont nécessairement complexes, un champ de gauge synthétique non nul (courbure de Berry) apparaît dans les équations dynamiques du mouvement ionique. En conséquence, les phonons non adiabatique sont polarisés de manière elliptique et des moments angulaires vibrationnels intrinsèques se produisent même pour des modes non dégénérés et sans sondes externes. Ces résultats sont validés en effectuant des calculs *ab-initio* entièrement relativistes sur des molécules de platine isolantes et un composé de manganèse métallique, à magnétisme non colinéaire. Dans les deux cas, les modes vibrationnels non adiabatiques portent des moments angulaires importants comparables à ceux électroniques orbitaux dans les ferroaimants itinérants.

Mots clés: *effets non-adiabatiques, moment cinétique des phonons, courbure de Berry, magnétisme non-colinéaire, couplage électron-phonon, symétrie par inversion du temps*

Acknowledgements

Most of the work carried out during the PhD has been supervised by Matteo Calandra which I gratefully acknowledge. He helped me since the very beginning up to the end of the project and assisted me in the transfer from one university to the other. Moreover, he guided me across all the hardships I faced during the three years with patience and dedication. Besides that, I express my gratitude to my french supervisor Tristan Cren who made possible the cotutelle with the University of Trento and to professor Francesco Mauri, my master's thesis advisor, who came up with the idea in the first place.

From a professional point of view, I also would like to thank my coworkers Davide, Cesare, Marco, Sky, Giovanni, with whom I often exchanged about physics, my thesis committee, professors Franck Vidal and Fabio Finocchi, as well as the doctoral school Physique en Île-de-France, who followed my doctorate, the whole research unit Institut de Nanosciences de Paris, the referees, professors Francesca Baletto and Ivo Souza, who kindly accepted to review my thesis, and the other members of the jury, professors Daniela Ascenzi and Jean-Noël Fuchs.

I acknowledge CINES, IDRIS, TGCC, PRACE and CINECA for high performance computational resources and Paolo Giannozzi for useful discussions.

During these 40 months many "adverse events" happened that strongly impacted on my work and my life. I believe the early months of the pandemics, the lockdown and all, have been the most challenging period for most of us. It would not have been the same without the support from all the people I met, first in Paris and then in Trento. Colleagues, flatmates, friends.

In this respect, I need to thank my closest friends in Paris, namely Serena, Gianluca, Juan Camilo, Angus, Violette and Mathis, for the wonderful time we spent together, and Marta, Andrea, Elena who almost adopted me during the past winter in Trento. I owe them a lot. I really enjoyed lunch breaks and beer evenings with interns, PhDs and postdocs from the laboratory and the department I worked in. Social moments, to me, have been the most gainful part of the university life. And even if they became less frequent since the healthcare crisis began, I could only appreciate them more. For this reason I wish to thank Marine, Thomas, Camille, Ronan, Sophie, Thibaut, Sarah, Ronei, Mehdi, Maryam, Thibault, Erika, Pedro, Sunniva and the association Doc'Up. Many thanks also to Roberto, Matteo, Santo, Piero, Daniele, Francesco, Silvia, Marco.

Many other people enriched the time spent working on the thesis. I would like to thank Farah and Caroline for being by my side for a while, Jean-Côme, my very first flatmate, Saverio who made the best panzerotti I remember, Claudio who recently joined me in Paris. I loved walking, dancing, laughing, eating, hiking with Ilaria, Ginevra, Laura, Marina, Koyomi, Federica, Prisca, Léon, Basile, Stelios, Juliette, Eugène, Alessandro, Omid and Guglielmo. Those I forget to mention shall forgive me.

Last but not least, I thank my dearest old friends from the previous life in Rome, especially the ones who came to visit me in Paris, and my family who always inspired me and stood by me. I am very attached to them all.

Contents

Introduction

Several experiments demonstrated the non-negligible interaction between vibrational modes and magnetic fields or optical probes. The phonon Hall effect [1, 2] and the phonon contribution to the gyromagnetic ratio detected in the Einstein de Haas effect [3, 4] are eminent examples. Moreover, it has been demonstrated that valley selective infrared optical absorption in transition metal dichalcogenides breaks time-reversal symmetry for the phonon field and can be used to probe the chirality of phonon modes at particular points in the Brillouin zone [5, 6].

In the absence of external probes, phonons are usually thought as static lattice vibration and, as such, they are considered as linearly polarized, namely they are invariant under time-reversal and they are not supposed to carry a finite angular momentum. In this case, a nonzero angular momentum of phonons can be obtained from twofold degenerate vibrational modes with a linear combination of the phonon eigenvectors, in the same way as circularly polarized light can arise from two linear polarizations. This case has been investigated in literature extensively [6–10], particularly for hexagonal crystal lattices[1].

For each circularly polarized phonon carrying an angular momentum $\boldsymbol{\ell}$ there exists another linearly independent combination of polarizations that leads to an angular momentum $-\boldsymbol{\ell}$, so that the total phonon angular momentum for the degenerate mode is zero. An external time-reversal symmetry breaking probe, such as optical absorption or magnetic field is then needed to break the degeneracy. The question is still open if a non-degenerate phonon mode can host an intrinsic angular momentum without external probes. Namely, can an intrinsic mechanism break time-reversal symmetry for the phonon field?

In condensed matter theory, the electronic problem is usually decoupled from the nuclear motion via the Born-Oppenheimer (adiabatic) approximation [11]. The vibrational properties of the system can then be described, from a microscopic point of view, in terms of static displacements of the ions (nuclei plus core electrons) from their equilibrium positions [12]. In density functional theory, these phonon displacements are usually handled as external perturbations to the electronic charge density and total energy of the system and in the *linear response* regime, where the density response

[1] In hexagonal crystal lattices with broken in-plane inversion symmetry, such as monolayer hexagonal boron nitride, single degenerate phonon modes carry opposite angular momenta at the Brillouin zone corners $\mathbf{K}$ and $\mathbf{K}' = -\mathbf{K}$. However, the phonon modes at $\mathbf{K}$ and $\mathbf{K}'$ have the same energy and if vibrations are described in a $\sqrt{3} \times \sqrt{3}\mathrm{R}30^{\circ}$ supercell, $\mathbf{K}$ and $\mathbf{K}'$ fold at $\mathbf{\Gamma}$ and the two single degenerate modes become twofold degenerate at zone center.

varies linearly with the perturbation. In this approach, the force constant matrix is obtained as the second derivative of the total energy with respect to the ionic displacement and the vibrational frequencies are equal to the square root of the eigenvalues of the dynamical matrix.

Even though the scenario outlined so far works pretty well for most systems, there are some cases in which the coupling between electrons and phonons cannot be ignored. Large non-adiabatic effects, so-called because they go beyond the *naive* Born-Oppenheimer approximation, have been predicted in two-dimensional systems and layered metals [13, 14], particularly in the vicinity of Kohn anomalies [15, 16], in the clean limit regime. In density functional perturbation theory (DFPT), non-adiabatic effects due to the electron-phonon coupling are taken into account by allowing the electrons to perceive the ionic vibrations by means of a time-dependent perturbation to the charge density [17]. In so doing, the dynamical matrix becomes a function of the frequency ω and the eigenvalue problem admits complex solutions. This framework is usually referred to as *dynamical* Born-Oppenheimer approximation since a dynamical phonon displacement is considered instead of a static one.

The thesis aims at demonstrating that, in systems with non-collinear magnetism, non-adiabatic (dynamical) effects due to the electron-phonon coupling are time-reversal symmetry breaking interactions for the vibrational field and hence entail an intrinsic angular momentum of phonons. In fact, for non-collinear magnetic systems, the electronic wavefunction can not be chosen as real and a nonzero geometric vector potential (Berry connection) arises in the Born-Oppenheimer approximation [18]. As a result, an intrinsic nonzero vibrational angular momentum occurs even for non-degenerate modes and in the absence of external probes. Phonons can then be seen as elementary quantum particles carrying a sizeable angular momentum driven by non-adiabatic effects.

The main advancements brought by the thesis can be summarized as follows:

1. We demonstrate that non-adiabatic effects are related to the geometric properties of the system. Namely, we show that the non-adiabatic dynamical matrix, to leading order in the low frequency expansion, yields the same eigenvalue problem as the *screened* Born-Oppenheimer approximation [19] in which the Berry curvature due to the electronic screening behaves as an effective magnetic field for the ionic motion.

2. In systems with spontaneously broken time-reversal symmetry (and relevant spin-orbit interaction), we prove that non-adiabatic effects lead to a sizeable intrinsic vibrational angular momentum even when the non-adiabatic frequencies are experimentally indistinguishable from the adiabatic ones ($\Delta\omega/\omega < 1\%$).

The reason why we consider non-collinear magnetic systems is that, for spin-diagonal hamiltonians, namely without magnetism or with collinear magnetism, the electronic wavefunctions can be chosen in such a way that the Berry curvature vanishes. In those cases therefore, the angular momentum of vibrational modes is zero. On the other hand, in non-collinear magnetic systems, the Berry curvature of electrons is nonzero

and the angular momentum of phonons can be finite. In other words, in non-collinear magnetic systems, the Berry curvature due to the screening of electrons becomes the intrinsic mechanism that breaks time-reversal symmetry for the phonon field. As a result, the vibrational modes may carry a finite angular momentum driven by non-adiabatic effects.

As a further development, the first-principles approach used for calculation of non-adiabatic effects [20] is generalized to study non-collinear magnetic systems and implemented in the phonon response code. In order to deal with periodic systems, particularly metals, the electron-phonon calculation is adapted following the method proposed in reference [21] based on the properties of the time-reversal operator.

The workflow can be summarized as follows. Firstly, a fully relativistic *ab-initio* calculation is carried on. Then, a self-consistent calculation of the adiabatic (static) phonon response is performed. Subsequently, the non-adiabatic dynamical matrix is obtained with a non-self-consistent procedure which makes use of a (force constant) functional that is stationary with respect to the variation of the electronic charge density. Finally, the angular momentum of phonons is obtained from the eigenvectors of the dynamical matrix [22].

As a proof of concept, we demonstrate the magnitude of the non-adiabatic effect in two insulating magnetic platinum clusters. These systems are ideal as the large spin-orbit coupling leads to a non-collinear arrangement of the magnetic moments and the energy gap between the highest occupied and lowest-unoccupied molecular orbitals is rather small compared to other magnetic molecular systems. Afterwards, the protocol developed for molecules is generalized to study periodic extended systems and applied to calculate non-adiabatic effects and phonon angular momenta in a metallic manganese compound with a non-collinear antiferromagnetic phase, namely Mn_3Pt. Such system has drawn our attention because recent studies have detected the anomalous Hall effect in epitaxial films of Mn_3Pt at room temperature [23–25]. In both the insulating platinum clusters and the metallic manganese compound we find that some vibrational modes host a sizeable intrinsic angular momentum driven by non-adiabatic effects. The magnitude of such phonon angular momenta is comparable to that of the electronic orbital angular momenta in itinerant ferromagnets, namely few percents of $\hbar$ [26]. Our work therefore provides the conceptual link between non-adiabatic effects, electron-phonon coupling and the existence of a finite angular momentum of vibrational modes in the absence of external fields.

Finally, the question arises if the angular momenta of phonons is observable in experiments. There are two cases in which it could be detected. The first is the case in which a twofold degenerate mode at zone center occurs in the adiabatic phonon frequencies of the non-collinear magnetic system. Since the time-reversal symmetry breaking non-adiabatic term related to the Berry connection lowers the crystal symmetry, the twofold degenerate mode could split in two different modes hosting different angular momenta. In this case, even if the angular momentum itself would not be observed, its effects on the phonon spectrum would be. The second case is inelastic scattering of light with circularly polarized modes (Raman spectroscopy). By comparing the polarizations of incident and scattered light, one can resolve the right or left circular polarization of a given vibrational mode.

The angular momentum of phonons is important for the control of intervalley scattering [27,28], for lattice modulation-driven electronic phase transitions [29,30] and for phonon-driven topological states [7]. It is involved in several opto-magnetic and chiral-driven effects, the most revelant being the phonon ac Stark and Zeeman effects [31,32], phonon rotoelectric and magnetochiral effects [33, 34], dynamical multiferroicity [32] and chiral-induced spin selectivity [35]. Moreover, the angular momentum of phonons can be used as a new degree of freedom in phonon integrated circuitry [36, 37].

Topics covered in the manuscript are organized as follows. Experimental evidences of the existence of the angular momentum of phonons as part of the interaction between vibrational fields and magnetic or optical probes are reviewed in the first chapter. Subsequently, we present the formalism usually employed to describe non-adiabatic effects in density functional theory as well as the definition of the Berry curvature and of the angular momentum of phonons. Then we establish the connection between non-adiabatic effects and the Berry curvature in insulating molecular systems. In this case the treatment is simplified and meaningful insights can be gained with little effort. Following this line, we demonstrate that an intrinsic vibrational angular momentum can arise in non-collinear magnetic platinum clusters as a result of the non-adiabatic vibronic coupling. Finally, we generalize the theoretical apparatus and numerical techniques to evaluate non-adiabatic effects and the phonon angular momentum in periodic systems with non-collinear magnetism. As proof, we carry out fully relativistic *ab-initio* calculations for a metallic manganese compound in the non-collinear antiferromagnetic phase. Because in this system we find sizeable angular momenta of non-degenerate modes, the overall theoretical framework is deemed to be reliable.

Chapter 1

Experimental framework

The interaction between phonons and magnetic fields is pivotal in the understanding of some physical phenomena such as the phonon Hall effect [1, 2, 38] and the phonon contribution to the Einstein-de Haas effect [3, 4, 39]. The former is the analog of the electron Hall effect for phonons, while the latter can be seen as the evidence of the conservation of the total angular momentum. In both effects, the external magnetic field breaks time-reversal symmetry for the phonon dynamics. In absence of external probes, phonons are usually understood in terms of springs and as such, they are solutions of the classical lattice dynamics, which is invariant under time-reversal[2]. When the magnetic field is applied, non-symmetric terms with respect to time-reversal appear in the phonon Hamiltonian and hence nontrivial effects occur.

In recent years, the interest in this domain of research has grown even further because it has been shown that phonons, i.e. collective modes of the crystal, can host a finite (pseudo)angular momentum[3]. In the semi-classical description, lattice vibrations are linearly polarized[4] and phonons do not carry angular momentum. However, two degenerate linearly polarized modes can give rise to opposite angular momenta, in the same way as circularly polarized light can arise from two linear polarizations. The total angular momentum of degenerate phonons would still vanish. Nevertheless, if the degeneracy between the two modes is lifted, by internal or external interactions, the circular polarization of each mode can be detected and the angular momentum of phonons can be nonzero.

First experimental evidence of pseudoangular momentum of phonons came forward when chiral phonons were observed at the corners of the Brillouin zone in monolayer WSe_2 using an optical pump-probe technique based on the intervalley transition of holes [5]. As in this system the broken inversion symmetry of the lattice lifts the degeneracy of valley phonon modes, a circular polarization of phonons can take place. In this chapter we review the main experimental facts that have led to the formulation of the angular momentum in the presence of external symmetry breaking fields (magnetic fields, optical probes).

[2] See appendix A.

[3] In the following we will use *pseudo* only when referring to other authors work.

[4] In this thesis we refer to the polarization of phonons as if they were charged particles. The meaning will be clearer later.

1.1 Phonon Hall effect

When a perpendicular magnetic field is applied on a slab of a paramagnetic material subject to a temperature gradient, a transverse thermal current can be observed, as shown in Fig. 1.1. This effect is known as phonon (or thermal) Hall effect (PHE) by analogy with the electron Hall effect in which, instead of a temperature gradient, there is an electric potential difference and, instead of a thermal current, it is observed a transverse charge current. The first experimental evidences of such effect have been reported in Refs. [1, 2] for a terbium gallium garnet $Tb_3Ga_5O_{12}$ at low temperature. Unlike the electron analogue, the phonon Hall effect is not justified by the Lorentz

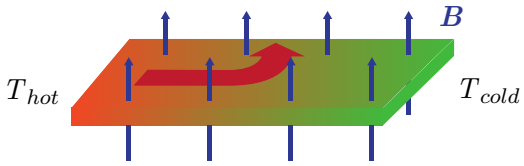

Figure 1.1: Schematic of the phonon Hall effect. A transverse heat current occurs in a paramagnetic material, perpendicularly to an applied temperature gradient and an external magnetic field.

force because phonons, being neutral quasiparticles, do not directly couple with the magnetic field. Therefore, after the phenomenological evidence, a sizeable effort has been devoted to study the PHE from a theoretical perspective [40–45]. Most of the articles published in this regard ascribe the PHE to the coupling between the pseudospin of the paramagnetic ions and lattice vibrations. Indeed, the Hamiltonian of the vibrating ions, for a ionic crystal lattice in a uniform external magnetic field, reads [46]

$$H = \sum_I \frac{1}{2M_I}\left[\mathbf{p}_I - \frac{e}{c}\mathbf{A}(\mathbf{u}_I)\right]^2 + \frac{1}{2}\sum_{IJ}\mathbf{u}_I\mathbf{C}_{IJ}(\mathbf{R})\mathbf{u}_J \tag{1.1}$$

where $\mathbf{u}_I$ is the phonon ionic displacement of the I-th ion, $\mathbf{p}_I$ is the conjugate momentum, M_I is the mass, $\mathbf{A}(\mathbf{u}_I)$ is the vector potential of the magnetic field, $\mathbf{C}_{IJ}(\mathbf{R})$ is the force constant matrix, e is the ionic charge and c the speed of light. In this section, we use the matrix notation in which vectors and matrices are bold and summations over the Cartesian indexes are implicit. For a constant magnetic field $\mathbf{B}$, the vector potential $\mathbf{A}$ can be written in a local symmetric gauge as $\mathbf{A}(\mathbf{u}) = -\mathbf{u}\times\mathbf{B}/2$. If the magnetic field is directed along the z axis and we consider only the two-dimensional motion (x and y directions) of the system, then the Hamiltonian can be expressed as

$$H = \sum_I \frac{1}{2M_I}(\mathbf{p}_I - \mathbf{\Lambda}\mathbf{u}_I)^T(\mathbf{p}_I - \mathbf{\Lambda}\mathbf{u}_I) + \frac{1}{2}\sum_{IJ}\mathbf{u}_I^T\mathbf{C}_{IJ}\mathbf{u}_J \tag{1.2}$$

where the conjugate variables are defined as $\mathbf{u}_I = (u_{Ix}, u_{Iy})^T$, $\mathbf{p}_I = (p_{Ix}, p_{Iy})^T$, the superscript T is used for transposed vectors and the antisymmetric matrix $\mathbf{\Lambda}$ is given by $\mathbf{\Lambda} = \begin{pmatrix} 0 & \lambda \\ -\lambda & 0 \end{pmatrix}$ where λ has the dimension of a frequency and it is proportional to

the magnetic field. Notice that $\mathbf{\Lambda}$ is independent on the ionic index in the mean-field approximation, so long as the magnetic field is constant.

The cross term in the kinetic energy product $\mathbf{u}_I^T \mathbf{\Lambda} \mathbf{p}_I / M_I$ can be interpreted as an isotropic Raman spin-phonon interaction [47–50] as it couples the pseudospin of the paramagnetic ions and lattice vibrations. In fact, the Raman spin-phonon interaction is usually expressed in the form of a spin-orbit interaction as $\mathcal{H}_R = g \sum_I \mathbf{s}_I \cdot (\mathbf{u}_I \times \mathbf{p}_I)$ where g is a constant of proportionality, $\mathbf{s}_I$ is the pseudospin of the lowest Kramers doublet[5] and $\mathbf{u}_I \times \mathbf{p}_I$ is the orbital angular momentum of the I-th ion. For an isotropic spin-phonon interaction, the average pseudospin is parallel to the magnetization $\mathbf{M}$. In the mean-field approximation, one can therefore replace $\langle \mathbf{s} \rangle = h\mathbf{M}$ into the equation of $\mathcal{H}_R$. Then, if the magnetic field is oriented along the z direction, the Raman spin-phonon interaction reads $\mathcal{H}_R = k \sum_I \mathbf{u}_I^T \mathbf{\Lambda} \mathbf{p}_I / M_I$ where k is another constant of proportionality.

When the magnetic field is present, the spin-phonon interaction breaks time-reversal symmetry for the ionic Hamiltonian as it introduces linear terms in the odd momentum $\mathbf{p}$ (velocities and momenta change sign when time is reversed). As a consequence, the phonon dynamics is governed by an effective non-hermitian Hamiltonian whose eigenstates include both positive and negative energies. This reflects on the energy current density and gives rise to a finite transverse thermal conductivity in the paramagnetic system. In reference [43] the interested reader can find the explicit calculation of the current density operator and of the phonon Hall conductivity. For our purposes, the important thing is that the Raman spin-phonon coupling constitutes a time-reversal symmetry breaking interaction for the phonon field that is responsible for the phonon Hall effect.

1.1.1 Topological nature of the phonon Hall effect

Some part of the literature enriched the theoretical demonstration of the phonon Hall effect from a topological point of view [43–45]. Namely, it was shown that the transverse thermal conductivity of the PHE can be expressed in terms of the *Berry curvature* of phonons, a geometrical object that is invariant under gauge transformation[6] and thus embeds a physical observable. The Berry curvature in question can be defined as

$$\Omega^{\nu}_{q_x,q_y} = \frac{\partial}{\partial q_x} \mathcal{X}^{\nu}_{q_y} - \frac{\partial}{\partial q_y} \mathcal{X}^{\nu}_{q_x} \tag{1.3}$$

where $\mathcal{X}^{\nu}_{\mathbf{q}}$ is the *Berry connection* of the phonon branch ν defined in the space of the phonon wavevector $\mathbf{q}$. It can be expressed in terms of the phonon eigenvectors $\boldsymbol{\varepsilon}_\nu$ as $\mathcal{X}^{\nu}_{\mathbf{q}} = i\boldsymbol{\varepsilon}^{\dagger}_{\nu} \frac{\partial}{\partial \mathbf{q}} \boldsymbol{\varepsilon}_\nu$. The Berry connection and the Berry curvature can be viewed, respectively, as a local gauge potential and gauge field associated with the *Berry phase* or geometric phase. The latter is defined as the loop integral of the vector potential $\mathcal{X}^{\nu}_{\mathbf{q}}$ in the parameter space, namely

$$\phi^{\nu} = \oint \mathcal{X}^{\nu}_{\mathbf{q}} \cdot d\mathbf{q}. \tag{1.4}$$

[5] Pair of degenerate electronic states. See appendix A.

[6] A transformation of the form $\mathbf{A} \to \mathbf{A} + \boldsymbol{\nabla} f$ where $f(\mathbf{r}, t)$ is a scalar function.

These concepts have been introduced by Micheal Berry in 1984 [51] and widely used over the past thirty years to explain and revisit a variety of phenomena in several domains of physics. In the next chapter, we will revise the main definitions and discuss one of the most popular effect due to the Berry phase, presented already in Berry's original paper, the Aharonov-Bohm effect.

In the standard Hall effect, the Berry phase of electrons has been related to the anomalous velocity of electrons in ferromagnetic materials [52–54] (topological nature of the anomalous Hall effect). In the thermal Hall effect instead, the Berry connection and curvature are associated with the phonon eigenvectors of the Hamiltonian Eq. 1.2 and they are defined in the space of the phonon wavevector $\mathbf{q}$ [55]. Going further with the parallel between phonon and electrons, the thermal current density in the phonon Hall effect exhibits off-diagonal elements equivalent to the anomalous velocity of electrons in the electron Hall effect. Moreover, the thermal Hall conductivity can be expressed by means of the phonon Berry curvature in a similar fashion as it can be done for electrons in the anomalous Hall effect. These similarities highlight the topological nature of the phonon Hall effect. However, even if the qualitative explanation of the phonon Hall effect and its topological nature has been given, a quantitative description is still missing. For example, what is the meaning of the spin-phonon interaction from a microscopic point of view?

1.2 Angular momentum of phonons

After the formulation of the topological nature of the phonon Hall effect, further studies on the interaction between phonons and magnetic fields have been carried on. In ionic crystals with Raman spin-phonon interaction, it has been shown that an external magnetic field breaks time-reversal symmetry for the phonon field [4]. As a result, non-degenerate vibrational modes can get a nonlinear polarization and host a finite angular momentum.

In a crystal lattice, the total angular momentum is equal to $\mathbf{J} = \mathbf{L} + \mathbf{S} + \mathbf{N}$ where $\mathbf{L}$ and $\mathbf{S}$ are the orbital and spin angular momenta of the electrons, respectively, and $\mathbf{N} = \sum_I \mathbf{R}_I \times \mathbf{P}_I$ is the orbital angular momentum of the nuclei, where $\mathbf{R}_I$ and $\mathbf{P}_I$ are respectively the equilibrium position and the momentum of the I-th nucleus. The spin of the nuclei is usually neglected because it is much smaller than the spin of the electrons. When considering a phonon ionic displacement $\mathbf{u}$ of the nuclei from the equilibrium positions $\mathbf{R}^0$, the angular momentum becomes

$$\mathbf{N} = \sum_I (\mathbf{R}_I^0 + \mathbf{u}_I) \times (\mathbf{P}_I + \mathbf{p}_I) = \mathbf{N}^{\text{lat}} + \mathbf{N}^{\text{ph}} \tag{1.5}$$

where $N^{\text{lat}} = \sum_I \mathbf{R}_I^0 \times \mathbf{P}_I$ is the angular momentum of the lattice which reflects a rigid-body rotation of the system and $\mathbf{N}^{\text{ph}} = \sum_I \mathbf{u}_I \times \mathbf{p}_I$ is the angular momentum of phonons. The cross terms vanish at equilibrium as the phonon ionic displacement and momentum average to zero on the timescale of the equilibrium variables. Within the classical theory of lattice dynamics, the phonon angular momentum can be defined as

$$\mathbf{N}^{\text{ph}} = \sum_I M_I \mathbf{u}_I \times \dot{\mathbf{u}}_I \tag{1.6}$$

where **u** is the phonon ionic displacement and M is the mass of the atom. In reference [4], it is demonstrated that the angular momentum of phonons as defined by Eq. 1.6 can be sizeable in systems with strong spin-phonon interaction and large magnetization. The magnitude of the angular momentum is related to the parameter λ that appears in Eq. 1.2. Such parameter can be estimated from the phonon Hall effect or measured by means of Raman scattering experiments, given that the spin-phonon interaction splits zone-center degenerate modes with an energy gap of 2λ.

The angular momentum of phonons can be observed in experiments that exploit the conservation law of the total angular momentum. Among them, it is worth mentioning the Einstein-de Haas effect which demonstrates that a change in the magnetization of a free body induces a mechanical rotation of the body itself. In the experiment, a ferromagnetic material is suspended into a cylindrical coil, that provides a uniform external magnetic field, as shown in Fig. 1.2.

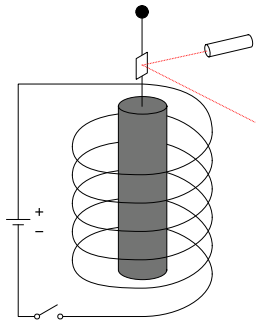

Figure 1.2: Schematic of the Einstein-de Haas effect. A cylinder of ferromagnetic material is suspended into a cylindrical coil which provides the external magnetic field. The variation of the magnetic field induces a finite variation of the magnetization of the system and, hence, a finite variation of the angular momentum of electrons. Due to the conservation of the total angular momentum, a rigid-body rotation of the system takes place. In presence of spin-phonon interaction, the phonon angular momentum is nonzero and it contributes to the macroscopic effect. The rotation of the system is measured with a laser beam reflecting on a mirror. Image by Jasper Olbrich, distributed under a CC BY-SA 3.0 licence.

The magnetization of the system **M** is proportional to the total angular momentum of electrons through the gyromagnetic ratio. A variation of the magnetization, namely a variation of the angular momentum of electrons, must therefore be compensated by a torque on the rigid-body due to the conservation of the total angular momentum. In other words, a variation of the magnetization induces a mechanical rotation of the free body that can be measured with a laser beam. In the presence of spin-phonon interaction, the spin angular momentum of electrons is coupled to the phonon angular momentum. A variation of the former thus modifies the latter. A phonon contribution can therefore be detected in the gyromagnetic ratio from the Einstein-de Haas effect [4].

Another possible experiment to detect the total angular momentum of phonons, based on the thermal Hall effect, has been proposed in reference [38]. Once again, the rigid body is free to rotate around a given vertical axis as shown in Fig. 1.3. A laser

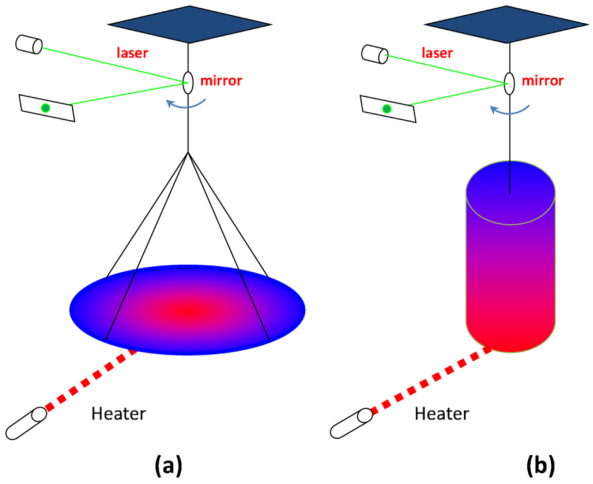

Figure 1.3: Experimental setup for measurement of mechanical rotation induced by a temperature gradient in a non-centrosymmetric material. (a) A thin rounded disk is heated in the center. (b) A cylinder is heated from the bottom. In both cases, a circular thermal current flows at the edge of the sample. A variation of the magnetization along the direction of the temperature gradient occurs. The result is a net variation of the microscopic angular momentum. For sufficiently low symmetric systems, the phonon angular momentum is nonzero. The mechanical rotation is measured by the laser-mirror setup. Image from *New Journal of Physics* 18, 103039 (2016), distributed under CC BY 3.0 licence.

beam is then used to heat the system up. As long as the material is heated, circular thermal currents flow at the edge of the sample perpendicularly to the temperature gradient. Therefore, a variation of the magnetization along the direction of the gradient must also take place [56]. Similarly to the Einstein-de Haas effect, the variation of the magnetization entails a variation of the angular momentum of electrons that is compensated by a mechanical rotation of the rigid body. If the system has sufficiently low crystallographic symmetries, such as polar or chiral crystal structures, the temperature gradient induces a finite phonon angular momentum due to the non-equilibrium phonon distribution [57]. In such cases, also the phonon angular momentum is compensated by the the rigid-body rotation of the system. In non-metallic materials with broken inversion symmetry, the mechanical torque is uniquely due to the phonon angular momentum. Note that in this experiment, the external magnetic field is unnecessary as the temperature gradient by itself breaks time-reversal symmetry.

1.3 Observation of chiral phonons

Chirality is a fundamental property of an object not identical to its mirror image. For elementary particles and quasiparticles, it is an important quantum concept at heart of modern physics. Much effort in the recent years has been addressed to demonstrate that bosonic collective excitations such as phonons can attain chirality. In this section,

we would like to focus on one particular experiment that showed that phonons can exhibit intrinsic chirality at the corners of the Brillouin zone in monolayer tungstene diselenide [5]. As in this system the broken inversion symmetry of the lattice lifts the degeneracy of valley phonon modes, a circular polarization of phonons can take place. Owing to the threefold rotational symmetry of the two-dimensional hexagonal lattice, the pseudoangular momentum l of phonons at K and K' can only be 0 or ± 1 [6], depending on the phase change of the atomic motion after a counterclockwise 120° rotation: $\hat{C}_3(u_q) = e^{-i(2\pi/3)l}u_q$. For example, the longitudinal optical mode LO(K) shown in the left side of Fig. 1.4 gains a negative phase after rotation and thus it carries pseudoangular momentum $l = 1$. In contrast, the longitudinal acoustic mode LA(K) is symmetric under C_3 rotations and thus it has $l = 0$.

Provided that time-reversal is a symmetry of the system, chiral phonons exist in pairs with identical energy, one in each valley. Namely, for each K phonon with pseudoangular momentum l, there exists a K' phonon with the same energy and pseudoangular momentum $-l$.

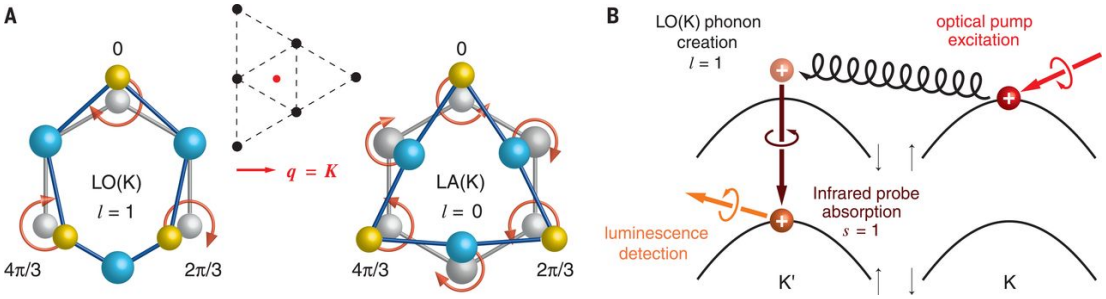

Figure 1.4: Phonons chirality at the corners of the Brillouin zone in WSe_2, probed via infrared optical absorption. (A) Phonon displacements of W and Se atoms (blue and yellow spheres, respectively) for two chiral phonon modes at the K point (red dot) of the reciprocal lattice (array of black dots). (B) Intervalley optical transition of holes through virtual scattering with a LO valley phonon. The pseudoangular momentum of the valley phonon is equal to the spin of the infrared photon due to angular momentum conservation. From *Science* 359, 579 (2018). Reprinted with permission from AAAS.

The chirality of phonons is probed with an optical pump-probe technique which allows to determine the pseudoangular momentum of valley phonons scattering with the holes. The intervalence band transition process is represented in the right hand side of Fig. 1.4. First, holes are injected at K valley by a left-circularly polarized optical pump pulse. K-valley polarized holes can then transit to K' valley in a virtual state by emitting a K phonon with pseudoangular momentum $l = 1$. The probe infrared pulse is sent to satisfy energy conservation and to place the hole in the spin-split band at K'. The pseudoangular momentum of the K phonon is determined by measuring the polarization selection of the absorbed photon. With a left-circularly polarized excitation, the intervalley transition of holes from the K-valley can either absorb a left-circularly polarized infrared photon to produce LO phonons with pseudoangular momentum $l = 1$ or absorb a right-circularly polarized infrared photon to excite TA/A_1 phonons with pseudoangular momentum $l = -1$.

From another perspective, the experiment proves that infrared optical probes break time-reversal symmetry for the phonon field. In fact, so long as valley phonons have the same energy, K and K' fold at Γ in a supercell $\sqrt{3}\times\sqrt{3}\mathrm{R}30^o$ reconstruction and the two phonon modes become doubly degenerate at zone center. The infrared absorption must therefore break valleys time-reversal symmetry to create chiral phonons.

1.4 Summary

In this first chapter, we introduced the experimental background in which our research has been carried on. The interaction between phonons and external magnetic fields is established through two main physical phenomena: the phonon Hall effect and the Einstein-de Haas effect. The former is usually explained in terms of the spin-phonon interaction, which breaks time-reversal symmetry for phonons when an external magnetic field is applied. The latter descends from the principle of conservation of the total angular momentum. Experimental setups based on these phenomena have been proposed to measure the angular momentum of phonons.

Alternatively, it has been demonstrated that valley phonons in lattice crystals with broken inversion symmetry can attain chirality. In particular, the chirality of some vibrational modes in monolayer tungstene diselenide has been probed by means of infrared optical absorption. It has been shown that circularly polarized phonons arise within the intervalence band transition process of holes from K to K' valley. Chiral phonons are important for electron-phonon coupling in solids, phonon-driven topological states, and energy-efficient information processing.

Chapter 2

Geometric phases and topology: general concepts

Geometric phases are at the heart of many physical phenomena. Here we present the formalism usually employed to define the Berry phase and related quantities in a general case. As a proof of concept, we discuss the Aharonov-Bohm (AB) effect and molecular AB effect in which geometric phases are crucial. The last sections are devoted to the parallel transport gauge, to the adiabatic approximation and to the geometric phase in periodic lattice structures. We refer the reader to [18] and [58] for the treatment of these topics.

2.1 Berry phase and related quantities

Let us consider a generic quantum system whose Hamiltonian depends on the parameter $\boldsymbol{\xi}$. The parameter can have more than one component. The time-independent Schrödinger equation reads

$$H(\boldsymbol{\xi})|\psi(\boldsymbol{\xi})\rangle = E(\boldsymbol{\xi})|\psi(\boldsymbol{\xi})\rangle \tag{2.1}$$

where the eigenstates $|\psi(\boldsymbol{\xi})\rangle$ of the system reside in a suitable Hilbert space. As an example, the parameter $\boldsymbol{\xi}$ can be the nuclear coordinates in a molecule and $H(\boldsymbol{\xi})$ the Hamiltonian of electrons. Let us consider a subset of $\boldsymbol{\xi}$ such that the ground state of the system $|\psi_0(\boldsymbol{\xi})\rangle$ is non-degenerate. In the following, we drop the subscript 0. The phase difference $\Delta\phi_{12}$ between the ground states at two different $\boldsymbol{\xi}$ points in the parameter space is given by

$$\Delta\phi_{12} = -\text{Im log } \langle\psi(\boldsymbol{\xi}_1)|\psi(\boldsymbol{\xi}_2)\rangle \tag{2.2}$$

$$e^{-i\Delta\phi_{12}} = \frac{\langle\psi(\boldsymbol{\xi}_1)|\psi(\boldsymbol{\xi}_2)\rangle}{|\langle\psi(\boldsymbol{\xi}_1)|\psi(\boldsymbol{\xi}_2)\rangle|}. \tag{2.3}$$

$\Delta\phi_{12}$ however, has no physical meaning. The state vectors are defined up to a global phase and an arbitrary change in the phase of the ground-states $|\psi(\boldsymbol{\xi}_{1,2})\rangle$ make the difference $\Delta\phi_{12}$ vary accordingly. However, if we consider a closed loop in the parameter

space, as shown in Fig. 2.1, the phase difference along the path can be written as

$$\begin{aligned}\phi &= \Delta\phi_{12} + \Delta\phi_{23} + \Delta\phi_{34} + \Delta\phi_{41} \\ &= -\mathrm{Im}\,\log\left[\langle\psi(\boldsymbol{\xi}_1)|\psi(\boldsymbol{\xi}_2)\rangle\langle\psi(\boldsymbol{\xi}_2)|\psi(\boldsymbol{\xi}_3)\rangle\langle\psi(\boldsymbol{\xi}_3)|\psi(\boldsymbol{\xi}_4)\rangle\langle\psi(\boldsymbol{\xi}_4)|\psi(\boldsymbol{\xi}_1)\rangle\right] \quad (2.4)\end{aligned}$$

where now the gauge-arbitrary phases cancel in pairs, making the overall phase ϕ a gauge invariant quantity. The sum Eq. 2.4, therefore, only depends on the path and the phase ϕ does have a physical meaning.

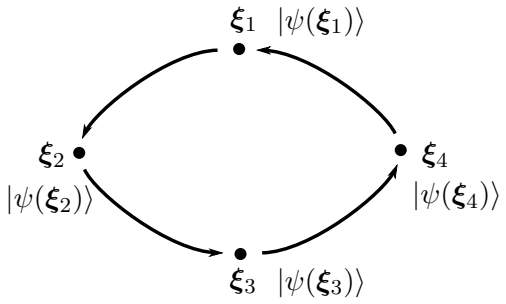

Figure 2.1: Closed loop in the parameter space.

In the continuum limit, the sum becomes an integral over the closed path γ and the Berry phase, defined modulo 2π, reads

$$\phi = \oint_\gamma \boldsymbol{\mathcal{X}}(\boldsymbol{\xi}) \cdot d\boldsymbol{\xi} = \oint_\gamma i\langle\psi(\boldsymbol{\xi})|\boldsymbol{\nabla}_{\boldsymbol{\xi}}\psi(\boldsymbol{\xi})\rangle \cdot d\boldsymbol{\xi} \quad (2.5)$$

where the vector potential $\boldsymbol{\mathcal{X}}(\boldsymbol{\xi})$, hereinafter called Berry potential or Berry connection[7], is defined as

$$\boldsymbol{\mathcal{X}}(\boldsymbol{\xi}) = i\langle\psi(\boldsymbol{\xi})|\boldsymbol{\nabla}_{\boldsymbol{\xi}}\psi(\boldsymbol{\xi})\rangle. \quad (2.6)$$

The latter is not a gauge invariant object as it transforms, under an arbitrary phase change of the wavefunction, in the following way:

$$\psi(\boldsymbol{\xi}) \to e^{if(\boldsymbol{\xi})}\psi(\boldsymbol{\xi}) \quad (2.7)$$

$$\boldsymbol{\mathcal{X}}(\boldsymbol{\xi}) \to \boldsymbol{\mathcal{X}}(\boldsymbol{\xi}) + \boldsymbol{\nabla}_{\boldsymbol{\xi}} f(\boldsymbol{\xi}) \quad (2.8)$$

where $f(\boldsymbol{\xi})$ is some differentiable scalar function of the parameter $\boldsymbol{\xi}$. The phase ϕ is given by a circuit integral in parameter space and it is independent of how the circuit is traversed, provided that the phase of the wavefunction is differentiable all along the path. The curl of the Berry potential in the parameter space is called Berry curvature and it is equal to

$$\Omega_{\mu\nu} = \frac{\partial\mathcal{X}_\nu}{\partial\xi_\mu} - \frac{\partial\mathcal{X}_\mu}{\partial\xi_\nu} = -2\mathrm{Im}\left\langle \frac{\partial\psi}{\partial\xi_\mu} \middle| \frac{\partial\psi}{\partial\xi_\nu} \right\rangle \quad (2.9)$$

where μ and ν label the components of $\boldsymbol{\xi}$. Notice that Ω is a real antisymmetric tensor. Since the curl of a gradient vanishes, the Berry curvature is gauge invariant

[7]The term *connection* is borrowed from differential geometry.

and hence, in principle, physically observable. According to Eq. 2.9, the curvature vanishes whenever the wavefunctions can be taken as real. This is the case of finite systems with no magnetic field and negligible spin-orbit interaction, as we will see in the following. When instead the wavefunctions are unavoidably complex, the curvature can be nonzero and the Berry phase can assume any value.

The main discovery of Berry's work is that geometric phases can be measurable. Namely, there exists a whole class of observables that cannot be cast as expectation value of any operator. Such geometric phases manifest themselves in many diverse unrelated domain of physics. Why these observables arise is explained in the original paper by Berry [51]. In a truly isolated system, no geometric phase can exist, as only conservative fields occur. However, no real system is isolated. Indeed, the first assumption that we made of a parametric Hamiltonian implies that the system is not isolated. The parameter $\boldsymbol{\xi}$ in fact plays the role of all the variables that are not included in the Hilbert space. In this sense the importance of the Berry phase can be appreciated: the parametric Hamiltonian can be used to describe some part of a larger system as if it were isolated, at the cost of introducing new observables that cannot be cast as the expectation value of hermitian operators [18].

The theory hereby presented works very well for those systems whose sub-parts are almost isolated relative to each other and the little coupled variables are static parameters compared to the rest, as for example the nuclear coordinates in crystals. Nowadays, the Berry phase is ubiquitous in physics and its effects have been detected in many diverse domain of research [59]. The first (recognized) and most known example of a manifestation of the Berry phase is the Aharonov-Bohm effect.

2.2 Aharonov-Bohm effect

The Aharonov-Bohm (AB) effect is an intriguing phenomenon by which a quantum system moving nearby a magnetic field $\mathbf{B}$ is affected by the vector potential $\mathbf{A}$ of the magnetic field, despite the latter is not invariant under a gauge transformation and thus not observable [60]. Experimental evidences of the effect have been sought and found since the 1960's [61].

The schematic of the AB effect for electrons, shown in Fig. 2.2, resembles the double-slit experiment that is commonly referred to in order to illustrate the wave-particle duality of light. The electrons are allowed to pass next to a region of space where the magnetic field is confined along two different paths encircling the solenoid as shown in Fig. 2.2. In classical electromagnetism, only the magnetic field is real and the vector potential does not affect the electrons. In quantum mechanics, instead, the vector potential is real and can modify the wavefunction of electrons in regions of space where the magnetic field identically vanishes. Indeed, when passing through a region with nonzero vector potential $\mathbf{A}$, the wavefunction undergoes the phase transformation

$$\psi(\mathbf{r},t) \to \exp\left[i\frac{e}{\hbar c}\int_{\gamma}\mathbf{A}(\mathbf{r},t)\cdot d\mathbf{r}\right]\psi(\mathbf{r},t) \tag{2.10}$$

where γ is the path of the particle, e is the electron charge and the phase of the wavefunction is referred to a given initial value in space coordinates. The magnetic

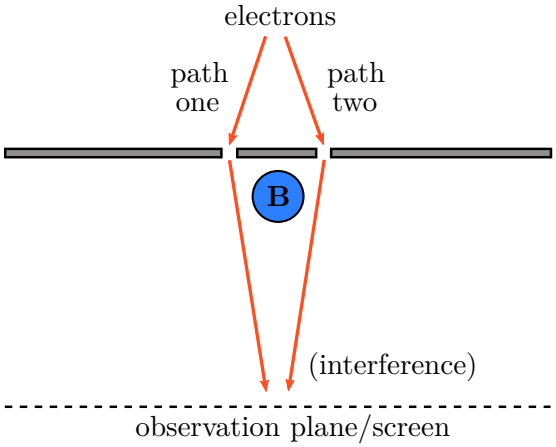

Figure 2.2: Schematic of the Aharonov-bohm effect.

vector potential thus modifies the phase of the vector state in a region where the magnetic field is absent. The phase change with respect to the initial value along the different paths can be detected in the interference pattern of the electrons on the observation screen. The intensity of the signal in the AB effect is related to the phase difference between the wavefunctions at the observation plane. Such quantity is equal to the line integral of the vector potential along the closed path, namely

$$\Delta\phi = \frac{e}{\hbar c}\oint \mathbf{A}(\mathbf{r},t)\cdot d\mathbf{r}, \tag{2.11}$$

and it is proportional to the flux of the magnetic field across the surface bounded by the path. In order to demonstrate that $\Delta\phi$ is a Berry phase, we consider an electron in a box (infinite potential well) subject to the time-independent Schrödinger equation

$$\left[\frac{p^2}{2m} + V(\mathbf{r})\right]\chi(\mathbf{r}) = E\chi(\mathbf{r}). \tag{2.12}$$

When the box is displaced by a vector $\mathbf{R}$, the Hamiltonian and the wavefunction become

$$H(\mathbf{R}) = \frac{p^2}{2m} + V(\mathbf{r}-\mathbf{R}) \tag{2.13}$$

$$\langle \mathbf{r}|\psi(\mathbf{R})\rangle = \chi(\mathbf{r}-\mathbf{R}) \tag{2.14}$$

while the eigenvalue is $\mathbf{R}$-independent. Suppose now that a magnetic field is switched on somewhere in space. The Hamiltonian becomes

$$H(\mathbf{R}) = \frac{1}{2m}\left[\mathbf{p} - \frac{e}{c}\mathbf{A}(\mathbf{r})\right]^2 + V(\mathbf{r}-\mathbf{R}) \tag{2.15}$$

where $\mathbf{A}(\mathbf{r})$ is the vector potential of the magnetic field. The formal solution of the Schrödinger equation can be written as

$$\langle \mathbf{r}|\psi(\mathbf{R})\rangle = \exp\left[i\frac{e}{\hbar c}\int_{\mathbf{R}}^{\mathbf{r}} \mathbf{A}(\mathbf{r}')\cdot d\mathbf{r}'\right]\chi(\mathbf{r}-\mathbf{R}). \tag{2.16}$$

The wavefunction so obtained is not a single-valued function of $\mathbf{r}$ as the integral in the phase factor depends on the path. Let us then consider a confined magnetic field and prevent the box from overlapping the region of the magnetic field. With such a choice, the wavefunction Eq. 2.16 is single-valued with respect to $\mathbf{r}$. If we let the box wind once around the flux tube of the magnetic field, the electronic wavefunction picks up a Berry phase ϕ. The Berry connection of the problem is equal to[8]

$$\boldsymbol{\mathcal{X}}(\mathbf{R}) = i\langle\psi(\mathbf{R})|\nabla_{\mathbf{R}}\psi(\mathbf{R})\rangle = \frac{e}{\hbar c}\mathbf{A}(\mathbf{R}), \tag{2.17}$$

and the Berry phase reads

$$\phi = \frac{e}{\hbar c}\oint_{\gamma}\mathbf{A}(\mathbf{R})\cdot d\mathbf{R} = \frac{e}{\hbar c}\iint_{S(\gamma)}\mathbf{B}(\mathbf{R})\cdot d\mathbf{S}, \tag{2.18}$$

that is to say, it is proportional to the flux of the magnetic field across the surface $S(\gamma)$ bounded by the path. The Berry curvature is proportional to the magnetic field, defined as the curl of the vector potential.

The AB effect is an example of manifestation of the Berry phase in which the geometric vector potential and the gauge field coincide with the magnetic vector potential and field, respectively. The Berry phase, in this case, is a topological object because it is due to a singular magnetic flux tube. In general, the Berry connection and curvature can be interpreted respectively as effective (synthetic) vector potential and magnetic field in the parameter space. In Table 2.1, we summarize the dualism between magnetism and the Berry related quantities. In the last column, the gauge invariance of each is specified.

magnetism	synthetic fields in the parameter space	gauge invariance
flux of the magnetic field across a closed surface	Berry phase ϕ	Y
vector potential $\mathbf{A}$	Berry connection $\boldsymbol{\mathcal{X}}$	N
magnetic field $\mathbf{B}$	Berry curvature Ω	Y

Table 2.1: Summary of the correspondence between magnetic flux, potential and field with the Berry related quantities. Gauge invariance is specified for each.

As a further consideration, the antisymmetric Berry curvature can be seen as the imaginary part of a more general quantum *geometric tensor* [62]. The real symmetric part instead represents the quantum *metric tensor* providing a natural means of measuring distances along paths in the parameter space. In the same way as the Berry curvature can be seen as a synthetic magnetic field, the gauge invariant metric tensor can be seen as synthetic electric field.

2.2.1 Molecular Aharonov-Bohm effect

Another interesting manifestation of the Berry phase is the molecular Aharonov-Bohm effect [63]. It concerns the ionic motion in the adiabatic approximation and it is observable in rotovibrational spectra of molecules. As parameter $\boldsymbol{\xi}$, we consider the nuclear

[8] The term $\int \chi(\mathbf{r}-\mathbf{R})\nabla_{\mathbf{R}}\chi(\mathbf{r}-\mathbf{R})d\mathbf{r}$ vanishes as we are considering normalized real wavefunctions.

coordinates $\mathbf{R}_s$, where s labels the nuclei in the molecule, and as parametric Hamiltonian we consider that of electrons in the Born-Oppenheimer approximation. Then the nuclear dynamics can be described by an effective Hamiltonian [18]

$$H^{nucl} = \sum_s \frac{1}{2M_s} \left[-i\hbar\boldsymbol{\nabla}_{\mathbf{R}_s} - \hbar\boldsymbol{\mathcal{X}}(\mathbf{R}_s)\right]^2 + E(\mathbf{R}) \tag{2.19}$$

where M_s is the mass of the s-th nucleus, $\boldsymbol{\mathcal{X}}(\mathbf{R})$ is the Berry connection of electrons defined by Eq. 2.6 and $E(\mathbf{R})$ is the Born-Oppenheimer energy surface of electrons. In molecular systems, one typically assumes vanishing wavefunctions at infinity. Then, in the absence of magnetic interactions, the Berry connection also vanishes and the nuclear dynamics reduces to the classical one.

When the wavefunctions are not real, as for example in the presence of a magnetic field, the Berry connection in Eq. 2.19 accounts for the screening of electrons to the nuclear dynamics. An illustrative example in this regard is the failure of the adiabatic approximation in the case of an hydrogen atom immersed into an external magnetic field. Within the *naive* Born–Oppenheimer approximation, the hydrogen atom is wrongly deflected by a Lorentz force according to its naked nuclear charge. The screening of the electron needs to be reinserted "by hand" to recover the correct result. When including the Berry connection in the description of the nuclear dynamics, the trajectory of the hydrogen atom is not affected by the magnetic field. The nuclear momentum in Eq. 2.19 can be replaced by

$$-i\hbar\boldsymbol{\nabla}_{\mathbf{R}} \rightarrow -i\hbar\boldsymbol{\nabla}_{\mathbf{R}} + \frac{e}{c}\mathbf{A}(\mathbf{R}) \tag{2.20}$$

where $\mathbf{A}(\mathbf{R})$ is the vector potential of the magnetic field $\mathbf{B}$. By expressing the potential $\mathbf{A}$ in the symmetric gauge, it can be shown that the electronic wavefunction $\psi(\mathbf{r})$ acquires a geometric phase of the kind $\Delta\phi = \frac{e}{2\hbar c}\mathbf{r}\cdot(\mathbf{B}\times\mathbf{R})$, analogously to what happens in the AB effect (see equation 2.10). The Berry connection $\boldsymbol{\mathcal{X}}(\mathbf{R})$ therefore reads

$$\boldsymbol{\mathcal{X}}(\mathbf{R}) = i\langle\psi_{\mathbf{R}}|\boldsymbol{\nabla}_{\mathbf{R}}\psi_{\mathbf{R}}\rangle = \frac{e}{2\hbar c}\langle\psi_{\mathbf{R}}|\mathbf{B}\times\mathbf{r}|\psi_{\mathbf{R}}\rangle = \frac{e}{2\hbar c}\mathbf{B}\times\mathbf{R} = \frac{e}{\hbar c}\mathbf{A}(\mathbf{R}), \tag{2.21}$$

namely it is equal, up to constants, to the vector potential at the proton site. When inserted into Eq. 2.19, the Berry connection, therefore, exactly cancels with the magnetic potential from Eq. 2.20. As a result, no Lorentz force is experienced by the neutral hydrogen atom moving in the magnetic field. In this example, the Berry connection provides the screening of the electron which is absent in the adiabatic approximation.

In the pre-Berry literature, this working framework is sometimes referred to as the *screened* Born-Oppenheimer approximation [19] and represents the first step beyond the *naive* Born-Oppenheimer approximation. It is therefore a good starting point for the description of non-adiabatic effects in solids and it will be the working topic of the next chapter.

2.3 The parallel transport gauge

One of the main attributes of the Berry curvature is the gauge invariance. The Berry curvature Ω as defined by Eq. 2.9, is invariant under the gauge transformation Eq. 2.7.

This allows for example to safely express the Berry curvature in perturbation theory without worrying about the gauge fixing. When we write the perturbed state as

$$|\psi_0(\boldsymbol{\xi}+\Delta\boldsymbol{\xi})\rangle = |\psi_0(\boldsymbol{\xi})\rangle + \sum_{n\neq 0} |\psi_n(\boldsymbol{\xi})\rangle \frac{\langle\psi_n(\boldsymbol{\xi})|H(\boldsymbol{\xi}+\Delta\boldsymbol{\xi}) - H(\boldsymbol{\xi})|\psi_0(\boldsymbol{\xi})\rangle}{E_0(\boldsymbol{\xi}) - E_n(\boldsymbol{\xi})} \tag{2.22}$$

we are implicitly assuming the *parallel transport* gauge fixing in which the phase of the state vector is kept constant as $\boldsymbol{\xi}$ is varied by an infinitesimal amount. As the excited states $|\psi_n(\boldsymbol{\xi})\rangle$ are orthogonal to the ground state $|\psi_0(\boldsymbol{\xi})\rangle$, the Berry connection, defined as $\boldsymbol{\mathcal{X}}(\boldsymbol{\xi}) = i\langle\psi(\boldsymbol{\xi})|\boldsymbol{\nabla}_{\boldsymbol{\xi}}\psi(\boldsymbol{\xi})\rangle$, vanishes along the path. However, the curvature is not necessarily zero and it can be written within the parallel transport gauge as

$$\Omega_{\mu\nu} = -2\mathrm{Im}\sum_{n\neq 0} \frac{\langle\psi_0(\boldsymbol{\xi})|\frac{\partial H(\boldsymbol{\xi})}{\partial\xi_\mu}|\psi_n(\boldsymbol{\xi})\rangle\langle\psi_n(\boldsymbol{\xi})|\frac{\partial H(\boldsymbol{\xi})}{\partial\xi_\nu}|\psi_0(\boldsymbol{\xi})\rangle}{\left[E_0(\boldsymbol{\xi}) - E_n(\boldsymbol{\xi})\right]^2}. \tag{2.23}$$

If the ground state is allowed to be degenerate with the first exited state, the curvature presents a singularity. This case is particularly interesting when the wavefunctions can be taken as real valued. Indeed, in these cases, a nontrivial change of sign in the wavefunction occurs, namely the Berry phase is equal to π, only if the path encircles these degeneracy points. This sign change has remarkable observable effects on the rotovibrational spectrum of some molecules, such as lithium trimer [64]. If the wavefunctions are complex, the Berry phase can assume any value.

2.4 The adiabatic approximation

In this paragraph we deal with the case in which the parameter $\boldsymbol{\xi}$ is a smooth function of time (we follow reference [58]). The adiabatic approximation consists in assuming that the variation of the parameter $\boldsymbol{\xi}(t)$ is so slow that the state vector $|\psi(\boldsymbol{\xi})\rangle$ is always well approximated by the static solution of the Schrödinger equation at the current value of $\boldsymbol{\xi}(t)$. As the Hamiltonian does not explicitly depend on time, the eigenvalue equation $H(\boldsymbol{\xi})|n(\boldsymbol{\xi})\rangle = E_n(\boldsymbol{\xi})|n(\boldsymbol{\xi})\rangle$ holds at any time. The index n labels the stationary solutions of the eigenvalue problem. If the parameter $\boldsymbol{\xi}$ had been time-independent, the time evolution of the state vector, solution of the time-dependent Schrödinger equation, would have been

$$|\psi(t)\rangle = \sum_n a_n(0)e^{-iE_nt/\hbar}|n\rangle \tag{2.24}$$

with coefficients $a_n(0)$ determined by the initial state. Now, if the parameter $\boldsymbol{\xi}$ slowly changes in time so that we can approximate it as constant in each interval of time dt, the phase evolution can be written as

$$|\psi(t)\rangle = \sum_n a_n(t)e^{-i\frac{1}{\hbar}\int_0^t E_n(t')dt'}|n(t)\rangle \tag{2.25}$$

where $|n(t)\rangle \equiv |n(\boldsymbol{\xi}(t))\rangle$ is the eigenstate of the time-independent problem $|n(\boldsymbol{\xi})\rangle$ evaluated at $\boldsymbol{\xi} = \boldsymbol{\xi}(t)$ and $a_n(t)$ is to be determined. We replace Eq. 2.25 into the time-dependent Schrödinger equation and multiply by $\langle n(t)|$ on the left. We end up with a

first order differential equation for $a_n(t)$, namely

$$\dot{a}_n(t) + a_n(t)\langle n(t)|\partial_t n(t)\rangle = 0 \tag{2.26}$$

that we solve by separation of variables as $a_n(t) = a_n(0)e^{i\phi_n(t)}$ where $\phi_n(t)$ is an open-path Berry phase in time which can be written as

$$\phi_n(t) = \int_0^t \mathcal{X}_n(t')dt' \tag{2.27}$$

and $\mathcal{X}_n(t) = i\langle n(t)|\partial_t n(t)\rangle$ is the Berry connection. Moreover, the Berry phase in Eq. 2.27 can be expressed as a function of the parameter $\boldsymbol{\xi}$ alone as

$$\phi_n(\boldsymbol{\xi}) = \int_{\boldsymbol{\xi}(0)}^{\boldsymbol{\xi}(t)} \boldsymbol{\mathcal{X}}_n(\boldsymbol{\xi}) \cdot d\boldsymbol{\xi} \tag{2.28}$$

where now $\boldsymbol{\mathcal{X}}_n(\boldsymbol{\xi}) = i\langle n(\boldsymbol{\xi})|\boldsymbol{\nabla}_{\boldsymbol{\xi}} n(\boldsymbol{\xi})\rangle$ is the Berry connection in the parameter space. Eq. 2.28 shows how the Berry phase of the time-dependent wavefunction is only related to the path travelled by the system in the parameter space and does not depend upon the rate at which the path is traversed, so long as the parametric evolution is sufficiently slow. The time evolution of the state vector in the adiabatic approximation is therefore given by

$$|\psi(t)\rangle = \sum_n a_n(0)e^{i\phi_n(\boldsymbol{\xi}(t))}e^{-i\frac{1}{\hbar}\int_0^t E_n(t')dt'}|n(t)\rangle \tag{2.29}$$

where the "normal" phase factor that usually determines the time evolution of the system is now accompanied by a Berry like phase factor that is absent in the time-independent picture (compare Eq. 2.29 with Eq. 2.24). It should be pointed out, however, that such phase is irrelevant in most treatments of physical problems as it cancels out when computing the expectation value of an hermitian operator. Nonetheless, as we already mentioned before, the Berry phase can sometimes play a role in interference processes such as the AB effect. The adiabatic approximation is very powerful in systems where "fast" and "slow" variables can be efficiently separated. A prototypical case is the one of electrons in molecules and crystals, which are much lighter than the nuclei and thus much faster. The electronic Hamiltonian can be handled in a very good approximation as if the nuclear coordinates $\mathbf{R}_I$ were classical variables varying slowly enough to solve the electronic problem as if they were still.

2.5 Berry phase in crystal lattices

Up until now in this chapter, we have considered Berry phases, connections and curvatures defined in the space of the generic parameter $\boldsymbol{\xi}$. In the following we will consider as parameter the phonon ionic displacement $\mathbf{u} = (u_{1x}, \ldots, u_{N_{\text{tot}}z})$ where N_{tot} is the total number of atoms in the system. The parametric Hamiltonian will be the Kohn-Sham Hamiltonian of electrons and the wavefunctions will be the Kohn-Sham eigenstates[9]. In periodic systems, the electronic wavefunctions can be written as $\psi_{\mathbf{k}i}(\mathbf{r}) = \langle \mathbf{r}|\psi_{\mathbf{k}i}\rangle$

[9]The Kohn-Sham formulation of density functional theory is discussed later on.

where $\mathbf{k}$ is the crystal momentum of electrons and i is the band index. These wavefunctions comply with the Bloch's theorem, namely $\psi_{\mathbf{k}i}(\mathbf{r}) = e^{i\mathbf{k}\cdot\mathbf{r}}u_{\mathbf{k}i}(\mathbf{r})$, where $u_{\mathbf{k}i}(\mathbf{r})$ is a lattice-periodic function such that $u_{\mathbf{k}i}(\mathbf{r}) = u_{\mathbf{k}i}(\mathbf{r}+\mathbf{R})$ with $\mathbf{R}$ vector of the Bravais lattice.

When defined using the Bloch's wavefunctions, the Berry connection and curvature also carry a $\mathbf{k}$-vector and band subscripts. According to Eqs. 2.6 and 2.9, they can be written as

$$\boldsymbol{\mathcal{X}}_{\mathbf{k}i}(\mathbf{u}) = i\langle\psi_{\mathbf{k}i}|\boldsymbol{\nabla}_{\mathbf{u}}\psi_{\mathbf{k}i}\rangle \tag{2.30}$$

$$\Omega_{\mu\nu,\mathbf{k}i}(\mathbf{u}) = \frac{\partial\mathcal{X}_{\nu,\mathbf{k}i}}{\partial u_\mu} - \frac{\partial\mathcal{X}_{\mu,\mathbf{k}i}}{\partial u_\nu} = -2\mathrm{Im}\left\langle\frac{\partial\psi_{\mathbf{k}i}}{\partial u_\mu}\middle|\frac{\partial\psi_{\mathbf{k}i}}{\partial u_\nu}\right\rangle. \tag{2.31}$$

Analogous relations can be established in terms of the periodic part of the wavefunction $u_{\mathbf{k}i}(\mathbf{r})$. We do not need to explicitly define the Berry phase in the crystal lattice formalism. In density functional perturbation theory, the derivative of the Kohn-Sham wavefunction with respect to the phonon ionic displacement $\mathbf{u}$ can be written in the parallel transport gauge as

$$\left|\frac{\partial\psi_{\mathbf{k}i}}{\partial u_\nu}\right\rangle = \sum_{\mathbf{k}'j}|\psi_{\mathbf{k}'j}\rangle\frac{\langle\psi_{\mathbf{k}'j}|\frac{\partial H_{\mathrm{KS}}}{\partial u_\nu}|\psi_{\mathbf{k}i}\rangle}{\epsilon_{\mathbf{k}i}-\epsilon_{\mathbf{k}'j}} \tag{2.32}$$

where H_{KS} is the Kohn-Sham Hamiltonian of electrons, $\partial H_{\mathrm{KS}}/\partial u_\nu$ is the deformation potential and $\epsilon_{\mathbf{k}i}$ are the Kohn-Sham eigenvalues. Replacing Eq. 2.32 into the definition of the Berry curvature Eq. 2.31, it can be shown that

$$\Omega^{\mathrm{KS}}_{\mu\nu,\mathbf{k}i}(\mathbf{u}) = -2\mathrm{Im}\sum_{\mathbf{k}'j}\frac{\langle\psi_{\mathbf{k}i}|\frac{\partial H_{\mathrm{KS}}}{\partial u_\mu}|\psi_{\mathbf{k}'j}\rangle\langle\psi_{\mathbf{k}'j}|\frac{\partial H_{\mathrm{KS}}}{\partial u_\nu}|\psi_{\mathbf{k}i}\rangle}{(\epsilon_{\mathbf{k}i}-\epsilon_{\mathbf{k}'j})^2}. \tag{2.33}$$

This expression for the gauge invariant Berry curvature, defined in the space of the phonon ionic displacement, for the Kohn-Sham electronic wavefunctions and Hamiltonian, is the particular case of the most general Eq. 2.23. In the following chapters we will show that such quantity is related with non-adiabatic effects due to the electron-phonon coupling.

2.6 Summary

In this second chapter we defined the Berry phase and related quantities. As a proof of concept, the Aharonov-Bohm effect is discussed as an example of manifestation of the Berry phase. It is also shown that the Berry phase, in the adiabatic approximation, has the meaning of the phase of the wavefunction.

In the next chapter we apply the adiabatic approximation to crystals and illustrate how the Berry connection of the electrons affects the nuclear dynamics. By analogy with the phonon Hall effect we demonstrate that the synthetic gauge field can break time-reversal symmetry for phonons and induce nonzero angular momentum.

Chapter 3

Theoretical background

3.1 Born-Oppenheimer approximation

In molecules as well as in solids the theory of vibrational modes is usually based on the Born-Oppenheimer (BO) adiabatic approximation which allows to decouple the ionic and electronic degrees of freedom. The two-particles Hamiltonian of the system of N_{tot} nuclei and N electrons, neglecting the spin-orbit interaction, is given by

$$H = -\sum_I \frac{\hbar^2}{2M_I}\boldsymbol{\nabla}^2_{\mathbf{R}_I} - \frac{\hbar^2}{2m}\sum_i \boldsymbol{\nabla}^2_{\mathbf{r}_i} + \frac{1}{2}\sum_{i\neq j}\frac{e^2}{|\mathbf{r}_i - \mathbf{r}_j|} - \sum_{iI}\frac{Z_I e^2}{|\mathbf{r}_i - \mathbf{R}_I|} + \frac{1}{2}\sum_{I\neq J}\frac{Z_I Z_J e^2}{|\mathbf{R}_I - \mathbf{R}_J|} \tag{3.1}$$

where the first two terms are the kinetic energies of the nuclei and of the electrons and the other three terms represent the two-particle Coulomb interactions. $\mathbf{R}_I$, M_I and Z_I are respectively the position, the mass and the atomic number of the I-th nucleus while $\mathbf{r}_i$ is the position of the i-th electron and m is the mass. In the BO approximation, it is assumed that the nuclei are much slower than the electrons because of the larger mass and thus we can neglect the gradient of the electronic wave function with respect to the nuclear coordinates. In this approximation, the total wavefunction can be factorized as $\Psi(\{\mathbf{R}\}, \mathbf{r})\Xi(\mathbf{R})$ where $\Psi(\{\mathbf{R}\}, \mathbf{r}_1, \ldots, \mathbf{r}_N)$ is the many-body electron wave function which depends parametrically on the nuclear coordinates $\{\mathbf{R}\} = \mathbf{R}_1, \ldots, \mathbf{R}_{N_{\text{tot}}}$ and $\Xi(\mathbf{R}_1, \ldots, \mathbf{R}_{N_{\text{tot}}})$ is the wave function of the nuclei.
We now make use of the Dirac notation to evaluate the action of the nuclear kinetic energy operator on the product wavefunction $\Psi(\{\mathbf{R}\}, \mathbf{r})\Xi(\mathbf{R})$. The canonical nuclear momentum $\mathbf{P}_I \equiv -i\hbar\boldsymbol{\nabla}_{\mathbf{R}_I}$ yields

$$\boldsymbol{P}_I|\Psi(\boldsymbol{R})\rangle\Xi(\boldsymbol{R}) = -i\hbar|\Psi(\boldsymbol{R})\rangle\boldsymbol{\nabla}_{\boldsymbol{R}_I}\Xi(\boldsymbol{R}) - i\hbar|\boldsymbol{\nabla}_{\boldsymbol{R}_I}\Psi(\boldsymbol{R})\rangle\Xi(\boldsymbol{R}). \tag{3.2}$$

Then we multiply on the left for the electronic wave function and integrate out. The resulting effective momentum acting on the ionic wave function therefore reads

$$\langle\Psi|\boldsymbol{P}_I|\Psi\rangle = [-i\hbar\boldsymbol{\nabla}_{\boldsymbol{R}_I} - i\hbar\langle\Psi|\boldsymbol{\nabla}_{\boldsymbol{R}_I}\Psi\rangle] \tag{3.3}$$

where we dropped the explicit dependence of $|\Psi\rangle$ on $\mathbf{R}$ for the sake of readability. In a similar way one may compute the averaged square momentum which yields

$$\langle\Psi|\boldsymbol{P}_I^2|\Psi\rangle = -\hbar^2\left[\boldsymbol{\nabla}^2_{\boldsymbol{R}_I} + 2\langle\Psi|\boldsymbol{\nabla}_{\boldsymbol{R}_I}\Psi\rangle\cdot\boldsymbol{\nabla}_{\boldsymbol{R}_I} + \langle\Psi|\boldsymbol{\nabla}^2_{\boldsymbol{R}_I}\Psi\rangle\right]. \tag{3.4}$$

Note that all these operators act on the nuclear wavefunction $\Xi(\boldsymbol{R})$. Let us also compute the variance of the momentum as it will be useful for later purpose:

$$\langle \boldsymbol{P}_I^2 \rangle - \langle \boldsymbol{P}_I \rangle^2 = \hbar^2 \left[\langle \boldsymbol{\nabla}_{\boldsymbol{R}_I} \Psi | \boldsymbol{\nabla}_{\boldsymbol{R}_I} \Psi \rangle - |\langle \Psi | \boldsymbol{\nabla}_{\boldsymbol{R}_I} \Psi \rangle|^2 \right]. \tag{3.5}$$

We are now ready to separate the problem in two Schrödinger equations, one for the electrons and one for the nuclei, namely

$$H^{\mathrm{el}}[\{\mathbf{R}\}, \mathbf{r}]\Psi(\{\mathbf{R}\}, \mathbf{r}) = E(\{\mathbf{R}\})\Psi(\{\mathbf{R}\}, \mathbf{r}) \tag{3.6}$$

$$\Big(\sum_I \frac{\langle \mathbf{P}_I^2 \rangle}{2M_I} + E(\{\mathbf{R}\}) \Big) \Xi(\mathbf{R}) = \mathcal{E}\Xi(\mathbf{R}) \tag{3.7}$$

where the electronic Hamiltonian reads

$$H^{\mathrm{el}} = -\frac{\hbar^2}{2m} \sum_i \boldsymbol{\nabla}_{\mathbf{r}_i}^2 + \frac{1}{2} \sum_{i \neq j} \frac{e^2}{|\mathbf{r}_i - \mathbf{r}_j|} - \sum_{iI} \frac{Z_I e^2}{|\mathbf{r}_i - \mathbf{R}_I|} + \frac{1}{2} \sum_{I \neq J} \frac{Z_I Z_J e^2}{|\mathbf{R}_I - \mathbf{R}_J|}, \tag{3.8}$$

$E(\{\mathbf{R}\})$ is the BO energy surface, which represents the ground-state energy of the interacting electrons moving in the field of the fixed nuclei, and $\mathcal{E}$ is the eigenenergy of the nuclei. In the Hamiltonian of the nuclei in Eq. 3.7, the quantity $\langle P_I^2 \rangle$ is equal to the average over the electronic state vector $|\Psi\rangle$ of the squared nuclear momentum $\mathbf{P}_I$ that we already calculated in Eq. 3.4.

Let us now suppose that we already solved the clamped-nuclei electronic problem[10] and we know the energy surface $E(\{\mathbf{R}\})$ that serves as scalar potential for the nuclei. Then let us focus on the nuclear dynamics. The *effective* kinetic energy $\sum_I \langle P_I^2 \rangle / 2M_I$ resembles very much the kinetic energy of a particle with charge q and mass m in an external magnetic field $\mathbf{B} = \boldsymbol{\nabla} \times \mathbf{A}$, namely

$$T = -\frac{\hbar^2}{2m} \nabla^2 + \frac{iq\hbar}{m} \mathbf{A} \cdot \boldsymbol{\nabla} + \frac{q^2}{2m} A^2 \tag{3.9}$$

where the Coulomb gauge condition $\boldsymbol{\nabla} \cdot \mathbf{A} = 0$ has been enforced. Indeed, the second term in Eq. 3.4, divided by the mass, can be written as

$$+ \frac{i\hbar^2}{M_I} \boldsymbol{\mathcal{X}}_I(\boldsymbol{R}) \cdot \boldsymbol{\nabla}_{\mathbf{R}_I} \tag{3.10}$$

where the Berry connection $\boldsymbol{\mathcal{X}}_I(\boldsymbol{R}) = i\langle \Psi | \boldsymbol{\nabla}_{\mathbf{R}_I} \Psi \rangle$ plays the role of the magnetic vector potential $\mathbf{A}$. The contribution from Eq. 3.10 is generally omitted when the coupling between electronic states is neglected. In the following discussion, however, this contribution to the kinetic energy will be fundamental and thus we keep it.

As for the last term of Eq. 3.4 instead, the quantity $-\hbar^2 \langle \Psi | \nabla^2 \Psi \rangle / 2M$ cannot be directly expressed in terms of the geometric potential squared. Despite this, we can write the *effective* Hamiltonian of the nuclei in a similar fashion as for the particle in an external magnetic field, namely

$$\mathcal{H}^{nucl}[\mathbf{R}] = \sum_I \frac{1}{2M_I} \left(-i\hbar \boldsymbol{\nabla}_{\mathbf{R}_I} - \hbar \boldsymbol{\mathcal{X}}_I \right)^2 + E(\{\mathbf{R}\}). \tag{3.11}$$

[10] In the next chapter we deal with the electronic problem and give an overview of the most common method employed to handle it, namely density functional theory.

By doing so, we neglect the difference between the mean squared momentum and the square of the average momentum, the variance in Eq. 3.5.

The effective Hamiltonian of Eq. 3.11 governs the trajectory of the nuclei along the BO energy surface. The Berry connection in the kinetic energy accounts for a back-interaction (*screening*) from the other electrons which is usually not taken into consideration. The reason is that, in time-reversal symmetric systems, one usually can choose real-valued electronic wavefunctions for which the Berry connection vanishes and the Schrödinger equation of the nuclei becomes unaware of the electronic states (naive adiabatic approximation). When instead time-reversal symmetry is broken, the electronic wavefunctions are necessarily complex and the nuclear dynamics is affected by the Berry potential (see discussion after Eq. 2.9).

3.1.1 Equations of motion

It is instructive to derive the equations of motion for the coordinates and momenta from the Hamiltonian of Eq. 3.11. Let us firstly rewrite for clarity the Hamiltonian in the Cartesian basis

$$\mathcal{H}^{nucl} = \sum_{I\alpha} \frac{1}{2M_I} \left(P_{I\alpha} - \hbar\mathcal{X}_{I\alpha}\right)^2 + E(\{\mathbf{R}\}) \tag{3.12}$$

where $P_{I\alpha} \equiv -i\hbar\partial/\partial R_{I\alpha}$. In the Heisenberg representation, the time-derivatives of the coordinates and momenta are related to the commutator with the Hamiltonian, namely

$$\dot{R}_{I\alpha} = \frac{i}{\hbar}[\mathcal{H}, R_{I\alpha}] \tag{3.13}$$

$$\dot{P}_{I\alpha} = \frac{i}{\hbar}[\mathcal{H}, P_{I\alpha}] \tag{3.14}$$

Then, by using canonical commutation relations such as $[R_{I\alpha}, P_{J\beta}] = i\hbar\delta_{IJ}\delta_{\alpha\beta}$ and $[f(\{\mathbf{R}\}), P_{I\alpha}] = i\hbar\ \partial f(\{\mathbf{R}\})/\partial R_{I\alpha}$ we can write down the equations of the nuclear motion stemming from the Hamiltonian of Eq. 3.12:

$$\dot{R}_{I\alpha} = \frac{1}{M_I}(P_{I\alpha} - \hbar\mathcal{X}_{I\alpha}) \tag{3.15}$$

$$\dot{P}_{I\alpha} = \hbar\sum_{J\beta} \frac{\partial\mathcal{X}_{J\beta}}{\partial R_{I\alpha}} \frac{1}{M_J}(P_{J\beta} - \hbar\mathcal{X}_{J\beta}) - i\frac{\hbar^2}{2}\sum_{J\beta}\frac{1}{M_J}\frac{\partial^2\mathcal{X}_{J\beta}}{\partial R_{I\alpha}\partial R_{J\beta}} - \frac{\partial E}{\partial R_{I\alpha}} \tag{3.16}$$

Compared to the classical equations of motion, the ones that we just derived exhibit many additional terms related to the Berry connection and its spacial derivatives. Once again, when the electronic wavefunctions are real, all these terms vanish and the nuclear trajectory along the BO surface is governed by classical Newton's equations. The second derivative of the coordinates with respect to time can be expressed solely in terms of the coordinates themselves as

$$M_I\ddot{R}_{I\alpha} + \hbar\sum_{J\beta}\Omega_{I\alpha,J\beta}\dot{R}_{J\beta} + \frac{\partial E}{\partial R_{I\alpha}} = 0 \tag{3.17}$$

where, we recall, the Berry curvature is given by

$$\Omega_{I\alpha,J\beta} = \frac{\partial \mathcal{X}_{J\beta}}{\partial R_{I\alpha}} - \frac{\partial \mathcal{X}_{I\alpha}}{\partial R_{J\beta}}. \tag{3.18}$$

In writing Eq. 3.17, we neglected a term proportional to the gradient of the curvature, for it is of higher order (in the derivative of the wavefunction) than other negligible terms in the adiabatic approximation.

When it comes to study the vibrational modes of molecules or solids, the Berry-like term in Eq. 3.17 can be thought as an effective Lorentz force (acting on the nuclei) induced by the geometric gauge field of the electrons. Note that there is no external magnetic field in the problem under investigation but, we can say, there is a *synthetic* gauge field due to the parametric dependence on $\mathbf{R}$ of the electronic Hamiltonian Eq. 3.8.

3.2 Lattice dynamics in the harmonic approximation

Let us put aside for one moment the Berry connection in the Hamiltonian of the nuclei and revise the theory of lattice dynamics where the phonons are treated as classical oscillators. The equations presented so far are valid for both molecules and solids. In the following, we specialize the theory to solids only. The equations for molecules will be given in a separate section.

Let us consider a (Bravais lattice) crystal with $N_{\rm at}$ atoms per unit cell and N_c cells. The total number of atoms be $N_{\rm tot} = N_{\rm at}N_c$. The vibrational modes in a crystal lattice are usually described in terms of the displacement of the ions (nuclei + valence electrons) with respect to the equilibrium sites. The position of each ion will therefore be equal to $\mathbf{R}_I \equiv \mathbf{R}_{Ls} = \mathbf{R}^0_{Ls} + \mathbf{u}_{Ls} = \mathbf{R}_L + \boldsymbol{\tau}_s + \mathbf{u}_{Ls}$ where $\mathbf{R}_L$ localizes the L-th unit cell, $\boldsymbol{\tau}_s$ identifies the equilibrium position of the s-th ion in the unit cell and $\mathbf{u}_{Ls}$ is the ionic displacement from the equilibrium position $\mathbf{R}^0_{Ls} \equiv \mathbf{R}_L + \boldsymbol{\tau}_s$. The index $I = \{Ls\}$ runs from 1 to $N_{\rm tot}$ while the indexes L and s run from 1 to $N_{\rm c}$ and from 1 to $N_{\rm at}$, respectively. The equilibrium positions of the ions are determined by nullifying the forces

$$F_{I\alpha} = -\frac{\partial E}{\partial R_{I\alpha}}\Big|_{\mathbf{u}=0}. \tag{3.19}$$

In the BO approximation, the total energy of the electronic system is a parametric function of the ionic coordinates. If the deviation of the ionic positions from the equilibrium is small, we can expand the total energy as a power series of the displacement $\mathbf{u}_I$. The harmonic approximation consists in truncating such series at the second order, namely

$$E(\{\mathbf{R}\}) = E(\{\mathbf{R}^0\}) + \frac{1}{2}\sum_{I\alpha,J\beta} u_{I\alpha} C_{I\alpha,J\beta}(\mathbf{R}) u_{J\beta} \tag{3.20}$$

where the first derivative has been omitted as it vanishes at equilibrium and the second derivative of the total energy has been used to define the interatomic force constant matrix

$$C_{I\alpha,J\beta}(\mathbf{R}) = C_{s\alpha,r\beta}(\mathbf{R}_L - \mathbf{R}_M) = \frac{\partial^2 E}{\partial u_{Ls\alpha}\partial u_{Mr\beta}}. \tag{3.21}$$

We stress out that $C_{I\alpha J\beta}$ is symmetric under exchange of the indexes and it is a function of the difference $\mathbf{R}_L - \mathbf{R}_M$ only, as consequence of the translational invariance of the crystal. The Fourier transform of the interatomic force constant matrix is given by

$$C_{s\alpha,r\beta}(\mathbf{q}) = \sum_L e^{-i\mathbf{q}\cdot\mathbf{R}_L} C_{s\alpha,r\beta}(\mathbf{R}_L) = \frac{1}{N_c} \frac{\partial^2 E}{\partial u^*_{\mathbf{q}s\alpha} \partial u_{\mathbf{q}r\beta}} \tag{3.22}$$

where, exploiting translational invariance, we have chosen $\mathbf{R}_M = 0$ and, in the right side of the equation, N_c is the number of unit cells in the crystal and $u_{\mathbf{q}s\alpha}$ is the Fourier transformed ionic displacement. The dynamical matrix is equal to the Fourier transformed force constant matrix divided by the square root of the masses

$$D_{s\alpha,r\beta}(\mathbf{q}) = \frac{1}{\sqrt{M_s M_r}} C_{s\alpha,r\beta}(\mathbf{q}). \tag{3.23}$$

M_s and M_r do not carry the cell index as the atoms have the same mass in every cell. The $3N_{\text{tot}}$ Newton's laws of motion read

$$M_s \ddot{u}_{Ls\alpha} = -\sum_{Mr\beta} C_{s\alpha,r\beta}(\mathbf{R}_L - \mathbf{R}_M) u_{Mr\beta}. \tag{3.24}$$

We seek for solution in the form

$$u_{Ls\alpha}(t) = \frac{1}{\sqrt{M_s}} \text{Re}\left[\varepsilon_{s\alpha}(\mathbf{q}) e^{i\mathbf{q}\cdot\mathbf{R}_L} e^{-i\omega_{\mathbf{q}}t}\right] \tag{3.25}$$

where $\varepsilon_{s\alpha}(\mathbf{q})$ and $\omega_{\mathbf{q}}$ are respectively the polarization vector and the frequency of the phonon with wavevector $\mathbf{q}$. The resulting equation delineates an eigenvalue problem for the dynamical matrix $D_{s\alpha,r\beta}(\mathbf{q})$, the solutions of which are labeled with a phonon mode index ν running from 1 to $3N_{\text{at}}$, namely

$$\sum_{r\beta} D_{s\alpha,r\beta}(\mathbf{q}) \varepsilon_{\nu r\beta}(\mathbf{q}) = \omega^2_{\mathbf{q}\nu} \varepsilon_{\nu s\alpha}(\mathbf{q}). \tag{3.26}$$

Following from the symmetry properties of the interatomic force constant matrix, the dynamical matrix is hermitian and such that $D(\mathbf{q}) = D(-\mathbf{q})$. Moreover, the phonon frequencies and eigenvectors fulfill the conditions $\omega_{\mathbf{q}} = \omega_{-\mathbf{q}}$ and $\varepsilon^*_{\nu s\alpha}(\mathbf{q}) = \varepsilon_{\nu s\alpha}(-\mathbf{q})$. The phonon polarization vectors also satisfy the orthogonality and the completeness relations:

$$\sum_{s\alpha} \varepsilon^*_{\nu s\alpha}(\mathbf{q}) \varepsilon_{\nu' s\alpha}(\mathbf{q}) = \delta_{\nu\nu'} \tag{3.27}$$

$$\sum_{\nu} \varepsilon_{\nu s\alpha}(\mathbf{q}) \varepsilon^*_{\nu r\beta}(\mathbf{q}) = \delta_{\alpha\beta}\delta_{sr}. \tag{3.28}$$

It is worth mentioning that phonon polarization vectors can be trivially complex, namely real vectors multiplied by a global phase, or nontrivially complex as in the case of polyatomic crystals at $\mathbf{q} \neq 0$. In the latter case, the ions perform elliptical trajectories around their equilibrium positions. Consequently, each ion gives rise to an orbital angular momentum perpendicular to the plane of the orbit. For each mode ν

and wavevector $\mathbf{q}$, the angular momentum of the lattice vibration is equal to the sum of the angular momenta of the rotating ions.

Note that all along this section, we treated phonons classically and we did not include any Berry phase effect in the derivation. We wonder now how the Berry connection in the Hamiltonian of the nuclei Eq. (3.12), stemming from the quantum derivation of the BO approximation, affects the lattice dynamics and, particularly, how the phonon eigenvalue problem Eq. (3.26) is modified. The angular momentum of phonons will be the object of the last section in this chapter.

3.2.1 How to deal with molecules

Molecules can be seen as crystals with one unit cell. The total number of ions is $N_{\text{tot}} = N_{\text{at}}$. The ionic index I coincides with the ionic index s in the unit cell. All the quantities that depends on the cell indexes in solids, are equal to themselves in reciprocal space for molecules. Therefore, all the equations of solids in reciprocal space are also valid for molecules provided that the wavevector $\mathbf{q}$ is set equal to zero. In particular, the eigenvalue equation of the dynamical matrix reads

$$\sum_{J\beta} D_{I\alpha,J\beta}\varepsilon_{\nu J\beta} = \omega_\nu^2 \varepsilon_{\nu I\alpha} \tag{3.29}$$

where D is real and ε is real up to a global phase. Vibrations of polyatomic molecules are described in terms of normal modes. Nonlinear molecules have 3 modes of translation (acoustic), 3 modes of rotation and $3N_{\text{tot}}-6$ optical modes. A molecular vibration is excited when the molecule absorbs an amount of energy corresponding to the vibrational frequency. The vibrational states of a molecule are typically probed via Infrared and Raman spectroscopy as vibrational frequencies typically range from less than 10^{13} Hz to approximately 10^{14} Hz. The non-adiabatic interaction (beyond the naive BO approximation) between electronic and nuclear vibrational motion in molecules is called vibronic coupling. It cannot be neglected when two adiabatic potential energy surfaces are close to each other as in presence of avoided crossings and conical intersections.

3.2.2 Harmonic lattice dynamics in the presence of the Berry connection

For ease of notation, the Cartesian indexes α and β will be omitted throughout this section. The Hamiltonian of the nuclei Eq. (3.12), when dealing with vibrational modes, can be expressed in the harmonic approximation as a quadratic function of the phonon ionic displacements $\mathbf{u}_I$ and its conjugate momenta $\mathbf{p}_I \equiv -i\hbar\boldsymbol{\nabla}_{\mathbf{u}_I}$ as

$$H = \sum_I \frac{1}{2M_I}\left(p_I - \hbar\mathcal{X}_I\right)^2 + \frac{1}{2}\sum_{IJ} u_I C_{IJ} u_J. \tag{3.30}$$

In the above equation, the *interionic* force constant matrix C_{IJ} is defined by Eq. 3.21 as the second derivative of the BO electronic energy with respect to the ionic displacement and the Berry connection $\mathcal{X}_I(\mathbf{u}) = i\langle\Psi(\mathbf{u})|\nabla_{u_I}\Psi(\mathbf{u})\rangle$ must be linear in the ionic displacement $\mathbf{u}$ since we only retain quadratic terms in the harmonic approximation.

In analogy with the electromagnetism, the Berry connection can be expressed in a proper gauge as (see appendix B)

$$\mathcal{X}_I = -\frac{1}{2}\sum_J \Omega_{IJ} u_J \tag{3.31}$$

where now the Berry curvature is constant and given by

$$\Omega_{IJ} = \frac{\partial \mathcal{X}_J}{\partial u_I} - \frac{\partial \mathcal{X}_I}{\partial u_J}. \tag{3.32}$$

The equation of motion (3.17) is then replaced by Eq. 3.24 with an additional velocity term proportional to the Berry curvature itself:

$$M_I \ddot{u}_I + \hbar \sum_J \Omega_{IJ} \dot{u}_J + \sum_J C_{IJ} u_J = 0. \tag{3.33}$$

We use the solution of Eq. 3.25 to obtain the phonon eigenvalue problem

$$\sum_r \frac{1}{\sqrt{M_s M_r}} \left[C_{sr}(\mathbf{q}) - i\hbar\omega_{\mathbf{q}} \Omega_{sr}(\mathbf{q}) \right] \varepsilon_r(\mathbf{q}) = \omega_{\mathbf{q}}^2 \varepsilon_s(\mathbf{q}) \tag{3.34}$$

where $\Omega_{sr}(\mathbf{q})$ is the Fourier component of the Berry curvature Ω_{IJ}. The phonon eigenvalue problem Eq. 3.34 has been obtained by retaining the Berry connection in the kinetic energy of the ionic Hamiltonian. It differs from Eq. 3.26 for a term in the dynamical matrix that is linear with the frequency and proportional to the Berry curvature in reciprocal space. Indeed, Eq. 3.34 is not a standard eigenvalue problem and needs to be solved carefully. First of all, we replace Eq. 3.31 into the equations of motion and we arrange it in the following way

$$\sqrt{M_I}\dot{u}_I = \sum_J \Sigma_{IJ} \sqrt{M_J} u_J + \frac{p_I}{\sqrt{M_I}} \tag{3.35}$$

$$\frac{\dot{p}_I}{\sqrt{M_I}} = -\sum_J D_{IJ} \sqrt{M_J} u_J + \sum_J \Sigma_{IJ} \frac{p_J}{\sqrt{M_J}} \tag{3.36}$$

where we defined a new antisymmetric matrix $\Sigma_{IJ} \equiv \frac{\hbar}{2}\Omega_{IJ}/\sqrt{M_I M_J}$, which is proportional to the Berry curvature divided by the square root of the masses, and also we defined $D_{IJ} \equiv C_{IJ}/\sqrt{M_I M_J} - \sum_K \Sigma_{IK}\Sigma_{KJ}$. Following Ref. [45] and the supplementary material of Refs. [4, 43], we then consider solutions in the form

$$u_I(t) = \varepsilon_s/\sqrt{M_s}\; e^{i\mathbf{q}\cdot\mathbf{R}_L} e^{-i\omega_{\mathbf{q}} t} \tag{3.37}$$

$$p_I(t) = \mu_s \sqrt{M_s}\; e^{i\mathbf{q}\cdot\mathbf{R}_L} e^{-i\omega_{\mathbf{q}} t} \tag{3.38}$$

where the polarization vectors ε_s and μ_s are related to the coordinates and the momenta, respectively. The equations of motion can therefore be written in a compact form as

$$-i\omega_{\mathbf{q}} \begin{pmatrix} \varepsilon_s \\ \mu_s \end{pmatrix} = \sum_r \begin{pmatrix} \Sigma_{sr} & \mathbb{I}_{sr} \\ -D_{sr} & \Sigma_{sr} \end{pmatrix} \begin{pmatrix} \varepsilon_r \\ \mu_r \end{pmatrix} \tag{3.39}$$

where Σ_{sr} is the Fourier transform of Σ_{IJ}, D_{sr} is the dynamical matrix and $\mathbb{I}_{sr}$ is the identity matrix. The momentum component is related to the coordinate one via $\mu_s = -i\omega_{\mathbf{q}}\varepsilon_s - \sum_r \Sigma_{sr}\varepsilon_r$. In addition, Eq. 3.39 can be seen as the Schrödinger equation of the effective non-hermitian Hamiltonian $\mathcal{H}_{sr} = i\begin{pmatrix} \Sigma_{sr} & \mathbb{I}_{sr} \\ -D_{sr} & \Sigma_{sr} \end{pmatrix}$ with eigenvectors $\xi_s = (\varepsilon_s, \mu_s)^T$ and eigenvalues $\omega_{\mathbf{q}}$, namely $\sum_r \mathcal{H}_{sr}\xi_r = \omega_{\mathbf{q}}\xi_s$. However, since the Hamiltonian is not a self-adjoint operator, we must consider also the eigenvalue equation of the hermitian conjugate operator, namely $\sum_r \zeta_r^T \mathcal{H}_{rs} = \omega_{\mathbf{q}}\zeta_s^T$, where $\zeta_s^T = (\mu_s^\dagger, -\varepsilon_s^\dagger)/(2i\omega_{\mathbf{q}})$ are the left eigenvectors of $\mathcal{H}$. The normalization has been chosen in such a way that the second quantization of the Hamiltonian is satisfied. The eigenvalue equations of the effective Hamiltonian are therefore given by

$$\sum_r \mathcal{H}_{sr}(\mathbf{q})\xi_{\nu r}(\mathbf{q}) = \omega_{\mathbf{q}\nu}\xi_{\nu s}(\mathbf{q}) \tag{3.40}$$

$$\sum_r \zeta_{\nu r}^T(\mathbf{q})\mathcal{H}_{rs}(\mathbf{q}) = \omega_{\mathbf{q}\nu}\zeta_{\nu s}^T(\mathbf{q}) \tag{3.41}$$

where the index ν labels the $3N_{\text{at}}$ solutions, $\omega_{\mathbf{q}\nu}$ are the eigenvalues, $\xi_{\nu s}(\mathbf{q})$ are the right eigenvectors and $\zeta_{\nu s}^T(\mathbf{q})$ are the left eigenvectors. The right and left eigenvectors obey the orthonormality condition $\sum_s \zeta_{\nu s}^T \xi_{\nu' s} = \delta_{\nu\nu'}$ and the completeness relation $\sum_\nu \xi_{\nu s} \otimes \zeta_{\nu r}^T = \mathbb{I}_{sr}$. The former can also be expressed solely in terms of the coordinate components as $\varepsilon^\dagger\varepsilon + \frac{i}{\omega_{\mathbf{q}}}\varepsilon^\dagger\Sigma\varepsilon = 1$. Since the Hamiltonian $\mathcal{H}$ is not hermitian, the complete set of solutions includes negative phonon branches. For the purposes of this thesis, we retain only positive phonon branches[11] ($\omega > 0$) and define the phonon *annihilation* and *creation* operator as $a_{\mathbf{q}\nu}$ and $a_{\mathbf{q}\nu}^\dagger$. Then the commutation relation $[a_{\mathbf{q}\nu}, a_{\mathbf{q}'\nu'}^\dagger] = \delta_{\mathbf{q}\mathbf{q}'}\delta_{\nu\nu'}$ holds. The time evolution of the annihilation and creation operators is respectively given by $a_{\mathbf{q}\nu}(t) = a_{\mathbf{q}\nu}e^{-i\omega_{\mathbf{q}\nu}t}$ and $a_{\mathbf{q}\nu}^\dagger(t) = a_{\mathbf{q}\nu}^\dagger e^{i\omega_{\mathbf{q}\nu}t}$. We therefore write the second quantization relations in the form

$$u_{Ls} = \sqrt{\frac{\hbar}{2N}} \sum_{\mathbf{q}\nu} \varepsilon_{\nu s}(\mathbf{q}) \frac{1}{\sqrt{M_s\omega_{\mathbf{q}\nu}}} \left(a_{\mathbf{q}\nu} + a_{-\mathbf{q}\nu}^\dagger\right) e^{i\mathbf{q}\cdot\mathbf{R}_L}, \tag{3.42}$$

$$p_{Ls} = \sqrt{\frac{\hbar}{2N}} \sum_{\mathbf{q}\nu} \mu_{\nu s}(\mathbf{q}) \sqrt{M_s\omega_{\mathbf{q}\nu}} \left(a_{\mathbf{q}\nu} - a_{-\mathbf{q}\nu}^\dagger\right) e^{i\mathbf{q}\cdot\mathbf{R}_L}. \tag{3.43}$$

The canonical commutation relations are satisfied $[u_{Ls}, p_{Mr}] = i\hbar\delta_{LM}\delta_{sr}$ and the Hamiltonian Eq. 3.30 in the harmonic approximation reads

$$H = \frac{1}{2}\sum_{\mathbf{q}\nu} \hbar\omega_{\mathbf{q}\nu}(a_{\mathbf{q}\nu}^\dagger a_{\mathbf{q}\nu} + \frac{1}{2}). \tag{3.44}$$

To summarize, in this section we have seen how the Berry phase in the Hamiltonian of the ions affect the lattice dynamics in the harmonic approximation. We found that the equations of motion of the ions Eq. 3.33 exhibit an additional viscous friction term proportional to the Berry curvature of the ionic displacements. Then we replaced

[11] Another approach is possible in which the negative branches are included (see Ref. [55]).

the standard solutions of the classical theory of lattice dynamics but we obtained a nonlinear eigenvalue problem for the dynamical matrix Eq. 3.34. To solve this problem we separated the polarization vectors of the coordinates and momenta and diagonalized the non-hermitian Hamiltonian $\mathcal{H}$ in order to write the solutions under the form of right and left orthonormal eigenvectors. We used second quantization relations to write the Hamiltonian in the familiar form, Eq. 3.44. The same procedure applies to solve the equations of motions for an ionic crystal into an external magnetic field, as shown in Ref. [4]. The electronic Berry curvature indeed behaves in the lattice dynamics as an effective magnetic field. Interestingly, it is found that, when the interaction term in the Hamiltonian is nonzero, the phonons host a finite angular momentum. In the next section therefore we want to take a closer look to this analogy. Our aim is to demonstrate that also the Berry connection can give rise to nonzero angular momentum in the phonon modes.

3.3 Phonon angular momentum

The Raman spin-phonon interaction plays a role in the appearance of the angular momentum of phonons in the presence of an external magnetic field [4]. In a crystal lattice the total angular momentum is equal to $\mathbf{J} = \mathbf{L} + \mathbf{S} + \mathbf{N}$ where $\mathbf{L}$ and $\mathbf{S}$ are the orbital and spin angular momentum of the electrons, respectively, and $\mathbf{N} = \sum_I \mathbf{R}_I \times \mathbf{P}_I$ is the orbital angular momentum of the nuclei. The spin of the nuclei is usually neglected because it is much smaller than the spin of the electrons. When considering a phonon ionic displacement from the equilibrium positions, the angular momentum becomes

$$\mathbf{N} = \sum_I (\mathbf{R}_I^0 + \mathbf{u}_I) \times (\mathbf{P}_I + \mathbf{p}_I) = \mathbf{N}^{\text{lat}} + \mathbf{N}^{\text{ph}} \tag{3.45}$$

where $N^{\text{lat}} = \sum_I \mathbf{R}_I^0 \times \mathbf{P}_I$ is the angular momentum of the lattice which reflects a rigid-body rotation of the system and $\mathbf{N}^{\text{ph}} = \sum_I \mathbf{u}_I \times \mathbf{p}_I$ is the angular momentum of phonons. The cross terms vanish at equilibrium. Within the classical theory of lattice dynamics, the phonon angular momentum can be defined as

$$\mathbf{N}^{ph} = \sum_{Ls} M_s \mathbf{u}_{Ls} \times \dot{\mathbf{u}}_{Ls} \tag{3.46}$$

where $\mathbf{u}_{Ls}$ is a displacement vector of the s-th atom in the L-th unit cell, and M_s is the mass of the atom. The z component of the phonon angular momentum can be expressed in terms of the x and y components of the phonon ionic displacements as $N_z^{ph} = \sum_{Ls} M_s(u_{Ls}^x \dot{u}_{ls}^y - u_{Ls}^y \dot{u}_{Ls}^x)$. By taking into account only positive eigenmodes, we use the second quantization relation Eq. 3.42 to express the z component of the total phonon angular momentum as[12]

$$N_z^{ph} = \frac{1}{2} \sum_{kk'} \ell_{kk',z} \left(\sqrt{\frac{\omega_k}{\omega_{k'}}} + \sqrt{\frac{\omega_{k'}}{\omega_k}} \right) \delta_{\mathbf{q},\mathbf{q}'} a_{k'}^\dagger a_k e^{i(\omega_{k'} - \omega_k)t} + \frac{1}{2} \sum_k \ell_{kk,z} \tag{3.47}$$

[12] A demonstration is available in the supplementary material of Ref. [4] and in appendix C of this thesis.

where $k = (\mathbf{q}, \nu)$ and $\ell_{kk',z} = \hbar \sum_s i(\varepsilon_{ksx}\varepsilon^*_{k'sy} - \varepsilon_{ksy}\varepsilon^*_{k'sx})$. At the equilibrium, the expectation value of the angular momentum reads

$$\langle N_z^{ph} \rangle = \sum_{\mathbf{q}\nu} \ell_{\mathbf{q}\nu,z} \left[b(\omega_{\mathbf{q}\nu}) + \frac{1}{2} \right] \tag{3.48}$$

where $b(\omega_{\mathbf{q}\nu}) = 1/(e^{\hbar\omega_{\mathbf{q}\nu}/K_BT} - 1)$ is the Bose-Einstein occupation function. We use the relation $\langle a^\dagger_{\mathbf{q}\nu'} a_{\mathbf{q}\nu} \rangle = b(\omega_{\mathbf{q}\nu})\delta_{\nu\nu'}$. At zero temperature, the total phonon angular momentum reads $\langle N_z^{\rm ph} \rangle (T = 0) = \frac{1}{2} \sum_{\mathbf{q}\nu} \ell_{\mathbf{q}\nu,z}$ which means that each mode has a zero-point angular momentum $\frac{1}{2}\ell_{\mathbf{q}\nu,z}$ in addition to a zero-point energy $\frac{1}{2}\hbar\omega_{\mathbf{q}\nu}$. In the high temperature limit, the phonon angular momentum is proportional to $1/T$ and vanishes (see Ref [4]):

$$\langle N_z^{ph} \rangle (T \to \infty) = \sum_{\mathbf{q}\nu} \ell_{\mathbf{q}\nu,z} \frac{\hbar\omega_{\mathbf{q}\nu}}{12 K_B T} \to 0. \tag{3.49}$$

At high temperatures, the classical statistical mechanics applies and the summation over quantum states is replaced by a phase space integral on the displacements and momenta. Then we can recast, through a change of variables, the kinetic energy in the usual form $p^2/2M$, removing the effect of the Berry connection. For such pure harmonic system the angular momentum is zero. It follows that the phonon angular momentum is meaningful only in low-temperature quantum systems. The angular momentum $\boldsymbol{\ell}_{\mathbf{q}\nu}$ of the phonon mode ν with wavevector $\mathbf{q}$ can also be expressed as a cross product between phonon polarization vectors as [22]

$$\boldsymbol{\ell}_{\mathbf{q}\nu} = -i\hbar \sum_s \boldsymbol{\varepsilon}^*_{\nu s}(\mathbf{q}) \times \boldsymbol{\varepsilon}_{\nu s}(\mathbf{q}) \tag{3.50}$$

where $\boldsymbol{\varepsilon}_{\nu s}(\mathbf{q})$ is the eigenvector of the dynamical matrix. When the polarization vectors are real, up to a global phase, the angular momentum vanishes, as the cross product in Eq. 3.50 is zero. Recalling Eq. 3.26, we therefore infer that the angular momentum $\boldsymbol{\ell}_{\mathbf{q}\nu}$ is zero when the dynamical matrix is real, namely in molecules and monoatomic crystals. Moreover, even when the dynamical matrix is complex, whenever the relation $\boldsymbol{\varepsilon}^*_{\nu s}(\mathbf{q}) = \boldsymbol{\varepsilon}_{\nu s}(-\mathbf{q})$ is valid, the angular momentum at $-\mathbf{q}$ will be equal to minus the angular momentum at $\mathbf{q}$, namely $\boldsymbol{\ell}_{-\mathbf{q}\nu} = -\boldsymbol{\ell}_{\mathbf{q}\nu}$, which implies, together with the relation $\omega_{\mathbf{q}\nu} = \omega_{-\mathbf{q}\nu}$, that the expectation value of the total angular momentum $\langle \mathbf{N}^{\rm ph} \rangle$ vanishes because the summation runs over both positive and negative wavevectors. In order to have nonzero total angular momentum of phonons, we thus need that $\boldsymbol{\varepsilon}^*_{\nu s}(\mathbf{q}) \neq \boldsymbol{\varepsilon}_{\nu s}(-\mathbf{q})$ or that $\omega_{\mathbf{q}\nu} \neq \omega_{-\mathbf{q}\nu}$. *This happens when the time-reversal symmetry is broken for phonons.*

3.3.1 Discussion and summary

In section 1.1, we have seen that the (Raman) spin-phonon interaction can be seen as a spin-orbit coupling for the ions. Since the external magnetic field takes action on the spin of the ions, the spin-phonon interaction breaks time-reversal (TR) symmetry for phonons. Namely, it transmits the information (about TR symmetry breaking) to the orbital sector of the ions, where phonons originate. It should be pointed out however

that the Raman spin-phonon interaction alone $\mathcal{H}_R \propto \sum_I \mathbf{s}_I \cdot (\mathbf{u}_I \times \mathbf{p}_I)$ is TR symmetric because $\mathbf{s}$ and $\mathbf{p}$ are odd under TR while $\mathbf{u}$ is even (see appendix A). It is therefore needed an external magnetic field to break TR symmetry.

In the harmonic lattice dynamics instead, when the Berry connection term is retained in the BO approximation, the phonon Hamiltonian Eq. 3.30 is not invariant under TR because the kinetic energy contains linear terms in the momentum $\mathbf{p}$, which is odd under TR. This reflects in the phonon eigenvalue problem Eq. 3.24 with a linear term in the frequency ω that is proportional to the Berry curvature $\mathbf{\Omega}$. In fact, even if there is no external magnetic field, we have a *synthetic* gauge field in the ionic dynamics representing the screening of electrons.

Differently from the spin-phonon interaction, moreover, the Berry connection $\boldsymbol{\mathcal{X}}$ in the Hamiltonian Eq. 3.30 *spontaneously* arises from the BO approximation as the only one track left of the electrons wavefunctions after integrating out the electronic problem. It is therefore the back-interaction of the electrons, as an external potential for the nuclei in the BO approximation, that breaks time-reversal symmetry for phonons irrespective of whether the electronic Hamiltonian is TR invariant [65]. As a consequence, the phonons are allowed to host a finite angular momentum. In this illustration, there is no need of external time-reversal symmetry breaking probes to get a finite phonon angular momentum. We just need a nonzero curvature from the electrons. We will therefore refer to it as an *intrinsic phonon angular momentum* to distinguish it from the phonon angular momentum "induced" by external probes.

Chapter 4

The electronic problem and linear response theory

We address now the problem of electrons moving in the field of the fixed nuclei and treat the displacement of the nuclei from the equilibrium position as a perturbation to the electronic wavefunction. Even when decoupled from the nuclear problem, the electronic problem is a many-body problem whose complexity grows exponentially with the number of particles. Many computational methods have then been developed to study such a problem. Among the most successful approach there is density functional theory. In this chapter we describe the Kohn-Sham (KS) formulation of density functional theory with and without spin and we present the theory of linear response with particular interest in the vibrational modes of molecules and crystals. We also discuss the effect of spin-orbit interaction and introduce the computational method that we use to evaluate the non-adiabatic dynamical matrix.

4.1 Density Functional Theory

Many physical properties of a system of interacting electrons are uniquely determined by its ground-state charge density distribution. The electronic problem is usually treated within the Kohn-Sham formulation of the density functional theory [66] which maps the interacting many-body problem onto a non-interacting single-particle one that has the same ground state density as the real one. The Kohn-Sham single-particle Hamiltonian reads

$$H_{\mathrm{KS}} = \frac{p^2}{2m} + V_{\mathrm{ext}}(\mathbf{r}) + V_{\mathrm{H}}^{[n]}(\mathbf{r}) + V_{\mathrm{xc}}^{[n]}(\mathbf{r}) \tag{4.1}$$

where $p^2/2m$ is the kinetic energy, $V_{\mathrm{ext}}(\boldsymbol{r})$ is the external potential due to the Coulomb interaction with the nuclei, namely

$$V_{\mathrm{ext}}(\boldsymbol{r}) = -\sum_I \frac{Z_I e^2}{|\mathbf{r} - \mathbf{R}_I|} + \frac{1}{2}\sum_{I \neq J} \frac{Z_I Z_J e^2}{|\mathbf{R}_I - \mathbf{R}_J|}, \tag{4.2}$$

$V_{\rm H}^{[n]}(\mathbf{r})$ and $V_{\rm xc}^{[n]}(\mathbf{r})$ are the Hartree and exchange-correlation potentials, that are functionals of the electronic density $n(\mathbf{r})$ and can be written as

$$V_{\rm H}^{[n]}(\mathbf{r}) = e^2 \int \frac{n(\mathbf{r}')}{|\mathbf{r}-\mathbf{r}'|} d\mathbf{r}' \tag{4.3}$$

$$V_{\rm xc}^{[n]}(\mathbf{r}) = \frac{\delta E_{\rm xc}[n]}{\delta n(\mathbf{r})}. \tag{4.4}$$

Here, $E_{\rm xc}[n]$ is the exchange-correlation energy functional and $\delta/\delta n$ is the functional derivative with respect to the electronic density $n(\mathbf{r})$. This last can be expressed in terms of the single-particle KS wavefunction $|\psi_i\rangle$ as

$$n(\mathbf{r}) = \sum_i f_i \langle\psi_i|\mathbf{r}\rangle\langle\mathbf{r}|\psi_i\rangle = \sum_i f_i \psi_i^*(\mathbf{r})\psi_i(\mathbf{r}) \tag{4.5}$$

where f_i is the occupation number (varying between 0 and 1 for empty and occupied states respectively). The single-particle KS equation reads

$$H_{\rm KS}|\psi_i\rangle = \epsilon_i|\psi_i\rangle \tag{4.6}$$

where $H_{\rm KS}$ is given by Eq. 4.1 and ϵ_i are the KS single-particle energies. The above set of equations forms a closed loop as the density is a function of the KS orbitals, the KS potential is a functional of the density and the KS Hamiltonian is diagonalized by the KS states. In practical calculations, the problem is thus handled with an iterative procedure known as *self-consistent field* (SCF) method. The procedure, together with other methodological techniques such as the *pseudopotential* approximation, is quickly reviewed in appendix D.

Up to here density functional theory is exact but the exact exchange-correlation energy functional $E_{\rm xc}[n]$ is unfortunately unknown. Some methods have therefore been developed to approximate the exchange-correlation energy functional. The most common one is the *local density approximation* (LDA) [67] according to which the functional is given by

$$E_{\rm xc}^{\rm LDA}[n] = \int n(\mathbf{r}) \mathcal{E}_{\rm xc}^{\rm hom}(n(\mathbf{r}))d\mathbf{r} \tag{4.7}$$

where $\mathcal{E}_{\rm xc}^{\rm hom}(n(\mathbf{r}))$ is the exact exchange-correlation energy density of a homogeneous electron gas with local density $n(\mathbf{r})$. LDA describes quite well the chemical bond, particularly for strong bonds like covalent and metallic. It also works well for vibrational properties. It is not accurate for strongly correlated systems. For spin-polarized systems, the LDA is replaced by the *local spin density approximation* (LSDA) [68] in which the exchange-correlation energy density is a function of the spin-up and spin-down electron density. The performance of the L(S)DA functional has then been improved by including the so-called gradient corrections [69–71]. Such approximation goes under the name of *generalized gradient approximation* (GGA) and the functional reads

$$E_{\rm xc}^{\rm GGA}[n] = \int n(\mathbf{r}) \mathcal{E}_{\rm xc}^{\rm GGA}(n(\mathbf{r}), \nabla n(\mathbf{r}))d\mathbf{r} \tag{4.8}$$

where the exchange-correlation energy density $\mathcal{E}_{\rm xc}^{\rm GGA}(n(\mathbf{r}), \nabla n(\mathbf{r}))$ is now also a function of the non-local gradient of the density. In most of the cases, the band structure in GGA

is very similar to LDA. However, GGA yields better total energies than LDA, better atomization energies and structural energy differences and it works slightly better than LDA for weak bonds, albeit it lacks the Van der Waals interaction. Several approaches based on hybrid functionals have been proposed [72]. These techniques incorporate a portion of exact exchange from Hartree–Fock theory [73, 74]. For a more complete description of the approximate functionals we refer the reader to [75].

4.1.1 Spin Density Functional Theory

In a spin-polarized system, the electronic wavefunction is a spinor, the components of which are $\psi_{i\sigma}(\mathbf{r})$. The spin density matrix can be written as:

$$\rho^{\sigma\sigma'}(\mathbf{r}) = \sum_i f_i \psi^*_{i\sigma}(\mathbf{r})\psi_{i\sigma'}(\mathbf{r}) \tag{4.9}$$

The electron density and magnetization density are obtained as

$$n(\mathbf{r}) = \sum_\sigma \rho^{\sigma\sigma}(\mathbf{r}) \tag{4.10}$$

$$m_\alpha(\mathbf{r}) = \mu_B \sum_{\sigma\sigma'} \rho^{\sigma\sigma'}(\mathbf{r})\sigma_\alpha^{\sigma\sigma'} \tag{4.11}$$

where μ_B is the Bohr magneton, α is a Cartesian index and the Pauli matrices σ_α are defined as

$$\sigma_x = \begin{pmatrix} 0 & 1 \\ 1 & 0 \end{pmatrix} \quad \sigma_y = \begin{pmatrix} 0 & -i \\ i & 0 \end{pmatrix} \quad \sigma_z = \begin{pmatrix} 1 & 0 \\ 0 & -1 \end{pmatrix}. \tag{4.12}$$

In this framework, the KS equation reads

$$\sum_{\sigma'} \left[\left(\frac{p^2}{2m} + V_\mathrm{H} + V_\mathrm{xc} \right) \delta^{\sigma\sigma'} + V_\mathrm{ext}^{\sigma\sigma'} - \mu_B \sum_\alpha B_{\mathrm{xc},\alpha} \sigma_\alpha^{\sigma\sigma'} \right] |\psi_{i\sigma'}\rangle = \varepsilon_i |\psi_{i\sigma}\rangle \tag{4.13}$$

where V_xc is the spin-diagonal exchange-correlation potential defined by Eq. 4.4 and $\boldsymbol{B}_\mathrm{xc}(\mathbf{r})$ is the exchange-correlation magnetic field, defined as the first derivative of the exchange-correlation energy with respect to the magnetization, namely

$$B_{\mathrm{xc},\alpha}(\mathbf{r}) = -\frac{\delta E_\mathrm{xc}}{\delta m_\alpha(\mathbf{r})}. \tag{4.14}$$

Note that V_ext can be non-diagonal in the spin components (we are considering a more general case than the pure ionic potential of Eq. 4.2). The Hamiltonian of Eq. 4.13 is not time-reversal symmetric due to the exchange correlation magnetic field. Indeed, we have

$$\mathcal{T} H_\mathrm{KS}^{[\mathbf{B}]} \mathcal{T}^{-1} = H_\mathrm{KS}^{[-\mathbf{B}]}. \tag{4.15}$$

Collinear magnetism

In the special case of collinear magnetism without spin-orbit coupling (SOC), the spin quantization axis can be taken parallel to the magnetization (usually the z direction).

The spin index σ therefore assumes the value $\uparrow$ and $\downarrow$, namely the two opposite directions on the quantization axis. The spin density matrix is diagonal:

$$\rho^{\sigma\sigma'}(\mathbf{r}) = \begin{pmatrix} \rho^{\uparrow\uparrow}(\mathbf{r}) & 0 \\ 0 & \rho^{\downarrow\downarrow}(\mathbf{r}) \end{pmatrix} \tag{4.16}$$

The charge and magnetization densities read:

$$n(\mathbf{r}) = \rho^{\uparrow\uparrow}(\mathbf{r}) + \rho^{\downarrow\downarrow}(\mathbf{r}) \tag{4.17}$$

$$m_z(\mathbf{r}) = \mu_B \left(\rho^{\uparrow\uparrow}(\mathbf{r}) - \rho^{\downarrow\downarrow}(\mathbf{r})\right) \tag{4.18}$$

where $\boldsymbol{m}(\mathbf{r})$ is always aligned with the spin quantization axis (chosen as the z-axis). The electronic problem is now separable (diagonal) in the spin components and the Kohn-Sham equations are given by

$$\left[\frac{p^2}{2m} + V_{\mathrm{H}} + V_{\mathrm{xc}} + V_{\mathrm{ext}} - \mu_B B_{\mathrm{xc},z}\right] |\psi_{i\uparrow}\rangle = \varepsilon_{i\uparrow} |\psi_{i\uparrow}\rangle \tag{4.19}$$

$$\left[\frac{p^2}{2m} + V_{\mathrm{H}} + V_{\mathrm{xc}} + V_{\mathrm{ext}} + \mu_B B_{\mathrm{xc},z}\right] |\psi_{i\downarrow}\rangle = \varepsilon_{i\downarrow} |\psi_{i\downarrow}\rangle \tag{4.20}$$

The case of collinear magnetism can therefore be exemplified within the LSDA in which the KS equations are time-reversal invariant. Namely, even when time-reversal symmetry is spontaneously broken and a collinear magnetic order emerges, the KS Hamiltonian is diagonal in the spin components and thus time-reversal symmetric. This is not true however when the spin-orbit coupling is non-negligible.

Spin-orbit coupling

In one-electron atoms, the spin angular momentum s and the orbital angular momentum ℓ are not separately conserved. Only the total angular momentum j in a good quantum number, namely the sum of the spin and the orbital angular momenta commutes with the Hamiltonian. The spin-orbit interaction

$$H_{\mathrm{SOC}} = \frac{\hbar}{2m^2c^2} \sum_i \boldsymbol{\nabla} V(\mathbf{r}_i) \times \mathbf{p}_i \cdot \mathbf{S}_i \tag{4.21}$$

is a relativistic effect that scales as the fourth power of the atomic number and it is negligible in light atoms. In the above equation, $V(\mathbf{r}) = -e\phi(r)$ is the potential felt by the electrons. Since $\boldsymbol{\nabla}\phi$ is strongest in the core region, H_{SOC} is often approximated by a sum of on-site contributions of the form $\xi(r)\mathbf{L}\cdot\mathbf{S}$ where $\mathbf{L} = \mathbf{r}\times\mathbf{p}$ and $\mathbf{S}$ are respectively the orbital and spin angular momenta on the site in question and $\xi(r)$ is a radial function given by

$$\xi(r) = \frac{\hbar}{2m^2c^2} \frac{1}{r} \frac{d\phi}{dr} \tag{4.22}$$

Spin-orbit coupling is responsible for the splitting of the electronic energy levels both in molecules and solids. However, such interaction, does not break the time-reversal

symmetry and, therefore, the Kramers degeneracy is not broken by the spin-orbit interaction alone. Nonetheless, when time-reversal symmetry is broken, as for example in the presence of magnetism, the spin-orbit coupling transfers the information to the orbital sector [58]. The time-reversal operator for spin-1/2 particles $\mathcal{T} = i\sigma_y\mathcal{K}$ (see appendix A), where $\mathcal{K}$ is the complex conjugation operator, acts on the spinor wavefunction in the following way

$$\mathcal{T}\begin{pmatrix}\psi_\sigma\\ \psi_{\sigma'}\end{pmatrix} = \begin{pmatrix}\psi^*_{\sigma'}\\ -\psi^*_\sigma\end{pmatrix} \tag{4.23}$$

where σ and σ' are equal to $\uparrow$ and $\downarrow$ when SOC is negligible, otherwise they just label the spinor components.

In the KS formulation of spin density functional theory, the spin-orbit coupling is usually included through the atomic pseudopotential (see appendix D), even though a relativistic density functional theory has also been proposed [76, 77]. The *fully relativistic* pseudopotential [78] is opposed to the *scalar relativistic* one [79] in which the radial Dirac equation is averaged over the total angular momentum.

As for the interplay of magnetism and spin-orbit interaction, in the absence of external fields, we may distinguish between the following situations:

- The system is nonmagnetic and spin-orbit interaction is negligible. Then the theory of the spinless electrons applies.
- The system is nonmagnetic but spin-orbit coupling is finite. Then the number of bands is doubled, the wavefunctions are spinors but time-reversal symmetry holds.
- The system is magnetic and spin-orbit coupling is negligible. Typically the spin are aligned and LSDA can be used. The direction of the magnetization is arbitrary and unrelated to the underlying lattice symmetry.
- The system is magnetic and spin-orbit coupling is non-negligible. The magnetization in an output of the calculation and its direction in space depends on the orientation of the crystal lattice. Time-reversal symmetry is broken for both the spin and orbital sectors.

4.2 Density functional perturbation theory

Let us consider a generic perturbation in the external potential and study the linear response of the system to this perturbation. According to the Hellmann-Feynman theorem [80,81], the first and second derivatives of the total energy with respect to the perturbation parameter read

$$\frac{\partial E}{\partial \lambda} = \int \frac{\partial V_{\text{ext}}(\mathbf{r})}{\partial \lambda} n(\mathbf{r}) d\mathbf{r} \tag{4.24}$$

$$\frac{\partial^2 E}{\partial \lambda \partial \eta} = \int \frac{\partial^2 V_{\text{ext}}(\mathbf{r})}{\partial \lambda \partial \eta} n(\mathbf{r}) d\mathbf{r} + \int \frac{\partial V_{\text{ext}}(\mathbf{r})}{\partial \lambda} \frac{\partial n(\mathbf{r})}{\partial \eta} d\mathbf{r} \tag{4.25}$$

where $n(\mathbf{r})$ is the electronic density in the absence of the perturbation. The first derivative of the electronic density with respect to the parameter $\partial n(\mathbf{r})/\partial\eta$ in the second term of Eq. 4.25 can be written in perturbation theory as [12]

$$\frac{\partial n(\mathbf{r})}{\partial \eta} = 2\sum_i \sum_{j\neq i} \frac{f_i - f_j}{\epsilon_i - \epsilon_j} \psi_i^*(\mathbf{r})\psi_j(\mathbf{r})\langle\psi_j|\frac{\partial H_{\mathrm{KS}}}{\partial \eta}|\psi_i\rangle. \tag{4.26}$$

Here, $|\psi_i\rangle$ are the KS orbitals, f_i are the occupation numbers and ϵ_i are the KS eigenvalues; the factor of 2 accounts for the spin degeneracy. The three equations above are generic and apply for any kind of perturbation, while, in the next sections, we will specialize perturbation theory to study the vibrational properties of molecular and periodic systems.

4.2.1 Spin density functional perturbation theory

When the perturbation is applied to a spin-polarized system, the equations of density functional perturbation theory must include the spin index. The first and second derivatives of the total energy can be written as

$$\frac{\partial E}{\partial \lambda} = \sum_{\sigma\sigma'} \int \frac{\partial V_{\mathrm{ext}}^{\sigma\sigma'}(\mathbf{r})}{\partial \lambda} \rho^{\sigma\sigma'}(\mathbf{r}) d\mathbf{r} \tag{4.27}$$

$$\frac{\partial^2 E}{\partial \lambda \partial \eta} = \sum_{\sigma\sigma'} \int \frac{\partial^2 V_{\mathrm{ext}}^{\sigma\sigma'}(\mathbf{r})}{\partial \lambda \partial \eta} \rho^{\sigma\sigma'}(\mathbf{r}) d\mathbf{r} + \sum_{\sigma\sigma'} \int \frac{\partial V_{\mathrm{ext}}^{\sigma\sigma'}(\mathbf{r})}{\partial \lambda} \frac{\partial \rho^{\sigma\sigma'}(\mathbf{r})}{\partial \eta} d\mathbf{r}. \tag{4.28}$$

In the above equation, the first derivative of the spin density matrix $\rho^{\sigma\sigma'}$ with respect to the perturbation η can be written as

$$\frac{\partial \rho^{\sigma\sigma'}(\mathbf{r})}{\partial \eta} = \sum_i \sum_{j\neq i} \frac{f_i - f_j}{\varepsilon_i - \varepsilon_j}\ \psi_{i\sigma}^*(\mathbf{r})\psi_{j\sigma'}(\mathbf{r}) \sum_{\sigma_1\sigma_2} \langle\psi_{j\sigma_1}|\frac{\partial H_{\mathrm{KS}}^{\sigma_1\sigma_2}}{\partial \eta}|\psi_{i\sigma_2}\rangle \tag{4.29}$$

where the bracket of the screened potential is summed over the spin indexes. The induced charge and magnetization densities are respectively given by

$$\frac{\partial n(\mathbf{r})}{\partial \eta} = \sum_\sigma \frac{\partial \rho^{\sigma\sigma}(\mathbf{r})}{\partial \eta} \tag{4.30}$$

$$\frac{\partial m_\alpha(\mathbf{r})}{\partial \eta} = \mu_B \sum_{\sigma\sigma'} \frac{\partial \rho^{\sigma\sigma'}(\mathbf{r})}{\partial \eta} \sigma_\alpha^{\sigma\sigma'}. \tag{4.31}$$

Up to here we considered static perturbations. Let us now move to dynamic ones.

4.2.2 Time-dependent perturbation

For time-dependent perturbations, the wavefunction and the density are time-dependent. Therefore, also the functionals of the density are time-dependent. In the adiabatic approximation, the Hartree and exchange-correlation potential at time t is a functional of

the density at the same time t. For a general time-dependent wavefunction satisfying the Schrödinger equation

$$i\hbar\frac{d}{dt}\psi_\lambda(t) = H_\lambda\psi_\lambda(t), \tag{4.32}$$

where λ is the perturbation parameter, the Hellmann–Feynman theorem is not valid [82] but the following relation holds

$$i\hbar\frac{d}{dt}\langle\psi_\lambda(t)|\frac{\partial\psi_\lambda(t)}{\partial\lambda}\rangle = \langle\psi_\lambda(t)|\frac{\partial H_\lambda}{\partial\lambda}|\psi_\lambda(t)\rangle. \tag{4.33}$$

It is still possible to evaluate response functions via time-dependent density functional perturbation theory. However, it is not practical to give the equations for a generic perturbation as we did in the static case because the response functions cannot be expressed as derivatives of the total energy. In the next section we write the specific equations for vibrational modes in molecules and solids. Then we apply the Kohn-Sham formalism to study non-adiabatic effects within the time-dependent linear response.

As a side note, when time-dependent density functional perturbation theory is employed, usually a monochromatic perturbation is considered so that response functions at different frequencies are decoupled.

4.3 Lattice dynamics in time-dependent density functional perturbation theory

In section 3.2, we presented the classical theory of lattice dynamics in the harmonic approximation and we solved the eigenvalue problem of the dynamical matrix. In density functional theory, the phonon response function is obtained through perturbation theory from the KS electronic problem. In the naive (static) Born-Oppenheimer (BO) approximation, the ionic motion is decoupled from electrons and static density functional perturbation theory can be used. However, non-adiabatic effects arise only when the electrons are allowed to exchange energy with the ions, namely when the electrons "perceive" the ionic motion. This can be obtained by considering a time-dependent perturbation instead of a static one. Such working framework is called *dynamical* BO approximation[13] and often referred to as *non-adiabatic* BO approximation.

In this section we derive the expression of the force constants using the time-dependent density functional perturbation theory in the harmonic approximation for periodic extended systems. Namely, we consider a time-dependent phonon ionic displacement $\mathbf{u}(t)$ as a monochromatic perturbation to the equilibrium ionic positions. The force acting on the J-th ion at time t due to the displacement $\mathbf{u}_I(t')$ of the I-th ion at time t' is labeled $\mathbf{F}_J(t)$. The matrix of the force constants is defined as

$$C_{I\alpha,J\beta}(t-t') = -\frac{\partial F_{J\beta}(t)}{\partial u_{I\alpha}(t')} \tag{4.34}$$

[13]The BO approximation still holds in the sense that non-adiabatic contributions beyond the electron-phonon coupling are still neglected.

for $t > t'$. In the following we omit the Cartesian indexes α and β where unnecessary. The ω transform of the force constant matrix is given by

$$C_{IJ}(\omega) = \int C_{IJ}(t) e^{i\omega t} dt \tag{4.35}$$

From section 3.2 we recall that the Fourier transform of the (frequency dependent) interatomic force constant matrix is given by

$$C_{sr}(\mathbf{q}, \omega) = \sum_{\mathbf{R}} e^{-i\mathbf{q}\cdot\mathbf{R}} C_{IJ}(\mathbf{R}, \omega). \tag{4.36}$$

The dynamical matrix is equal to the hermitian part of force constant matrix in reciprocal space divided by the square root of the masses, namely

$$D_{sr}(\mathbf{q}, \omega) = \frac{1}{2\sqrt{M_s M_r}} \left[C_{sr}(\mathbf{q}, \omega) + C_{rs}(\mathbf{q}, \omega)^* \right]. \tag{4.37}$$

The antihermitian part on the contrary is related to the phonon damping which determines the phonon linewidth. When the antihermitian part of $C_{sr}(\mathbf{q}, \omega)$ is much smaller than the hermitian part, then non-adiabatic phonon frequencies $\tilde{\omega}$ and polarization vectors $\tilde{\boldsymbol{\varepsilon}}$ are obtained as the square root of the eigenvalues and as the eigenvectors of the dynamical matrix respectively (the tilde to distinguish from the adiabatic case).

However, unlike the adiabatic case, the dynamical matrix of Eq. 4.37 depends on the frequency ω itself. We may therefore define the non-adiabatic phonons as solutions of the nonlinear eigenvalue problem

$$\sum_r D_{sr}(\mathbf{q}, \tilde{\omega}_{\mathbf{q}\nu}) \tilde{\boldsymbol{\varepsilon}}_{\nu r}(\mathbf{q}) = \tilde{\omega}^2_{\mathbf{q}\nu} \tilde{\boldsymbol{\varepsilon}}_{\nu s}(\mathbf{q}) \tag{4.38}$$

where $\tilde{\omega}_{\mathbf{q}\nu}$ and $\tilde{\boldsymbol{\varepsilon}}_{\nu r}(\mathbf{q})$ are respectively the frequency and the non-adiabatic polarization vector of the phonon mode ν with wavevector $\mathbf{q}$. Finally, by analogy with the static case, the angular momentum of non-adiabatic phonons can be defined as

$$\boldsymbol{\ell}_{\mathbf{q}\nu} = -i\hbar \sum_s \tilde{\boldsymbol{\varepsilon}}^*_{\nu s}(\mathbf{q}) \times \tilde{\boldsymbol{\varepsilon}}_{\nu s}(\mathbf{q}). \tag{4.39}$$

4.3.1 Linear response theory

The force-constant matrix in the frequency domain can be evaluated in time-dependent linear response. The force acting on the J-th ion at time t can be evaluated in terms of the variation in the external potential as

$$F_J(t) = -\int n(\mathbf{r}, t) \frac{\partial V_{\text{ext}}(\mathbf{r})}{\partial R_J} d\mathbf{r} \tag{4.40}$$

where $n(\mathbf{r}, t)$ is the electron charge density and $V_{\text{ext}}(\mathbf{r})$ is the external potential due to the ions defined by Eq. 4.2. In time-dependent linear response the force constant matrix in the frequency domain can then be evaluated as [20]

$$C_{IJ}(\omega) = \int \frac{\partial n(\mathbf{r}, \omega)}{\partial u_I} \frac{\partial V_{\text{ext}}(\mathbf{r})}{\partial u_J} d\mathbf{r} + \int n_0(\mathbf{r}) \frac{\partial^2 V_{\text{ext}}(\mathbf{r})}{\partial u_I \partial u_J} d\mathbf{r} \tag{4.41}$$

where $\partial n(\mathbf{r},\omega)/\partial u_I$ is the induced density, $n_0(\mathbf{r})$ is the unperturbed density and $V_{\rm ext}(\mathbf{r})$ is the external potential of the nuclei which does not depends explicitly on time but only through the dependence of the phonon ionic displacement $\mathbf{u}(t)$. The derivatives of the external potential in Eq. 4.41 are evaluated at the equilibrium position of the nuclei ($\mathbf{u}=0$) and they are real and time-independent quantities. The induced density $\partial n(\mathbf{r},\omega)/\partial u_I$ instead is complex. We can evaluate it by using the time-dependent density functional perturbation theory as shown in the previous section. For solids, the derivative of the density with respect to the ionic displacement as a function of the frequency is given by

$$\frac{\partial n(\mathbf{r},\omega)}{\partial u_I} = 2\sum_{\mathbf{k}i,\mathbf{k}'j}^{N_k} \frac{f_{\mathbf{k}i}-f_{\mathbf{k}'j}}{\epsilon_{\mathbf{k}i}-\epsilon_{\mathbf{k}'j}+\omega+i\eta}\langle\psi_{\mathbf{k}'j}|\frac{\partial V_{\rm KS}(\mathbf{r},\omega)}{\partial u_I}|\psi_{\mathbf{k}i}\rangle\psi^*_{\mathbf{k}i}(\mathbf{r})\psi_{\mathbf{k}'j}(\mathbf{r}) \tag{4.42}$$

where the wavefunctions and the energies are labeled with a wavevector $\mathbf{k}$ of the reciprocal lattice (the quasimomentum of the electrons) and a band index i, N_k is the number of k-points necessary to converge the sum, the Fermi occupation functions $f_{\mathbf{k}i}=f(\epsilon_{\mathbf{k}i})$ only depend on the energy $\epsilon_{\mathbf{k}i}$, η is a small positive real number[14] and the factor of 2 accounts for the spin degeneracy. The derivative of the KS potential with respect to the ionic displacement $\partial V_{\rm KS}(\omega)/\partial u_I$ is a complex object that can be written as

$$\frac{\partial V_{\rm KS}(\mathbf{r},\omega)}{\partial u_I} = \frac{\partial V_{\rm ext}(\mathbf{r})}{\partial u_I} + \int K_{\rm Hxc}(\mathbf{r},\mathbf{r}')\frac{\partial n(\mathbf{r}',\omega)}{\partial u_I}d\mathbf{r}' \tag{4.43}$$

where $K_{\rm Hxc}(\mathbf{r},\mathbf{r}')$ defined as $K_{\rm Hxc}(\mathbf{r},\mathbf{r}') = \frac{\delta^2 E_{\rm Hxc}}{\delta n(\mathbf{r})\delta n(\mathbf{r}')}$ is the Hartree and exchange-correlation kernel which we assume to be real and independent on the frequency ω. Following Ref. [20], we use both Eq. 4.42 and Eq. 4.43 to rewrite the force constant matrix of Eq. 4.41 as

$$\begin{aligned} C_{IJ}(\omega) = 2\sum_{\mathbf{k}i,\mathbf{k}'j}^{N_k} \frac{f_{\mathbf{k}i}-f_{\mathbf{k}'j}}{\epsilon_{\mathbf{k}i}-\epsilon_{\mathbf{k}'j}+\omega+i\eta}\langle\psi_{\mathbf{k}'j}|\frac{\partial V_{\rm KS}(\mathbf{r},\omega)}{\partial u_I}|\psi_{\mathbf{k}i}\rangle\langle\psi_{\mathbf{k}i}|\frac{\partial V_{\rm KS}(\mathbf{r},\omega)}{\partial u_J}|\psi_{\mathbf{k}'j}\rangle + \\ + \int d\mathbf{r}\frac{\partial^2 V_{\rm ext}(\mathbf{r})}{\partial u_I \partial u_J}n_0(\mathbf{r}) - \iint d\mathbf{r}d\mathbf{r}'\frac{\partial n(\mathbf{r},\omega)}{\partial u_I}K_{\rm Hxc}(\mathbf{r},\mathbf{r}')\frac{\partial n(\mathbf{r}',\omega)}{\partial u_J}. \end{aligned} \tag{4.44}$$

This formulation is different from Eq. 4.41, as it involves the derivative of the screened potential in both the matrix elements in the first term. As a consequence the symmetry of the force constant matrix under exchange of the ionic and Cartesian indexes is made explicit in Eq. 4.44 at the cost of introducing a negative double counting term (last one). The advantage is that the formulation given in Eq. 4.44 allows to introduce a functional that is stationary with respect to the variation in the self-consistent charge density [20] and, as a consequence, permits the calculation of the vibrational frequencies in a non-self-consistent way with a negligible error.

In the next section, we present the main passages of the scheme proposed in Ref. [20] to compute non-self-consistently the non-adiabatic force constant matrix $C_{IJ}(\omega)$ taking advantage of the formulation of Eq. 4.44.

[14] The small imaginary part prevents divergences. See for example Ref. [83].

4.4 First-principles scheme for calculation of non-adiabatic phonons

Equations 4.42 and 4.44 constitute a frequency-dependent self-consistent scheme that allows the calculation of the non-adiabatic force constant matrix. However, the self-consistent calculation of the perturbed KS potential as a function of the frequency is no easy task, both at the numerical stage and in terms of implementation in the ab-initio code. We therefore resort to the scheme depicted in Ref. [20] to evaluate the non-adiabatic force constant matrix using a functional that is stationary in the variation of the self-consistent charge density. Such procedure allows to avoid the self-consistent calculation of the derivative of the KS potential at the cost of a small error. The force constant functional is given by

$$\begin{aligned} F_{IJ}[x(\mathbf{r}),\bar{x}(\mathbf{r}),\omega,T] = 2\sum_{\mathbf{k}i,\mathbf{k}'j}^{N_k(T)} & \frac{f_{\mathbf{k}i}(T)-f_{\mathbf{k}'j}(T)}{\epsilon_{\mathbf{k}i}-\epsilon_{\mathbf{k}'j}+\omega+i\eta} \\ & \times \langle\psi_{\mathbf{k}'j}|\frac{\partial V_{\text{ext}}(\mathbf{r})}{\partial u_I}+\int K_{\text{Hxc}}(\mathbf{r},\mathbf{r}')x(\mathbf{r}')d\mathbf{r}'|\psi_{\mathbf{k}i}\rangle \\ & \times \langle\psi_{\mathbf{k}i}|\frac{\partial V_{\text{ext}}(\mathbf{r})}{\partial u_J}+\int K_{\text{Hxc}}(\mathbf{r},\mathbf{r}')\bar{x}(\mathbf{r}')d\mathbf{r}'|\psi_{\mathbf{k}'j}\rangle \\ & + \int d\mathbf{r}\frac{\partial^2 V_{\text{ext}}(\mathbf{r})}{\partial u_I \partial u_J}n_0(\mathbf{r}) - \iint d\mathbf{r}d\mathbf{r}'x(\mathbf{r})K_{\text{Hxc}}(\mathbf{r},\mathbf{r}')\bar{x}(\mathbf{r}') \end{aligned} \tag{4.45}$$

where $f_{\mathbf{k}i}(T)$ is the Fermi occupation function at the electronic temperature T (see appendix D). With this definition, the force constant matrix C_{IJ} at frequency ω and temperature T reads

$$C_{IJ}(\omega,T) = F_{IJ}[n_I^{(1)}(\mathbf{r},\omega,T), n_J^{(1)}(\mathbf{r},\omega,T),\omega,T] \tag{4.46}$$

where $n_I^{(1)}(\mathbf{r},\omega,T) \equiv \partial n(\mathbf{r},\omega)/\partial u_I$ is the first derivative of the charge density with respect to the ionic displacement, given by Eq. 4.42. The functional of Eq. 4.45 is stationary with respect to the first-order perturbation of the electronic charge density,

$$\frac{\delta F_{IJ}[x(\mathbf{r}),\bar{x}(\mathbf{r}),\omega,T]}{\delta x(\mathbf{r})}\Big|_{x(\mathbf{r})=n_I^{(1)}(\mathbf{r},\omega,T),\ \bar{x}(\mathbf{r})=n_J^{(1)}(\mathbf{r},\omega,T)} = 0. \tag{4.47}$$

The same relation holds upon derivation with respect to $\bar{x}(\mathbf{r})$. As a consequence, an error in the derivative of the density $n_I^{(1)}(\mathbf{r},\omega,T)$ affects the force constants $C_{IJ}(\omega,T)$ only at second order.

4.4.1 Approximate force constant functional

The most precise force-constant matrix $C_{IJ}(\omega,T)$ is obtained when T coincides with the physical temperature T_0 (e.g., room temperature) of the system. However, in a metal, the number of k-points required to converge the summation of Eq. 4.45 at $T = T_0$, namely $N_k(T_0)$, can be so large (T so small) as to make the calculation

unfeasible. In addition, the self-consistent calculation of $n_I^{(1)}(\mathbf{r},\omega,T)$ at finite $\omega \neq 0$ requires to increase further the number of k-points with respect to the standard static linear response calculation $n_I^{(1)}(\mathbf{r},0,T)$.

In order to overcome these problems, we approximate the force constant matrix as

$$\tilde{C}_{IJ}(\omega,T_0) = F_{IJ}[n_I^{(1)}(\mathbf{r},0,T_{\rm ph}), n_J^{(1)}(\mathbf{r},0,T_{\rm ph}),\omega,T_0] \tag{4.48}$$

where the induced densities $n_I^{(1)}(\mathbf{r},\omega,T)$ and $n_J^{(1)}(\mathbf{r},\omega,T)$ are evaluated at $\omega = 0$ and $T = T_{\rm ph} \gg T_0$. That is, the static limit is considered and the temperature is increased so that the number of k-points needed to converge is diminished. Thanks to the stationary property of the functional, these approximations only introduce an error that is quadratic in the difference $|n_I^{(1)}(\mathbf{r},\omega,T_0) - n_I^{(1)}(\mathbf{r},0,T_{\rm ph})|$ and thus negligible.

The approximate force constant matrix does not need a self-consistent calculation of the non-adiabatic phonon response as the only frequency dependence left is in the weighting factor of the first term of Eq. 4.44. In this approximation, by summing and subtracting $C_{IJ}(0,T_{\rm ph})$ on the right hand side of Eq. 4.48, the non-adiabatic force constant matrix can be written as

$$\tilde{C}_{IJ}(\omega,T_0) = \Pi_{IJ}(\omega,T_0) + C_{IJ}(0,T_{\rm ph}) \tag{4.49}$$

where $C_{IJ}(0,T_{\rm ph})$ is the standard linear-response self-consistent force constant matrix at temperature $T_{\rm ph}$ and $\Pi_{IJ}(\omega,T_0)$ is the phonon self-energy at frequency ω and temperature T_0 given by (see appendix E)

$$\begin{aligned}\Pi_{IJ}(\omega,T_0) = 2 \sum_{\mathbf{k}i,\mathbf{k}'j}^{N_k(T_0)} & \frac{f_{\mathbf{k}i}(T_0) - f_{\mathbf{k}'j}(T_0)}{\epsilon_{\mathbf{k}i} - \epsilon_{\mathbf{k}'j} + \omega + i\eta} \langle\psi_{\mathbf{k}'j}| \frac{\partial V_{\rm KS}}{\partial u_I} |\psi_{\mathbf{k}i}\rangle \langle\psi_{\mathbf{k}i}| \frac{\partial V_{\rm KS}}{\partial u_J} |\psi_{\mathbf{k}'j}\rangle \\ - 2 \sum_{\mathbf{k}i,\mathbf{k}'j}^{N_k(T_{\rm ph})} & \frac{f_{\mathbf{k}i}(T_{\rm ph}) - f_{\mathbf{k}'j}(T_{\rm ph})}{\epsilon_{\mathbf{k}i} - \epsilon_{\mathbf{k}'j}} \langle\psi_{\mathbf{k}'j}| \frac{\partial V_{\rm KS}}{\partial u_I} |\psi_{\mathbf{k}i}\rangle \langle\psi_{\mathbf{k}i}| \frac{\partial V_{\rm KS}}{\partial u_J} |\psi_{\mathbf{k}'j}\rangle. \end{aligned} \tag{4.50}$$

Here $\mathbf{k}$ and $\mathbf{k}'$ are crystal momenta, i and j are band indexes, $|\psi_{\mathbf{k}i}\rangle$ is the Bloch wavefunction, $\partial V_{\rm KS}/\partial u_I$ is the derivative of the static KS potential with respect to the phonon ionic displacement u_I (also known as deformation potential), $f_{\mathbf{k}i}(T)$ is the Fermi occupation function at temperature T and η is an arbitrarily small number.

4.4.2 Characterization of the phonon self-energy

The phonon self-energy of Eq. 4.50 consists of the difference between two terms related to the non-adiabatic and to the adiabatic response, respectively. This is due to the approximation that we have used to evaluate the force-constant matrix $C_{IJ}(\omega,T)$.

The product of the deformation potential matrix elements on the right side of Eq. 4.50 is the same for both terms. It represents the electron-phonon interaction. The product also determines the symmetry properties of the self-energy, namely hermiticity and reality conditions (see appendix E) as the weighting factors, albeit relevant for symmetry, are independent on the ionic indexes.

The weighting factors in the summations of Eq. 4.50 differ for the quantity $\omega + i\eta$ in the denominator. The second one (without $\omega + i\eta$) is the standard coefficient of linear responses in solids. It basically selects KS states $|\psi_{\mathbf{k}i}\rangle$ and $|\psi_{\mathbf{k}'j}\rangle$ that have different occupation numbers and close enough energies (as for states far apart in energy the denominator suppresses the function). In practical calculations, when two states with different occupations are degenerate in metals, the weighting function is replaced with its limiting value, namely minus the density of states at the Fermi energy.

The weighting factor in the first summation of Eq. 4.50 instead selects KS states that are resonant with the vibrational frequency ω. The imaginary part η of the frequency ω ensures that the denominator does not vanish when the difference $\epsilon_{\mathbf{k}'j} - \epsilon_{\mathbf{k}i}$ is equal to ω. Though necessary for mathematical reasons, the parameter η has also the meaning of electron momentum-scattering rate [84]. Indeed the imaginary part of the self-energy is related to the phonon linewidth and to the phonon damping coefficients.

4.4.3 Practical calculation

The main advantage of approximating the force constant functional with Eq. 4.48 is that the calculation of the phonon self-energy $\Pi_{IJ}(\omega, T_0)$ does not require the knowledge of the self-consistent deformation potential on the dense grid $N_k(T_0)$ and thus it is much faster than calculating the non-adiabatic force constant matrix without the approximation.

The practical calculation of the approximate force constant matrix is carried out in reciprocal space. By taking the Fourier transform, Eq. 4.49 becomes

$$\tilde{C}_{sr}(\mathbf{q}, \omega, T_0) = \Pi_{sr}(\mathbf{q}, \omega, T_0) + C_{sr}(\mathbf{q}, 0, T_{\mathrm{ph}}) \tag{4.51}$$

where s and r label the positions of the ions in the unit cell and $\mathbf{q}$ is the phonon wavevector. The phonon self-energy in reciprocal space reads (see appendix E)

$$\begin{aligned}\Pi_{sr}(\mathbf{q}, \omega, T_0) = \frac{2}{N_k(T_0)} \sum_{\mathbf{k}ij}^{N_k(T_0)} \frac{f_{\mathbf{k}+\mathbf{q}i}(T_0) - f_{\mathbf{k}j}(T_0)}{\epsilon_{\mathbf{k}+\mathbf{q}i} - \epsilon_{\mathbf{k}j} + \omega + i\eta} \langle u_{\mathbf{k}j} | \frac{\partial v_{\mathrm{KS}}}{\partial u_{-\mathbf{q}s}} | u_{\mathbf{k}+\mathbf{q}i} \rangle \langle u_{\mathbf{k}+\mathbf{q}i} | \frac{\partial v_{\mathrm{KS}}}{\partial u_{\mathbf{q}r}} | u_{\mathbf{k}j} \rangle \\ - \frac{2}{N_k(T_{\mathrm{ph}})} \sum_{\mathbf{k}ij}^{N_k(T_{\mathrm{ph}})} \frac{f_{\mathbf{k}+\mathbf{q}i}(T_{\mathrm{ph}}) - f_{\mathbf{k}j}(T_{\mathrm{ph}})}{\epsilon_{\mathbf{k}+\mathbf{q}i} - \epsilon_{\mathbf{k}j}} \langle u_{\mathbf{k}j} | \frac{\partial v_{\mathrm{KS}}}{\partial u_{-\mathbf{q}s}} | u_{\mathbf{k}+\mathbf{q}i} \rangle \langle u_{\mathbf{k}+\mathbf{q}i} | \frac{\partial v_{\mathrm{KS}}}{\partial u_{\mathbf{q}r}} | u_{\mathbf{k}j} \rangle .\end{aligned} \tag{4.52}$$

where $|u_{\mathbf{k}i}\rangle$ is the periodic part of the Bloch wavefunction, v_{KS} is the periodic part of the static self-consistent potential and $u_{\mathbf{q}s}$ is the Fourier component of the phonon displacement.

The calculation of the force constant matrix $\tilde{C}_{sr}(\mathbf{q}, \omega, T_0)$ is carried out as follows. Firstly, $C_{sr}(\mathbf{q}, 0, T_{\mathrm{ph}})$ is calculated self-consistently on the $N_K(T_{\mathrm{ph}})$ k-points grid at the high temperature T_{ph}. Secondly, the band energies and wavefunctions are calculated on the denser grid $N_K(T_0)$ and the deformation potential of the sparse grid is interpolated to the denser one. Finally, the two summations in the phonon self-energy Eq. 4.52 are calculated on the dense and on the sparse grids respectively. The force constant matrix in reciprocal space is then given by the sum Eq. 4.51.

At the given temperature, the dynamical matrix is equal to the hermitian part of force constant matrix in reciprocal space divided by the square root of the masses, namely

$$\tilde{D}_{sr}(\mathbf{q},\omega) = \frac{1}{2\sqrt{M_s M_r}} \left[\tilde{C}_{sr}(\mathbf{q},\omega) + \tilde{C}_{rs}(\mathbf{q},\omega)^* \right]. \tag{4.53}$$

Density functional perturbation theory ensures that phonon responses at different $\mathbf{q}$ vectors and frequencies ω are decoupled (monochromatic perturbation). The non-adiabatic phonon frequencies $\tilde{\omega}$ and polarization vectors $\tilde{\boldsymbol{\varepsilon}}$ are obtained as the square root of the eigenvalues and as the eigenvectors of the dynamical matrix, respectively. Namely, they solve the nonlinear eigenvalue problem

$$\sum_r \tilde{D}_{sr}(\mathbf{q},\tilde{\omega}_{\mathbf{q}\nu})\tilde{\boldsymbol{\varepsilon}}_{\nu r}(\mathbf{q}) = \tilde{\omega}^2_{\mathbf{q}\nu}\tilde{\boldsymbol{\varepsilon}}_{\nu s}(\mathbf{q}) \tag{4.54}$$

where ν labels the phonon branches. The nonlinear eigenvalue problem Eq. 4.54 can be solved numerically with an iterative procedure. The adiabatic vibrational frequencies $\omega_{\mathbf{q}\nu}$ are replaced for each mode in the phonon self-energy Eq. 4.52. Then the non-adiabatic dynamical matrix is computed using Eq. 4.53 and diagonalized to yield the new guess frequency $\tilde{\omega}_{\mathbf{q}\nu}$. The procedure is iterated until the input and the output frequencies agree within a given threshold. Usually, no more than one iteration is necessary to converge.

The method discussed so far allows to calculate the non-adiabatic force constant matrix $\tilde{C}_{sr}(\mathbf{q},\omega,T_0)$ at a given $\mathbf{q}$ vector with a non-self-consistent procedure on the dense grid $N_k(T_0)$ at temperature T_0. In Ref. [20] the whole method is detailed and a technique based on Wannier functions which allows to interpolate the dynamical matrix onto the whole Brillouin zone is also described. We refer to the article for a complete coverage of the argument.

4.5 Discussion and summary

The non-adiabatic dynamical matrix as defined in Eq. 4.53, where $\tilde{C}_{sr}(\mathbf{q},\omega)$ is the time-dependent linear response force constant matrix, comprehends the screening of electrons. As a matter of fact, in the present framework, non-adiabatic effects are due to the electron-phonon interaction. In the *dynamical* BO approximation, electrons are coupled with phonons by means of the time-dependent perturbation parameter $\mathbf{u}(t)$. When the approximation Eq. 4.51 is introduced in the context of the first-principles scheme, non-adiabatic effects are affected to second order in the variation of the induced charge density thanks to the properties of the functional F_{IJ}.

By comparing the nonlinear eigenvalue problem Eq. 4.54, which embodies the non-adiabatic effects due to the electron-phonon interaction, with the eigenvalue problem of the harmonic lattice dynamics in the presence of the Berry connection Eq. 3.34, one can reasonably argue that the former looks simply like a particular case of the latter. Namely the case in which

$$\tilde{C}_{sr}(\mathbf{q},\omega) = C_{sr}(\mathbf{q}) - i\hbar\omega\Omega_{sr}(\mathbf{q}). \tag{4.55}$$

It is therefore interesting to investigate the relation between non-adiabatic effects in the *dynamical* BO approximation and topological effects in the *screened* BO approximation. In particular, we wonder if non-adiabatic effects can be time-reversal symmetry breaking interactions for the phonon field just like the Berry connection is for adiabatic phonons (see section 3.2.2). In such case, do non-adiabatic phonons carry angular momentum?

4.5.1 Summary

In this chapter we have addressed the electronic problem in the Born-Oppenheimer approximation. We illustrated the Kohn-Sham formulation of density functional theory with and without spin. The interplay between magnetic and spin-orbit interactions is also analysed. The equations of density functional perturbation theory are then specialized to study lattice dynamics in time-dependent linear response. A first-principles method to calculate the non-adiabatic force constant matrix with non-self-consistent evaluation of the deformation potential is presented. Non-adiabatic phonons are finally obtained from iterative diagonalization of the dynamical matrix.

In the next chapter we demonstrate that non-adiabatic effects are related, at least in the low frequency limit, to the topology of the system. By doing so, we provide a first-principles derivation of the spin-phonon interaction (discussed in chapter 1). This demonstrates that non-adiabatic phonons can carry finite angular momentum.

Chapter 5

Non-adiabatic effects and the gauge field

Now we want to relate the non-adiabatic effects to the geometric properties of the system, and in particular to the gauge invariant Berry curvature that we introduced in chapter 2. In insulators with vibrational frequencies much smaller than the bandgap, we expand the non-adiabatic force constant matrix to linear order in the frequency ω and demonstrate that the coefficients of the linear term of the expansion can be expressed in terms of the Berry curvature of the Kohn-Sham states with respect to the phonon ionic displacement. This result demonstrates the microscopic link between non-adiabatic effects and geometrical properties.

By analogy with the theory of lattice dynamics in the screened Born-Oppenheimer (BO) approximation, we infer that a nonzero vibrational angular momentum can arise due to non-adiabatic effects. For insulators with vibrational frequencies much smaller than the bandgap, time-dependent linear response allows to determine the symmetry conditions required to obtain a finite angular momentum of vibrational modes in the absence of external probes. We show that the KS Berry curvature vanishes in nonmagnetic and collinear magnetic systems since in these systems the electronic wavefunctions can be taken as real and the curvature is proportional to the imaginary part of the deformation potential matrix elements. Consequently, we expect that an intrinsic vibrational angular momentum can arise in non-collinear magnetic materials. We therefore extend the equations of section 4.3 and the first-principles scheme for calculation of non-adiabatic effects to the case of non-collinear magnetism. Finally, we resume the discussion on the phonon angular momentum and thoroughly explain why the non-adiabatic effects are time-reversal symmetry breaking interactions for the vibrational field.

In metals and insulators with vibrational frequencies greater than the bandgap, the calculation is slightly more complicated because the phonon self-energy is divergent for infinite electron lifetime ($\eta = 0$). The non-adiabatic force constant matrix thus cannot be expanded in power series of the frequency ω without including the parameter η. We therefore delay the treatment of this class of materials to chapter 7.

5.1 Non-adiabatic effects in molecular systems

Let us consider, in the first place, non-adiabatic effects in the simpler case of molecules which can be handled as solids with one unit cell. As we have seen in section 3.2.1, the vibrational modes in molecules are obtained as solutions of the eigenvalue equation of the force constant matrix

$$\sum_r C_{sr}\varepsilon_r = \omega^2\varepsilon_s \tag{5.1}$$

where the indexes s and r label the ionic positions (different from I and J that also include a cell index for periodic systems) and the Cartesian indexes are omitted.

In the adiabatic (static) description of vibrational modes, the force constant matrix is real and the polarization vectors are real, up to a global phase. In this case, vibrational modes are linearly polarized and no vibrational angular momentum can arise.

The non-adiabatic interaction (beyond the static BO approximation) between electronic and nuclear vibrational motion in molecules is called vibronic coupling. It cannot be neglected when two adiabatic potential energy surfaces are close to each other as in presence of avoided crossings and conical intersections [85].

The theory of non-adiabatic effects discussed for solids can be straightforwardly adapted to molecular systems by setting $\mathbf{k} = \mathbf{k}' = \mathbf{q} = 0$ everywhere. The nonlinear eigenvalue problem thus reads

$$\sum_r C_{sr}(\omega)\varepsilon_r = \omega^2\varepsilon_s \tag{5.2}$$

where the non-adiabatic force constant matrix can be written in time-dependent density functional perturbation theory as

$$C_{sr}(\omega) = 2\sum_{ij}\frac{f_i - f_j}{\epsilon_i - \epsilon_j + \omega + i\eta}\langle\psi_j|\frac{\partial V_{\mathrm{KS}}(\mathbf{r},\omega)}{\partial u_s}|\psi_i\rangle\langle\psi_i|\frac{\partial V_{\mathrm{KS}}(\mathbf{r},\omega)}{\partial u_r}|\psi_j\rangle + \\ + \int d\mathbf{r}\frac{\partial^2 V_{\mathrm{ext}}(\mathbf{r})}{\partial u_s \partial u_r}n_0(\mathbf{r}) - \iint d\mathbf{r}d\mathbf{r}'\frac{\partial n(\mathbf{r},\omega)}{\partial u_s}K_{\mathrm{Hxc}}(\mathbf{r},\mathbf{r}')\frac{\partial n(\mathbf{r}',\omega)}{\partial u_r}. \tag{5.3}$$

The solutions of the eigenproblem Eq. 5.2 will be the non-adiabatic vibrational frequencies $\tilde{\omega}$ and the non-adiabatic polarization vectors $\tilde{\boldsymbol{\varepsilon}}$. Since the frequency dependent force constant matrix $C_{sr}(\omega)$ is complex, also the polarization vectors can be nontrivially complex. Therefore, a nonzero angular momentum can arise in vibrational modes of molecules. Following section 3.3, the expectation value of the angular momentum of non-adiabatic modes over the quantum vibron ground state can be defined as

$$\langle\mathbf{N}^{\mathrm{ph}}\rangle = \sum_\nu \tilde{\boldsymbol{\ell}}_\nu\left[b(\tilde{\omega}_\nu) + \frac{1}{2}\right] \tag{5.4}$$

where ν labels the phonon branches, $b(\tilde{\omega}_\nu)$ is the Bose-Einstein occupation function and the angular momentum $\tilde{\boldsymbol{\ell}}_\nu$ of vibrational mode ν can be expressed in terms of the non-adiabatic vibrational polarization vectors as

$$\tilde{\boldsymbol{\ell}}_\nu = -i\hbar\sum_s \tilde{\boldsymbol{\varepsilon}}^*_{\nu s}\times\tilde{\boldsymbol{\varepsilon}}_{\nu s}. \tag{5.5}$$

We underline that the expectation value of the angular momentum of phonons over the vibron ground state is not a quantized object as the (pseudo)angular momentum does not commute with the phonon Hamiltonian [86] and the vibron ground state is not its eigenvector.

According to Eq. 5.5, the non-adiabatic vibrational polarization vectors must be nontrivially complex in order to generate a nonzero angular momentum of phonons. However, Eq. 5.3 for the non-adiabatic force constant matrix does not allow to determine in which cases the phonon eigenvectors are non-trivially complex and give rise to a finite angular momentum. We therefore adapt the first-principles scheme presented for solids in Sec. 4.4 to evaluate the non-adiabatic force constant matrix $C_{sr}(\omega)$. For the sake of simplicity, in this section, we neglect the dependence on the temperature. The approximate force constant functional at frequency ω reads

$$\tilde{C}_{sr}(\omega) = \Pi_{sr}(\omega) + C_{sr}(0) \tag{5.6}$$

where $C_{sr}(0)$ is the standard linear-response self-consistent force constant matrix and $\Pi_{sr}(\omega)$ is the phonon self-energy at frequency ω. In molecules, the self-energy of vibrational modes can be written as (the equation is the same as Eq. 4.50 for solids)

$$\Pi_{sr}(\omega) = 2\sum_{ij}\left[\frac{f_i - f_j}{\epsilon_i - \epsilon_j + \omega + i\eta} - \frac{f_i - f_j}{\epsilon_i - \epsilon_j}\right]\langle\psi_j|\frac{\partial V_{\mathrm{KS}}}{\partial u_s}|\psi_i\rangle\langle\psi_i|\frac{\partial V_{\mathrm{KS}}}{\partial u_r}|\psi_j\rangle \tag{5.7}$$

where the square bracket contains the weighting function of the frequency ω and the matrix elements on the right account for the vibronic coupling. Note that the self-energy Eq. 5.7 is well defined even for metals thanks to the small imaginary part η of the frequency ω in the denominator of the first fraction. In section 4.4.2 we already discussed the behavior of the weighting function in the general case: the first fraction selects KS states with different occupations that are resonant with the vibrational frequency ω; the second fraction is well behaved even when $\epsilon_i = \epsilon_j$ as the limiting value exists and it is finite. The nonlinear eigenvalue equation of the force constant matrix in the frequency domain $\tilde{C}_{sr}(\omega)$ reads

$$\sum_r \frac{1}{2\sqrt{M_s M_r}}\left[\tilde{C}_{sr}(\tilde{\omega}_\nu) + \tilde{C}^*_{rs}(\tilde{\omega}_\nu)\right]\tilde{\varepsilon}_{\nu r} = \tilde{\omega}^2_\nu \tilde{\varepsilon}_{\nu s} \tag{5.8}$$

where $\tilde{\omega}_\nu$ and $\tilde{\varepsilon}_{\nu s}$ are the non-adiabatic vibrational frequencies and polarization vectors, respectively.

5.2 The insulating case

If we limit our considerations to insulating molecular systems with vibrational frequencies smaller than the gap, the denominator in the first fraction of Eq. 5.7 never vanishes and the parameter η can be set to 0. Indeed, in insulators, the phonon broadening can be neglected. Then, we can expand the self-energy as a power series of the frequency ω, that is[15]

$$\Pi_{sr}(\omega) = \sum_{n=1}^{\infty}\frac{1}{n!}\Pi^{(n)}_{sr}\omega^n, \tag{5.9}$$

[15]Here we use the fact that $\frac{1}{1-x} = \sum_{n=0}^{\infty} x^n$ when $|x| < 1$.

where the coefficients $\Pi^{(n)}$ are given by the n-th derivative of the self-energy with respect to ω evaluated at $\omega = 0$ and they can be explicitly written as

$$\Pi^{(n)}_{sr} = 2n! \sum_i \sum_{j \neq i} \frac{f_i - f_j}{\epsilon_i - \epsilon_j} \frac{(-1)^n}{(\epsilon_i - \epsilon_j)^n} \langle \psi_j | \frac{\partial V_{\mathrm{KS}}}{\partial u_s} | \psi_i \rangle \langle \psi_i | \frac{\partial V_{\mathrm{KS}}}{\partial u_r} | \psi_j \rangle. \tag{5.10}$$

In insulators, the coefficients $\Pi^{(n)}_{sr}$ are well defined because two bands with the same energy have also the same occupation number (0 or 1) and two bands with different occupation numbers have always different energies. The difference $\epsilon_i - \epsilon_j$ is always greater than or equal to the gap between the highest occupied molecular orbital (HOMO) and the lowest unoccupied molecular orbital (LUMO).

Since the weighting function in Eq. 5.10 is odd/even under exchange of the indexes $i \leftrightarrow j$ according to the parity of n, the overall matrix $\Pi^{(n)}_{sr}$ is antisymmetric (symmetric) in s and r for n odd (even), namely

$$\Pi^{(n)}_{sr} = -\Pi^{(n)}_{rs} \quad \text{for } n \text{ odd} \tag{5.11}$$

$$\Pi^{(n)}_{sr} = \Pi^{(n)}_{rs} \quad \text{for } n \text{ even}. \tag{5.12}$$

This, together with the hermiticity condition $\Pi_{sr}(\omega) = \Pi^*_{sr}(\omega)$, implies that odd (even) coefficients in the series expansion of the self-energy Eq. 5.9 are purely imaginary (real).

5.2.1 The Kohn-Sham Berry curvature

When the vibrational frequencies are much smaller than the HOMO-LUMO gap, we can neglect higher than linear order terms in the series expansion and evaluate the phonon self-energy as

$$\Pi_{sr}(\omega) \simeq -2\omega \sum_i \sum_{j \neq i} \frac{f_i - f_j}{(\epsilon_i - \epsilon_j)^2} \langle \psi_j | \frac{\partial V_{\mathrm{KS}}}{\partial u_s} | \psi_i \rangle \langle \psi_i | \frac{\partial V_{\mathrm{KS}}}{\partial u_r} | \psi_j \rangle. \tag{5.13}$$

Since we retained only the first order of the expansion, the phonon self-energy is now purely imaginary as it can be shown by rewriting it in the form

$$\Pi_{sr}(\omega) \simeq -4i\omega \ \mathrm{Im} \sum_i \sum_{j \neq i} \frac{f_i}{(\epsilon_i - \epsilon_j)^2} \langle \psi_j | \frac{\partial V_{\mathrm{KS}}}{\partial u_s} | \psi_i \rangle \langle \psi_i | \frac{\partial V_{\mathrm{KS}}}{\partial u_r} | \psi_j \rangle, \tag{5.14}$$

where we used the fact that $d^s_{ij} = (d^s_{ji})^*$. The attentive reader may recognize here the Berry curvature expressed in perturbation theory from Eq. 2.23. The phonon self-energy, to leading order in the low-frequency expansion, can thus be expresses in insulators as a summation over the occupied states of the Berry curvature $\Omega^{\mathrm{KS}}_{sr,i}$ associated with the KS state $|\psi_i\rangle$ and the phonon ionic displacements u, namely

$$\Pi_{sr}(\omega) \simeq -i\omega \Omega^{\mathrm{KS}}_{sr} = -i\omega \sum_i f_i \Omega^{\mathrm{KS}}_{sr,i}, \tag{5.15}$$

where $\Omega^{\mathrm{KS}}_{sr,i}$ is given by

$$\Omega^{\mathrm{KS}}_{sr,i} = 4\mathrm{Im} \sum_{j \neq i} \frac{1}{(\epsilon_i - \epsilon_j)^2} \langle \psi_j | \frac{\partial V_{\mathrm{KS}}}{\partial u_s} | \psi_i \rangle \langle \psi_i | \frac{\partial V_{\mathrm{KS}}}{\partial u_r} | \psi_j \rangle. \tag{5.16}$$

The matrix $\Omega^{\mathrm{KS}}_{sr}$ is a real antisimmetric matrix that plays the role of the Berry curvature in the case of Kohn-Sham independent electrons. When replacing the phonon self-energy Eq. 5.15 into the approximate force constant matrix Eq. 5.6, we can write the nonlinear eigenvalue problem as

$$\sum_r \frac{1}{\sqrt{M_s M_r}} \left[C_{sr} - i\hbar\tilde{\omega}_\nu \Omega^{\mathrm{KS}}_{sr} \right] \tilde{\varepsilon}_{\nu r} = \tilde{\omega}^2_\nu \tilde{\varepsilon}_{\nu s} \tag{5.17}$$

which is equal to the phonon eigenvalue problem of the harmonic crystal lattice in the presence of the Berry connection, Eq. 3.34. The difference between the present derivation and the latter is that, in chapter 3, the Berry curvature directly arises from the BO approximation as the effect of the back-interaction of the electrons whereas, in this section, the KS Berry curvature represents, to leading order in the low-frequency expansion, the non-adiabatic effects due to the vibronic coupling.

We stress that, in the present calculation, Eq. 5.17 holds because the force constant matrix has been evaluated in time-dependent linear response with the approximation of section 4.4. The coupling between electrons and vibrational modes is accounted for via the dynamical BO approximation and the KS Berry curvature can only be expressed in density functional perturbation theory as in Eq. 5.16. On the other hand, the Berry curvature in the screened BO approximation Eq. 3.34 is exact, namely it includes the full electronic wavefunction. The two equations coincide when the latter is also evaluated in linear response.

5.2.2 Time-reversal symmetry breaking

Since the KS Berry curvature in Eq. 5.17 is real, the force constant matrix and polarization vectors become complex and thus a nonzero angular momentum of vibrational modes can arise. The present derivation also allows to establish what are the conditions that the molecule must meet in order to have nonzero vibrational angular momentum.

If time-reversal symmetry holds, the matrix elements in Eq. 5.16 are real and therefore the KS Berry curvature vanishes. Indeed, a necessary condition to have nonzero vibrational angular momentum is that time-reversal symmetry is broken. In experimental works reviewed in chapter 1, it has been shown that phonon angular momentum arises in presence of external time-reversal symmetry breaking probes, such as the magnetic field. However, time-reversal symmetry is broken as well in the magnetic phase of insulators without external probes. Since we are looking for an intrinsic mechanism to induce nonzero vibrational angular momentum in molecules, we need to exclude from the analysis nonmagnetic systems and generalize the theory to include spin.

Moreover, collinear magnetism with negligible spin-orbit coupling, can be dealt with as if the spin up and down sectors were independent (local spin density approximation). The collinear KS Hamiltonian is therefore diagonal in the spin components and the KS equations are time-reversed of each other (see section 4.1.1). Linear response functions can therefore be written as the sum of a spin-up and a spin-down term. The KS Berry curvature then vanishes because the deformation potential matrix elements are real. Another way to prove it is the following. In magnetic systems with negligible spin-orbit coupling, time-reversal symmetry is broken in the spin sector of electronic

wavefunctions. The KS Berry curvature accounting for the electron-vibron coupling must therefore vanish to prevent time-reversal symmetry breaking in the orbital sector since spin-orbit is negligible.

In order to observe non-adiabatic effects in molecules and nonzero vibrational angular momentum we must consider non-collinear magnetic systems in which the spin components cannot be decoupled. A specific class of non-collinear magnetic phase is the case in which the spin-orbit interaction is sizeable along with magnetic interactions. However non-collinear magnetism can arise also in the absence of relativistic effects (see geometric frustration). An example of frustrated non-collinear magnetic molecular systems with large spin-orbit coupling are platinum clusters that we present in the next chapter.

5.2.3 Few more considerations

Equations 5.16 and 5.17 are the microscopic link between the electron-vibron interaction, non-adiabatic (dynamical) effects and the occurrence of a finite angular momentum in molecules. In insulators with vibrational frequencies much smaller than the bandgap, non-adiabatic effects can be expressed as a KS Berry curvature in the space of the ionic displacement. This result allows one to determine the conditions that the system must meet in order to get a nonzero vibrational angular momentum, namely the KS Berry curvature is nonzero in non-collinear magnetic systems. Furthermore, the equation of the non-adiabatic force constant matrix provides a practical computational scheme to evaluate the vibrational quantum angular momentum based on the method presented in Sec. 4.4.

In section 5.2.1, we showed that non-adiabatic effects are time-reversal symmetry breaking interactions for the vibrational field in insulating molecules with vibrational frequencies much smaller than the HOMO-LUMO gap. When the vibrational frequencies are not much smaller (but still smaller) than the electronic gap, higher order terms in the power series expansion of the self-energy can be relevant. However, the second order term quadratic in ω is real and thus it can be incorporated in the adiabatic real force constant matrix. Indeed, it does not change the qualitative result. Third order and higher terms in the power series expansion can safely be neglected as they are related with anharmonic effects which we do not take into account. In practical calculations, the linear term in the frequency ω, with the aim of evaluating the vibrational angular momentum, is the only one that should be considered in molecules with vibrational frequencies smaller than the HOMO-LUMO gap.

Insulating systems with vibrational frequencies equal to or greater than the bandgap will be dealt with in chapter 7 together with metals. In the latter case, the parameter η cannot be set equal to zero because the self-energy Eq. 5.7 diverges in the limit $\eta \to 0$. Nonetheless, a Taylor series expansion around $\omega = 0$ can still be performed keeping $\eta \neq 0$ and a generalized KS Berry curvature can be defined for both insulating and metallic systems.

As a final remark, we notice that $\Omega_{sr}^{\mathrm{KS}}$ is directly proportional to the square of the deformation potential and inversely proportional to the HOMO-LUMO gap (Eq. 5.16). The requirement of non-collinear magnetism and such proportionalities suggest that

large non-adiabatic (dynamical) effects and vibrational angular momenta could be found in insulating non-collinear magnetic molecules with a small gap and a large electron-vibron interaction.

5.3 Non-adiabatic effects in non-collinear magnetic molecular systems

Non-adiabatic effects due to the electron-phonon interaction, expressed through the KS Berry curvature to leading order in the low-frequency expansion, break time-reversal symmetry in the eigenvalue problem of the force constant matrix. However, the Berry curvature itself is nonzero only when the deformation potential matrix elements are complex. The complete electron-phonon interaction, on the other side, does not necessarily break time-reversal symmetry for vibrational modes unless the symmetry has already been broken for electrons (magnetism). In this section we generalize the theory illustrated so far to the spin-dependent case as we expect that non-adiabatic effects induce a nonzero angular momentum in non-collinear magnetic systems.

In sections 4.1.1 and 4.2.1 we introduced the spin density matrix $\rho^{\sigma\sigma'}$ and spin density functional perturbation theory. When dealing with time-dependent linear response, however, it is more convenient to introduce a 4-vector notation. We define the 4-vector density $\rho(\mathbf{r}) = (n(\mathbf{r}), m_x(\mathbf{r}), m_y(\mathbf{r}), m_z(\mathbf{r}))$ in such a way that the spin density matrix is equal to $\rho^{\sigma\sigma'} = \sum_\lambda \rho_\lambda \sigma_\lambda^{\sigma\sigma'}$, where the index λ runs from 0 to 3 and σ is the 4-vector of the identity and Pauli matrices.

The equations that we present in the following are analogous to those given in section 4.3.1 for spin-independent extended periodic systems. The first derivative of the frequency dependent KS potential can be written in this framework as

$$\frac{\partial V_{\mathrm{KS},\lambda}(\mathbf{r},\omega)}{\partial u_s} = \frac{\partial V_{\mathrm{ext},\lambda}(\mathbf{r})}{\partial u_s} + \sum_\mu \int K_{\mathrm{Hxc},\lambda\mu}(\mathbf{r},\mathbf{r}') \frac{\partial \rho_\mu(\mathbf{r}',\omega)}{\partial u_s} d\mathbf{r}', \tag{5.18}$$

where $V_{\mathrm{KS},\lambda}$ and $V_{\mathrm{ext},\lambda}$ are the components of the Kohn-Sham and external potentials in the basis of the identity and Pauli matrices, u_s is the phonon ionic displacement, $K_{\mathrm{Hxc},\lambda\mu}(\mathbf{r},\mathbf{r}')$ is the Hartree and exchange-correlation kernel defined as the second derivative of the Hartree and exchange-correlation energy with respect to the 4-vector density,

$$K_{\mathrm{Hxc},\lambda\mu}(\mathbf{r},\mathbf{r}') = \frac{\delta^2 E_{\mathrm{Hxc}}[\rho]}{\delta\rho_\lambda(\mathbf{r})\delta\rho_\mu(\mathbf{r}')}, \tag{5.19}$$

and the first derivative of the 4-vector spin density in the frequency domain can be written in density functional perturbation theory as

$$\frac{\partial \rho_\mu(\mathbf{r},\omega)}{\partial u_s} = \sum_{ij} \frac{f_i - f_j}{\epsilon_i - \epsilon_j + \omega + i\eta} \sum_{\sigma_1\sigma_2} \langle \psi_{j\sigma_1} | \frac{\partial V_{\mathrm{KS}}^{\sigma_1\sigma_2}(\mathbf{r},\omega)}{\partial u_s} | \psi_{i\sigma_2} \rangle \sum_{\sigma\sigma'} \psi^*_{i\sigma}(\mathbf{r}) \psi_{j\sigma'}(\mathbf{r}) \sigma_\mu^{\sigma\sigma'}. \tag{5.20}$$

The frequency dependent force constant matrix, as a second derivative of the total energy, is given by

$$C_{sr}(\omega) = \sum_\lambda \int \frac{\partial \rho_\lambda(\mathbf{r},\omega)}{\partial u_s} \frac{\partial V_{\mathrm{ext},\lambda}(\mathbf{r})}{\partial u_r} d\mathbf{r} + \sum_\lambda \int \rho^0_\lambda(\mathbf{r}) \frac{\partial^2 V_{\mathrm{ext},\lambda}(\mathbf{r})}{\partial u_s \partial u_r} d\mathbf{r}, \tag{5.21}$$

where $\rho^0(\mathbf{r})$ is the unperturbed 4-vector spin density and $V_{\text{ext}}(\mathbf{r})$ is the external potential of the nuclei, which does not depend explicitly on time. We allow the external potential to have 4 components in order to include the spin-orbit interaction and the eventual external magnetic field as well.

Replacing Eq. 5.20 into Eq. 5.21 and replacing the derivative of the external potential in the first term as obtained from Eq. 5.18, the force constant matrix can be expressed as

$$C_{sr}(\omega) = \sum_{ij} \frac{f_i - f_j}{\epsilon_i - \epsilon_j + \omega + i\eta} \sum_{\sigma_1\sigma_2} \langle \psi_{j\sigma_1} | \frac{\partial V_{\text{KS}}^{\sigma_1\sigma_2}(\mathbf{r},\omega)}{\partial u_s} | \psi_{i\sigma_2} \rangle \sum_{\sigma_3\sigma_4} \langle \psi_{i\sigma_3} | \frac{\partial V_{\text{KS}}^{\sigma_3\sigma_4}(\mathbf{r},\omega)}{\partial u_r} | \psi_{j\sigma_4} \rangle + \sum_{\lambda} \int d\mathbf{r} \frac{\partial^2 V_{\text{ext},\lambda}(\mathbf{r})}{\partial u_s \partial u_r} \rho^0_\lambda(\mathbf{r}) - \sum_{\lambda\mu} \iint d\mathbf{r} d\mathbf{r}' \frac{\partial \rho_\lambda(\mathbf{r},\omega)}{\partial u_s} K_{\text{Hxc},\lambda\mu}(\mathbf{r},\mathbf{r}') \frac{\partial \rho_\mu(\mathbf{r}',\omega)}{\partial u_r}. \tag{5.22}$$

The above equation generalizes Eq. 4.44 to the spin-dependent case in molecular systems. The force constant matrix as a function of the frequency can be written as a quadratic form of the 4-vector spin density just like in the spin-independent framework.

5.3.1 First-principles scheme

Following the line of section 4.4, we may define a spin-dependent functional of the density to evaluate the non-adiabatic force constant matrix with a non-self-consistent procedure. Then, the non-adiabatic force constant matrix can be approximated as in the spin-independent case with a negligible error due to the stationary properties of the functional. The force constant functional of the generic 4-vector spin density $y(\mathbf{r})$ reads

$$\begin{aligned} F_{sr}[y(\mathbf{r}), \bar{y}(\mathbf{r}), \omega] = & \sum_{ij} \frac{f_i - f_j}{\epsilon_i - \epsilon_j + \omega + i\eta} \\ & \times \sum_{\sigma_1\sigma_2} \langle \psi_{j\sigma_1} | \frac{\partial V_{\text{ext}}^{\sigma_1\sigma_2}(\mathbf{r})}{\partial u_s} + \int K_{\text{Hxc}}(\mathbf{r},\mathbf{r}') y^{\sigma_1\sigma_2}(\mathbf{r}') d\mathbf{r}' | \psi_{i\sigma_2} \rangle \\ & \times \sum_{\sigma_3\sigma_4} \langle \psi_{i\sigma_3} | \frac{\partial V_{\text{ext}}^{\sigma_3\sigma_4}(\mathbf{r})}{\partial u_r} + \int K_{\text{Hxc}}(\mathbf{r},\mathbf{r}') \bar{y}^{\sigma_3\sigma_4}(\mathbf{r}') d\mathbf{r}' | \psi_{j\sigma_4} \rangle \\ & + \sum_{\lambda} \int d\mathbf{r} \frac{\partial^2 V_{\text{ext},\lambda}(\mathbf{r})}{\partial u_s \partial u_r} \rho^0_\lambda(\mathbf{r}) \\ & - \sum_{\lambda\mu} \iint d\mathbf{r} d\mathbf{r}' y_\lambda(\mathbf{r}) K_{\text{Hxc},\lambda\mu}(\mathbf{r},\mathbf{r}') \bar{y}_\mu(\mathbf{r}'). \end{aligned} \tag{5.23}$$

Eq. 5.23 generalizes Eq. 4.45 to the spin-dependent molecular systems. The force constant matrix in the frequency domain reads

$$C_{sr}(\omega) = F_{sr}\left[\rho_s^{(1)}(\mathbf{r},\omega), \rho_r^{(1)}(\mathbf{r},\omega), \omega\right], \tag{5.24}$$

where $\rho_s^{(1)}(\mathbf{r},\omega) = \partial\rho(\mathbf{r},\omega)/\partial u_s$. The functional is stationary with respect to the first-order perturbation of the spin charge density which means that an error on the induced density affects the force constants only at second order.

We approximate the force constant matrix with a functional of the frequency-independent spin density which does not need a self-consistent evaluation of the non-adiabatic linear response. The approximate force constant functional in the frequency domain therefore reads

$$\tilde{C}_{sr}(\omega) = \Pi_{sr}(\omega) + C_{sr}(0) \tag{5.25}$$

where $C_{sr}(0)$ is the usual linear response to the vibrational field, while the self-energy $\Pi_{sr}(\omega)$ embodies the non-adiabatic part of the response function. In the spin-dependent framework the self-energy is equal to

$$\begin{aligned}\Pi_{sr}(\omega) = &\sum_{ij} \frac{f_i - f_j}{\epsilon_i - \epsilon_j + \omega + i\eta} \sum_{\sigma_1\sigma_2} \langle \psi_{j\sigma_1} | \frac{\partial V_{\mathrm{KS}}^{\sigma_1\sigma_2}}{\partial u_s} | \psi_{i\sigma_2} \rangle \sum_{\sigma_3\sigma_4} \langle \psi_{i\sigma_3} | \frac{\partial V_{\mathrm{KS}}^{\sigma_3\sigma_4}}{\partial u_r} | \psi_{j\sigma_4} \rangle \\ &- \sum_{i\neq j} \frac{f_i - f_j}{\epsilon_i - \epsilon_j} \sum_{\sigma_1\sigma_2} \langle \psi_{j\sigma_1} | \frac{\partial V_{\mathrm{KS}}^{\sigma_1\sigma_2}}{\partial u_s} | \psi_{i\sigma_2} \rangle \sum_{\sigma_3\sigma_4} \langle \psi_{i\sigma_3} | \frac{\partial V_{\mathrm{KS}}^{\sigma_3\sigma_4}}{\partial u_r} | \psi_{j\sigma_4} \rangle. \end{aligned} \tag{5.26}$$

Eq. 5.26 is an adaptation of Eq. 4.52 to spin-dependent molecular insulating and metallic systems.

The study of non-adiabatic effects in molecules is easier than periodic systems because there is just one unit cell and we do not have to worry about Fourier transforms. Moreover, in solids, the Bloch wavefunctions at $\mathbf{k}$ are related with the Bloch wavefunctions at $-\mathbf{k}$ (the same for phonon linear response at $\mathbf{q}$ and $-\mathbf{q}$) via time-reversal symmetry. Most of the ab-initio codes and first-principles methods enforce this symmetry in the calculation of vibrational modes. The evaluation of the non-adiabatic force constant matrix in reciprocal space thus would need major modifications of the existing code. Luckily, the linear response theory for adiabatic lattice dynamics has been recently extended to study non-collinear magnetic systems (see references [21] and [87]). We take care of these aspects in chapter 7 when dealing with solids.

5.4 Discussion and summary

If we consider the phonon self-energy in the low frequency expansion, the KS Berry curvature breaks time-reversal symmetry for the vibrational field (see Eq. 5.17). We have shown in section 5.2.2 that the KS Berry curvature is nonzero in non-collinear magnetic systems. In this class of materials, we therefore expect to observe a nonzero angular momentum of vibrational modes driven by non-adiabatic effects.

On the other hand, if we consider the full self-energy Eq. 5.7 accounting for the dynamical electron-vibron interaction, time-reversal symmetry holds. However, broken time-reversal symmetry in the orbital sector of the electronic wavefunctions can be transferred to the vibrational field via the electron-vibron interaction.

The magnetic interactions break time-reversal symmetry in the spin sector of the electronic wavefunctions. But, if the spin and orbit sectors of the electronic wavefunctions are coupled, magnetism becomes non-collinear and time-reversal symmetry breaking occurs in both the electronic and ionic dynamical equations.

Molecular systems with non-collinear magnetism and large spin-orbit coupling are therefore ideal candidates to host a finite vibrational angular momentum driven by

non-adiabatic effects. Since the spin-orbit coupling scales with the fourth power of the nuclear charge, in the next chapter we will evaluate this non-adiabatic effect in non-collinear magnetic clusters of platinum (atomic number Z= 78).

5.4.1 Summary

In this chapter we addressed the connection between non-adiabatic effects and geometrical properties of the system. We demonstrated that non-adiabatic effects due to the vibronic coupling are time-reversal symmetry breaking interactions for the vibrational field in non-collinear magnetic molecules with vibrational frequencies much smaller than the electronic gap. As in these systems the deformation potential matrix elements cannot be real valued, a nonzero synthetic field arises (KS Berry curvature). As a result, an intrinsic nonzero vibrational angular momentum occurs even for non-degenerate modes and in the absence of external time-reversal symmetry breaking probes. Our work provides the conceptual link between the Berry's formalism, the electron-vibron interaction, and the existence of a nonzero intrinsic vibrational angular momentum in insulating non-collinear magnetic molecules.

Chapter 6

Vibrational angular momentum in non-collinear magnetic platinum clusters

The angular momentum of vibrational modes in molecules can be nonzero when time-reversal symmetry is broken for the ionic motion. This last circumstance eventually occurs in three stages: the magnetic interaction ensures that time-reversal symmetry is broken in the Kohn-Sham (KS) equations of electrons; spin-orbit coupling guarantees that time-reversal symmetry breaking is communicated to the orbital sector of the electronic wavefunctions; the vibronic interaction transmits time-reversal symmetry breaking to the vibrational field. Molecular systems with non-collinear magnetism and large spin-orbit coupling are therefore ideal candidates to host circularly polarized vibrational modes in the absence of external fields. The magnitude of the angular momentum is expected to be inversely proportional to the HOMO-LUMO gap and proportional to the absolute magnetization of the system.

Here, we demonstrate the occurrence of an intrinsic total vibrational angular momentum driven by non-adiabatic (dynamical) effects in two small platinum clusters with an odd number of atoms, namely platinum trimer Pt_3 and platinum pentamer Pt_5. These systems are ideal as they are (i) magnetic, (ii) the large spin-orbit coupling leads to a non-collinear magnetic order and (iii) the HOMO-LUMO gap is quite small compared to other magnetic molecules ($\sim 10^2$ meV). We calculate the electronic structure and vibrational properties (adiabatic and non-adiabatic) by performing fully relativistic calculations using version 6.4.1 of the Quantum-Espresso suite [88, 89] and the compatible version of Thermo_pw [21] for the non-collinear treatment of the magnetization densities. We used version 3.3.0 of the fully relativistic ONCV pseudopotential [90, 91] with Perdew-Burke-Ernzerhof exchange-correlation functional [92] and a kinetic energy cutoff of 90 Ry. A simple cubic Bravais lattice structure with a parameter of 10.6 Å was used in order to minimize the interaction between the clusters and their copies. Then we study the vibrational properties of the platinum clusters using linear response theory and compare the results with the few data present in the literature. Finally, the nonlinear eigenvalue equation is solved by evaluating the force

constant matrix as a function of the frequency ω and by diagonalizing it. For each mode, the non-adiabatic (dynamical) vibrational frequency and polarization vectors can be found when the square root of the eigenvalue is equal to the value of the frequency fed into the force constant matrix. The non-adiabatic vibrational angular momentum is ultimately obtained from the polarization vectors in platinum trimer and pentamer with non-collinear alignment of the magnetic moments.

6.1 Electronic structure properties

In fully relativistic density functional calculations, it is found that the non-collinear magnetic order minimizes the total energy in platinum trimer and pentamer. The lowest energy structure of the two platinum clusters is shown in Fig. 6.1. In both systems, a small Jahn-Teller distortion takes place. Pt_3 arranges in a isosceles triangular shape with interatomic distances of 2.49 Å and 2.50 Å whereas Pt_5 stabilizes in a trigonal bipyramid configuration with the atoms at the vertexes of the pyramids slightly shifted towards one side of the basis triangle. In platinum pentamer, the interatomic distance is 2.59 Å for in-plane atoms and 2.58 Å and 2.62 Å for out-of-plane atoms.

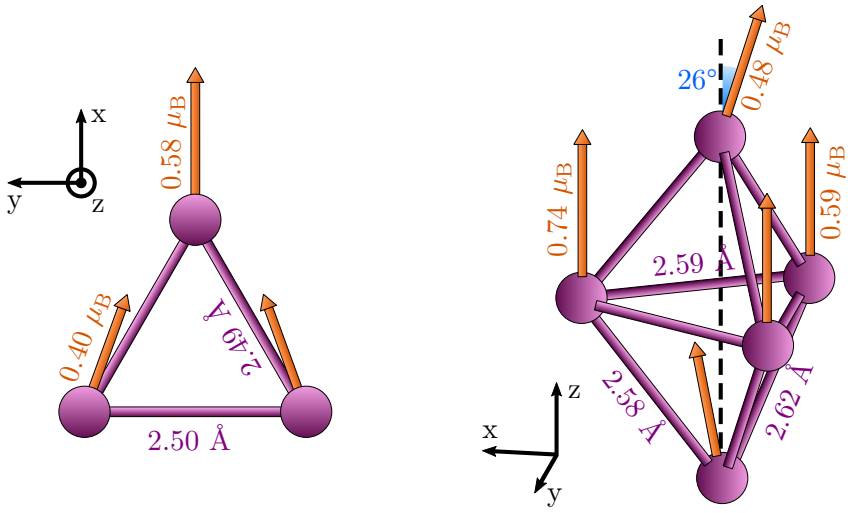

Figure 6.1: Non-collinear magnetic ground state of Pt_3 (left) and Pt_5 (right): geometric structure, interatomic distances and magnetic moments.

The magnetic phase of platinum clusters is also reported in Fig. 6.1. The arrows correspond to the magnetic moments of the atoms and the value is given in units of μ_B/atom. It is found that relativistic effects lower the energy of the non-collinear magnetic configuration with respect to the collinear one. In Pt_3 the magnetic moments of the two atoms in the basis of the triangle are tilted towards the center compared to the collinear phase. The same occurs for the atoms at the vertexes of the pyramids in Pt_5 whose magnetic moments are tilted in opposite directions with respect to the vertical axis. The total magnetization is 1.58 μ_B for platinum trimer and 3.63 μ_B for platinum pentamer, in agreement with Ref. [93].

The binding energy per atom of each cluster is obtained as $(nE_1 - E_n)/n$ where n is the number of atoms in the cluster and E_1 is the energy of the isolated atom. The calculated binding energy per atom in Pt_3 and Pt_5 is respectively 2.177 eV and 2.835 eV, in agreement with Ref. [94]. The HOMO-LUMO gap is 137 meV for Pt_3 in agreement with [93, 95] and 92 meV for Pt_5, in agreement with [93]. The small value of the electronic gap suggests the occurrence of large non-adiabatic effects and sizeable angular momentum of vibrational modes both in platinum trimer and pentamer.

The results obtained in the present electronic structure calculation are compared with available data from literature in Table 6.1 for platinum trimer and Table 6.2 for platinum pentamer. In the second column it is specified whether the spin-orbit coupling (SOC) was included or not in the calculation. Columns 3 to 7 report in order the geometrical structure, interatomic distances in Angstrom, the binding energy per atom in electronVolt, the HOMO-LUMO energy gap in electronVolt, the magnetic moment per atom in units of the Bohr magneton.

Table 6.1: Comparison of electronic structure properties in triangular arrangements of platinum trimer from several different studies (referred to in the first column). Our results are shown in the first line. In column 2 it is specified whether spin-orbit coupling was included or not in the calculation. Columns 3 to 7 report, in the cited reference, the geometrical structure (equilateral or isosceles triangular), interatomic distances, the binding energy per atom, the HOMO-LUMO energy gap and the magnetic moment per atom (0 for nonmagnetic configurations). Blank spaces correspond to unavailable data.

	SOC	structure	d (Å)	E_b/atom (eV)	gap (eV)	μ_B/atom
this work	Y	is. △	2.489, 2.501	2.177	0.1365	0.379, 0.584
[96]	Y	eq. △	2.52	1.85	1.85	
[93]	Y	is. △	2.502, 2.512	2.90	0.13	0.443, 0.644
	N	eq. △	2.465	3.13	0.09	0.012
[94]	Y	is. △	2.50, 2.51	2.22		0.43, 0.65
[97]	N	eq. △	2.49	2.41		
[98]	N	eq. △	2.49	2.063	0.1139	
[95]	Y	is. △	2.509, 2.558	2.210	0.128	
	N	eq. △	2.476	2.443	0.479	
[99]	N	eq. △	2.47	2.33	0.034	0
[100]	N	eq. △	2.58	2.40		

In platinum trimer there is general agreement on the structure, interatomic distances and binding energy while the value of the HOMO-LUMO gap is uncertain (although our result agrees well with the relativistic calculations of references [95] and [93]). Most of referenced articles agree on the structure that minimizes the total energy, namely isosceles or equilateral triangle depending on whether SOC is included or not. The non-collinear magnetic configuration of platinum trimer has only been analysed in Ref. [93] and Ref. [94] and the resulting magnetic moments are reasonably similar to ours.

For what concerns platinum pentamer, there is in general less agreement between

Table 6.2: Comparison of electronic structure properties of bipyramidal platinum pentamer from several different studies (referred to in the first column). Our results are shown in the first line. Description of the columns is given in the caption of Tab. 6.1.

	SOC	d (Å)	E_b/atom (eV)	gap (eV)	μ_B/atom
this work	Y	2.59/ 2.58, 2.62	2.835	0.092	0.59, 0.74/ 0.48
[96]	Y		2.25		
[93]	Y	2.599, 2.609/ 2.620, 2.625	2.75	0.09	0.653, 0.685/ 0.378
	N	2.569/2.634	2.99	0.39	0.790/0.485
[94]	Y	2.60/2.62	2.8		0.64/0.36
[98]	N	2.61	2.593	0.387	
[95]	Y	2.607/2.619	2.748		
	N	2.574/2.633	2.956		
[99]	N	2.57/2.63	2.91	0.63	0.8
[100]	N	2.58, 2.85, 2.71, 2.84	2.59		

different studies on which is the lowest energy isomer. In Table 6.2 we consider the bipyramid isomer only as the non-collinear magnetic phase seems to be the lowest-energy configuration. Our calculated interatomic distances and binding energy are in agreement with other relativistic calculations and in line with the rest of the data. The result obtained for the HOMO-LUMO energy gap agrees with Ref. [93] but not with others. The magnetic configuration of platinum pentamer is more difficult to compare with the literature as the non-collinear magnetic phase is difficult to stabilize in the fully relativistic calculation. Still, the values of the magnetic moments obtained in our work (last field in the first row of Table 6.2) lie within the range of magnetic moments from other calculations.

6.2 Static vibrational modes

After studying the magnetic ground state, we investigate the vibrational properties of the platinum clusters using static linear response theory. Nonlinear molecules have 3 modes of translation (acoustic), 3 modes of rotation and $3N_{\rm tot}-6$ optical modes. In the following we will consider only optical modes because translations and rotations have zero energy. The vibrational frequencies of the optical modes in platinum trimer and pentamer obtained from static linear response calculations are reported in Table 6.3 in $\rm cm^{-1}$ and meV. Roto-translational modes are not shown. Notice that all the listed frequencies are much smaller than the electronic energy gap both in Pt_3 and Pt_5.

The ionic displacements of the static vibrational modes of the two platinum clusters are represented in Fig. 6.2. In this case, the polarization vectors are real and no vibrational angular momentum can arise. It is worth mentioning that modes $\nu = 1$ and

Table 6.3: Adiabatic vibrational frequencies of the optical modes in platinum trimer and pentamer obtained from static linear response calculations.

	ν	ω_ν (cm^{-1})	ω_ν (meV)
	1	102.4	12.7
Pt_3	2	121.7	15.1
	3	217.7	27.0
	1	54.0	6.7
	2	71.1	8.8
	3	97.0	12.0
	4	103.3	12.8
Pt_5	5	119.6	14.8
	6	134.8	16.7
	7	138.6	17.2
	8	169.4	21.0
	9	210.4	26.1

$\nu = 2$ in trimer are degenerate in the absence of magnetism and spin-orbit interaction. The same occurs for the asymmetric stretching modes $\nu = 6$ and $\nu = 7$ of platinum pentamer.

To our knowledge, only one experimental work on vibrational properties of platinum trimer is available in the literature [101]. It dates back to 1988. The technique employed is photoelectron spectroscopy and the reported optical frequencies are equal to 105 cm^{-1} and 225 cm^{-1}. The vibrational modes of platinum trimer have been studied in density functional theory in Ref. [100], where a non-self-consistent LDA functional method has been used and in Ref. [96] where time-dependent density functional theory is claimed to be used with relativistic core potentials. Our result is partly in agreement with the experiment (one mode is not observed) but disagrees with the other density functional calculations. We could not find any study on vibrational properties of platinum pentamer instead.

6.3 Non-adiabatic effects

Using the first-principles scheme in the spin-dependent framework introduced in section 5.3.1, non-adiabatic effects due to the vibronic coupling are now taken into consideration. By using our own code, we calculate the non-adiabatic vibrational frequencies of platinum clusters in the following two ways.

1. The approximate non-adiabatic force constant matrix $\tilde{C}_{sr}(\omega)$ is calculated as a function of the frequency ω using the vibron self-energy $\Pi_{sr}(\omega)$ of Eq. 5.26.

2. Since vibrational frequencies are much smaller than the electronic gap, we enforce the low-frequency expansion and evaluate the non-adiabatic force constant matrix $\tilde{C}_{sr}(\omega)$ using the KS Berry curvature Eq. 5.16.

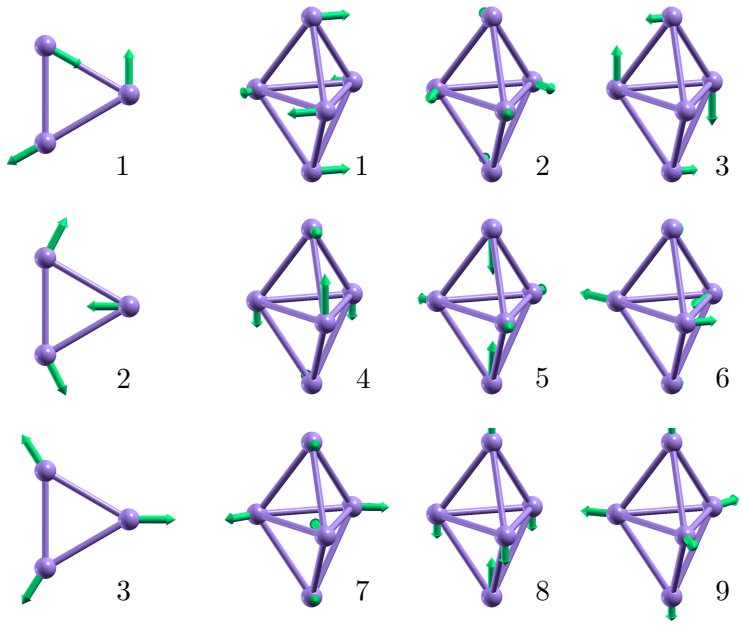

Figure 6.2: Vibrational ionic displacements of the optical modes of platinum trimer and pentamer obtained from self-consistent static linear response. The corresponding vibrational frequencies are listed in Table 6.3.

In both cases, we need the KS eigenvalues and the deformation potential matrix elements of the static self-consistent linear response calculation to evaluate the vibron self-energy or the KS Berry curvature. The nonlinear eigenvalue equation 5.8 is then solved by evaluating the force constant matrix $\tilde{C}_{sr}(\omega)$ at the adiabatic frequency ω_ν of each mode and by diagonalizing its hermitian part divided by the mass. The non-adiabatic vibrational frequencies and polarization vectors are obtained as the square root of the eigenvalues and as the eigenvectors of the force constant matrix, respectively.

For platinum trimer and pentamer the vibrational frequencies thus obtained are shown in the third column of Tab. 6.4 for calculation 1 ($\tilde{\omega}_\nu$) and in the fourth column for calculation 2 ($\tilde{\omega}'_\nu$). Compared to the results of the static linear response theory, it is found that both in Pt_3 and Pt_5 the non-adiabatic corrections on vibrational frequencies are relatively small. Moreover, we notice that the non-adiabatic frequencies obtained from the low-frequency expansion $\tilde{\omega}'_\nu$ are almost identical to the adiabatic ones. This does not mean that the KS Berry curvature vanishes but tells us that vibrational frequencies are not affected by first order terms in the low-frequency expansion of the vibron self-energy.

So far our result can be summarized as follows. Even by considering non-collinear magnetic platinum clusters, which fulfill all the requirements to exhibit non-adiabatic effects due to the electron-vibron interaction (small gap, spin-orbit coupling, etc.), the vibrational frequencies are not sensitive enough to observe such effects. In the following section we will show that other quantities than the vibrational frequencies, such as the vibrational angular momentum, are actually affected by the KS Berry curvature.

Table 6.4: Non-adiabatic vibrational frequencies of optical modes in platinum trimer and pentamer. From left to right, adiabatic mode index ν, adiabatic vibrational frequencies ω_ν, non-adiabatic frequencies $\tilde{\omega}_\nu$ calculated using the vibron self-energy $\Pi_{sr}(\omega)$ of Eq. 5.26, non-adiabatic frequencies $\tilde{\omega}'_\nu$ calculated using the KS Berry curvature Eq. 5.16.

	ν	ω_ν (cm^{-1})	$\tilde{\omega}_\nu$ (cm^{-1})	$\tilde{\omega}'_\nu$ (cm^{-1})
	1	102.4	100.6	102.5
Pt_3	2	121.7	121.2	121.7
	3	217.7	217.7	217.7
	1	54.0	53.6	54.0
	2	71.1	71.1	71.1
	3	97.0	96.6	96.7
	4	103.3	103.5	103.5
Pt_5	5	119.6	119.5	119.6
	6	134.8	134.7	134.7
	7	138.6	138.6	138.6
	8	169.4	169.4	169.5
	9	210.4	209.9	210.5

6.4 Vibrational angular momentum

Even if non-adiabatic effects are small on the frequencies, it is nonetheless worthwhile to calculate the angular momentum of vibrational modes in platinum clusters. In the adiabatic linear response, the vibrational modes are linearly polarized, the eigenvectors of the force constant matrix are real and the vibrational angular momentum vanishes.

Non-adiabatic effects modify the oscillatory motion of the ions around their equilibrium positions in such a way that the eigenvectors are nontrivially complex in platinum clusters. The real ionic displacement is related to the polarization vector through $u_s = \mathrm{Re}\left[\tilde{\varepsilon}_{\nu s} e^{-i\tilde{\omega}_\nu t}\right]$. Therefore, even if the vibrational frequency is not modified by non-adiabatic effects, the trajectory of the ions around equilibrium positions is. As a consequence, each ion gives rise to an orbital angular momentum perpendicular to the plane of the trajectory. For each vibrational mode, the angular momentum of the cluster is equal to the sum of the angular momenta of the rotating ions. Such intrinsic vibrational angular momentum driven by non-adiabatic effects can be evaluated by replacing the non-adiabatic polarization vectors $\tilde{\varepsilon}_{\nu s}$, obtained from time-dependent linear response, into Eq. 5.5.

Because non-adiabatic effects act as local magnetic fields on every atom, the phonon Hamiltonian does not commute with the phonon angular momentum operator $\boldsymbol{N}^{\mathrm{ph}} = \sum_s M_s \boldsymbol{u}_s \times \dot{\boldsymbol{u}}_s$. What we calculate here then is the expectation value of the angular momentum operator over the ground state of the Hamiltonian, namely $\langle N_\alpha \rangle = \frac{1}{2}\sum_\nu \ell_{\nu\alpha}$, where $\alpha = x, y, z$. Hence, this quantity is not a quantized object and it makes sense to list the three Cartesian components $\ell_{\nu\alpha}$. Indeed, when driven by non-adiabatic ef-

fects, $\ell_{\nu\alpha}$ is not equal to the eigenvalue of the phonon angular momentum but rather it is equal to its expectation value over the quantum vibron ground state. It becomes observable in the form of the angular momentum of the classical ionic motion.

As an illustrative example, we represent in Fig. 6.3 the adiabatic and non-adiabatic polarization vectors of two stretching modes of platinum trimer and pentamer obtained as solutions of the nonlinear eigenvalue problem of the force constant matrix $\tilde{C}_{sr}(\omega)$ as described in section 6.3. In both cases the polarization vectors acquire an imaginary part, although small compared to the real part, and the non-adiabatic modes carry nonzero angular momentum as shown in the right hand side of Fig. 6.3 (red arrows).

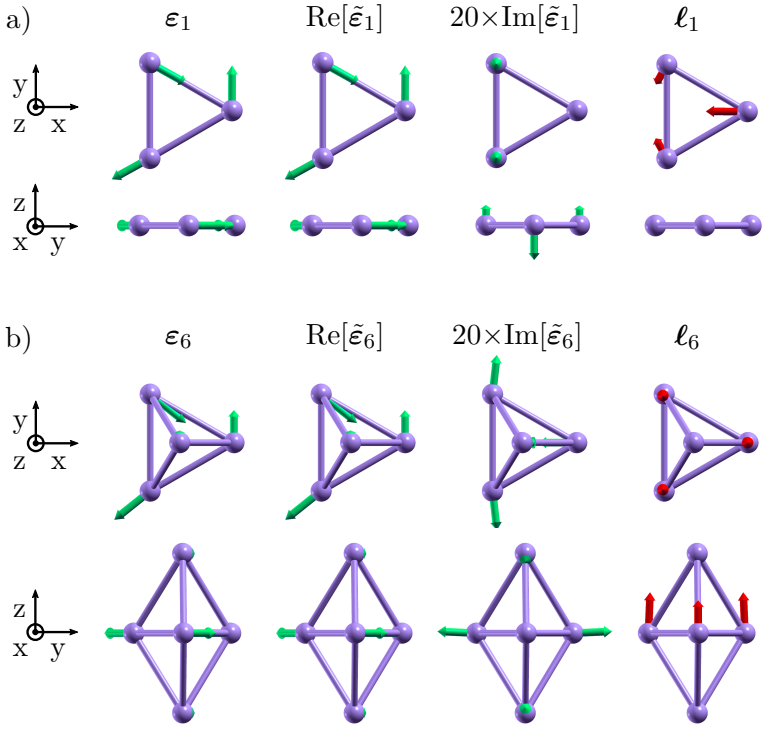

Figure 6.3: Angular momentum of two selected vibrational modes in platinum clusters. From left to right: adiabatic (static) polarization vectors $\boldsymbol{\varepsilon}_\nu$, real and imaginary parts of the non-adiabatic (dynamical) polarization vectors $\tilde{\boldsymbol{\varepsilon}}_\nu$, vibrational angular momentum $\boldsymbol{\ell}_\nu$. From top to bottom: a) top representation (x-y) of platinum trimer, side representation (y-z) of platinum trimer; b) top representation (x-y) of platinum pentamer, side representation (y-z) of platinum pentamer.

In platinum trimer, the imaginary part of the polarization vectors is perpendicular to the the plane of the cluster. The angular momentum of vibrational mode $\nu = 1$ is coplanar with the cluster which means that the atomic vibrations around equilibrium position have a small out-of-plane component.

In platinum pentamer, the optical mode $\nu = 6$ shown in Fig. 6.3 (b) is approximately the same as the asymmetric stretching mode of the trimer. Namely, the eigendisplacements of the vertex atoms are much smaller than the eigendisplacements of the 3

atoms in the basis of the pyramids and these last have high overlap[16] with the eigendisplacements of the trimer shown in Fig. 6.3 (a). However, the imaginary parts of the polarization vectors and consequently the vibrational angular momentum behave differently with respect to the trimer. Notably, the angular momenta of the basis atoms are mainly orthogonal to the basis plane whereas in platinum trimer they are coplanar with the cluster. The non-adiabatic trajectories of the basis atoms in Pt_5 therefore do not come out of the plane.

It is interesting to remark that the imaginary part of the asymmetric stretching mode $\nu = 6$ in platinum pentamer exhibits a similar character as the adiabatic mode $\nu = 7$ (see Fig. 6.2). In the absence of a magnetic order, the two modes are degenerate and a finite angular momentum can be obtained from a linear combination of the polarization vectors. In the present calculation, magnetism and spin-orbit interaction break the degeneracy between the vibrational modes, already in the static linear response. However, a nonzero angular momentum arises only when we include the electron-vibron interaction in the calculation, namely when non-adiabatic effects are taken into account.

The angular momentum of vibrational modes shown in Fig. 6.3 (sum of the angular momenta of the ions) is reported together with the other modes in Tab. 6.5 for platinum trimer and pentamer in units of $\hbar$. We notice that y and z components (with reference to Fig. 6.3 (a) of the angular momentum in platinum trimer always vanish. The same occurs for x and y components in platinum pentamer. This is actually related to the orientation of the atomic magnetic moments and more in general to the non-collinear magnetic order in the two clusters: in trimer the total magnetization is directed along

Table 6.5: Vibrational angular momentum driven by dynamical effects in platinum clusters. The Cartesian components (with reference to Fig. 6.3) of the angular momentum $\boldsymbol{\ell}_\nu$ are listed in units of $\hbar$.

	ν	$\ell_{\nu x}$ ($\hbar$)	$\ell_{\nu y}$ ($\hbar$)	$\ell_{\nu z}$ ($\hbar$)
	1	−0.048	0.000	0.000
Pt_3	2	0.000	0.000	0.000
	3	0.001	0.000	0.000
	1	0.000	0.000	−0.064
	2	0.000	0.000	−0.094
	3	0.001	0.000	−0.089
	4	0.002	0.000	−0.086
Pt_5	5	0.002	0.000	0.000
	6	−0.003	0.000	0.071
	7	0.000	0.000	0.093
	8	0.000	0.000	0.001
	9	0.000	0.000	−0.003

[16]The overlap between polarization vectors of two given vibrational modes can be used as a measure of the matching between the character of the two modes.

the x-axis while in pentamer it is parallel to the z-axis.

Unexpectedly, we record a sizeable vibrational angular momentum even where the vibrational frequency is marginally altered by the non-adiabatic (dynamical) effects. The reason is that vibrational frequencies are affected by non-adiabatic effects only in the second order of the low-frequency expansion of section 5.2 while the polarization vectors and the angular momentum are affected already at the first order. The magnitude of these vibrational angular momenta is of the same order of the typical values of the electron orbital momenta in itinerant ferromagnets [26].

The expectation value of the total angular momentum $\langle \boldsymbol{N}^{\mathrm{ph}} \rangle = \frac{1}{2} \sum_\nu \boldsymbol{\ell}_\nu$ is nonzero too because the Cartesian components of $\boldsymbol{\ell}_\nu$ have been calculated for each mode at different frequencies (namely at the frequencies $\tilde{\omega}_\nu$). Since the angular momentum of the cluster must be conserved, a non-adiabatic variation of the electron angular momentum (spin plus orbital) must also occur in order to compensate the phonon contribution. The calculation of such variation, however, requires simulating the non-adiabatic dynamics of the whole cluster, which goes beyond the purpose of this work.

6.5 Summary

Non-adiabatic effects due to the vibronic coupling are time-reversal symmetry breaking interactions for the vibrational field in non-collinear magnetic molecules with vibrational frequencies much smaller than the electronic gap. As a proof of concept, we studied non-adiabatic effects in two platinum clusters with non-collinear magnetic order, namely a trimer and a pentamer.

In these systems, we calculated the electronic structure and vibrational properties by performing fully relativistic ab-initio calculations. The non-collinear magnetic arrangement together with a geometrical distortion of the symmetric structure was found to minimize the total energy in both platinum clusters. We then compared the electronic structure properties with existing data in literature, resulting in good agreement with some of the previous studies.

Subsequently, we analysed adiabatic and non-adiabatic vibrational properties. We found that non-adiabatic corrections to the vibrational frequencies of platinum clusters are not observable notwithstanding magnetism, spin-orbit coupling and the small electronic gap. However, we recorded a nonzero vibrational angular momentum for some modes in platinum clusters, the magnitude of which being of the same order of electrons orbital momenta in itinerant ferromagnets. Such result confirms that non-adiabatic effects can induce a finite intrinsic vibrational angular momentum in non-collinear magnetic molecules.

As the same conclusions obtained for molecules can be easily generalized to insulating crystals, we expect that in any non-collinear magnetic system (solid or molecule) with strong electron-phonon interaction and sufficiently small gap non-adiabatic effects break time-reversal symmetry for the vibrational field and induce sizeable phonon angular momenta in the absence of external probes.

Chapter 7

Non-adiabatic effects in non-collinear magnetic periodic systems

Let us now move on to the most general results obtained for solids. Insulating solids with vibrational frequencies smaller than the bandgap can be handled in the same way as molecular systems and therefore they do not present particular difficulties. Still, they constitute an intermediate step between molecules and metals and thus it is useful to rapidly go through it. We show that the non-adiabatic force constant matrix in insulating periodic systems is related to the Berry curvature of the Kohn-Sham (KS) states defined in the space of the ionic displacements. When the curvature vanishes, in time-reversal symmetric systems, the vibrational modes are linearly polarized and do not carry angular momentum. On the other hand, in non-collinear magnetic systems, one can get a nonzero vibrational angular momentum driven by non-adiabatic effects.

Here, we generalize the definition of the KS Berry curvature to all insulating and metallic systems. In this case the phonon self-energy can be expanded in power series of the frequency by retaining a nonzero broadening η. Although nonlinear order terms in the expansion cannot in principle be neglected, the non-adiabatic force constant matrix in the low-frequency limit can be expressed in terms of the generalized Berry curvature as in molecular systems. We compare the nonlinear eigenvalue problem of the non-adiabatic dynamical matrix with the theory of lattice dynamics presented in section 3.2.2. Because the KS Berry curvature breaks time-reversal symmetry for the lattice dynamics, a finite angular momentum can be obtained for non-degenerate modes in the absence of external fields.

In the second part of the chapter, we extend the first-principles scheme described in section 4.4 to calculate non-adiabatic phonons in non-collinear magnetic insulating and metallic periodic systems by exploiting the properties of the time-reversal operator. In doing so, we adopt the method proposed in references [21,87] and presently implemented in the phonon linear response package of Quantum-Espresso. In the suite, we modify the electron-phonon calculation accordingly and write a code to implement the first-principles scheme and calculate the phonon angular momentum.

7.1 Non-adiabatic effects and topology in solids

The non-adiabatic dynamical matrix, as approximated in section 4.4, can be expressed in power series of the frequency ω, even for metals provided that the parameter η is kept finite. The first term of the expansion is related to the KS Berry curvature expressed in linear response theory.

Here, we generalize the results obtained in section 5.2 for insulating molecules to periodic extended systems, insulators and metals. Throughout this section we do not explicitly include the spin dependence in the deformation potential matrix elements and the temperature in the phonon self-energy. For periodic systems, the phonon self-energy $\Pi_{IJ}(\omega)$, as a function of the frequency ω, is given by

$$\Pi_{IJ}(\omega) = 2 \sum_{\mathbf{k}i,\mathbf{k}'j}^{N_k} \left[\frac{f_{\mathbf{k}i} - f_{\mathbf{k}'j}}{\epsilon_{\mathbf{k}i} - \epsilon_{\mathbf{k}'j} + \omega + i\eta} - \frac{f_{\mathbf{k}i} - f_{\mathbf{k}'j}}{\epsilon_{\mathbf{k}i} - \epsilon_{\mathbf{k}'j}} \right] \langle \psi_{\mathbf{k}'j} | \frac{\partial V_{\mathrm{KS}}}{\partial u_I} | \psi_{\mathbf{k}i} \rangle \langle \psi_{\mathbf{k}i} | \frac{\partial V_{\mathrm{KS}}}{\partial u_J} | \psi_{\mathbf{k}'j} \rangle \tag{7.1}$$

where, compared to the molecular case, the band index i is now accompanied with a crystal momentum index $\mathbf{k}$ both in KS eigenvalues and eigenfunctions, and the ionic indexes I and J also include the cell indexes, unlike s and r.

7.1.1 Insulators with vibrational frequencies smaller than the bandgap

In insulators with vibrational frequencies smaller than the bandgap, the non-adiabatic part of the force constant matrix can be expanded in power series of the frequency ω, by setting $\eta = 0$ in Eq. 7.1. In this case, the phonon self-energy

$$\Pi_{IJ}(\omega) = \sum_{n=1}^{\infty} \left[2 \sum_{\mathbf{k}i,\mathbf{k}'j}^{N_k} \frac{f_{\mathbf{k}i} - f_{\mathbf{k}'j}}{\epsilon_{\mathbf{k}i} - \epsilon_{\mathbf{k}'j}} \frac{(-1)^n}{(\epsilon_{\mathbf{k}i} - \epsilon_{\mathbf{k}'j})^n} \langle \psi_{\mathbf{k}'j} | \frac{\partial V_{\mathrm{KS}}}{\partial u_I} | \psi_{\mathbf{k}i} \rangle \langle \psi_{\mathbf{k}i} | \frac{\partial V_{\mathrm{KS}}}{\partial u_J} | \psi_{\mathbf{k}'j} \rangle \right] \omega^n \tag{7.2}$$

is hermitian in the ionic indexes I and J and the coefficient of the n-th term of the expansion is equal to the n-th derivative of the self-energy with respect to ω, evaluated at $\omega = 0$. As for molecular systems, the odd (even) coefficients of the expansion are purely imaginary (real). We stress that the self-energy Eq. 7.2 is well defined in insulators because the difference $\epsilon_{\mathbf{k}i} - \epsilon_{\mathbf{k}'j}$ is always greater than or equal to the electronic bandgap when the numerator $f_{\mathbf{k}i} - f_{\mathbf{k}'j}$ is nonzero.

If the vibrational frequencies are much smaller than the electronic bandgap, then we can neglect higher than linear order terms in the series expansion and rewrite the non-adiabatic part of the self-energy in the form

$$\Pi_{IJ}(\omega) \simeq -i\omega\Omega_{IJ}^{KS} = -2i\omega \sum_{\mathbf{k}i}^{N_k} f_{\mathbf{k}i} \Omega_{IJ,\mathbf{k}i}^{KS} \tag{7.3}$$

$$\Omega_{IJ,\mathbf{k}i}^{KS} = 2\mathrm{Im} \sum_{\mathbf{k}'j}^{N_k} \frac{\langle \psi_{\mathbf{k}'j} | \frac{\partial V_{\mathrm{KS}}}{\partial u_I} | \psi_{\mathbf{k}i} \rangle \langle \psi_{\mathbf{k}i} | \frac{\partial V_{\mathrm{KS}}}{\partial u_J} | \psi_{\mathbf{k}'j} \rangle}{(\epsilon_{\mathbf{k}i} - \epsilon_{\mathbf{k}'j})^2} \tag{7.4}$$

where $\Omega_{IJ,\mathbf{k}i}^{KS}$ is the Berry curvature associated with the KS eigenstate $|\psi_{\mathbf{k}i}\rangle$ and the phonon ionic displacements u_I, u_J (see Eq. 2.33).

In analogy with the case of insulating molecular systems, the phonon self-energy in the low-frequency limit can therefore be expressed in terms of a real antisymmetric matrix Ω_{IJ}^{KS} that plays the role of the Berry curvature in the case of KS independent electrons.

If the vibrational frequencies range between roughly half of the energy gap and the energy gap, the expansion Eq. 7.2 is still valid but higher than linear order terms cannot be neglected. In any event, the ω^2 order term is real and symmetric. Thence, it can be incorporated in the adiabatic force constant matrix as it does not significantly modify the eigenvalue problem. Higher order terms in the frequency ω are not harmonic.

7.1.2 Insulators with vibrational frequencies larger than the bandgap and metals

In insulators with the vibrational frequencies similar to bandgap as well as in metals, the phonon self-energy cannot be expanded in power series as in Eq. 7.2 because the coefficients in the square brackets diverge. Non-adiabatic effects can be obtained from the full self-energy $\Pi_{IJ}(\omega)$ with $\eta \neq 0$. We already pointed out that η is not just a mathematical workaround but it physically represents the electron momentum-scattering rate. Notice that for $\omega = 0$ and $\eta \neq 0$ the phonon self-energy Eq. 7.1 does not vanish, namely the non-adiabatic force constant matrix does not coincide with the adiabatic one in the zero frequency limit due to the finite broadening. Then, one can relate the phonon self-energy with a more generally defined KS Berry curvature, demonstrating the link between non-adiabatic effects and geometric properties also in metals.

Even if a proper series expansion of the phonon self-energy is not possible in metals, it is still interesting to see how the non-adiabatic part of the force constant matrix behaves in the low-frequency limit. Since we are interested in the calculation of the dynamical matrix, let us consider the hermitian part of the self-energy $\Pi_{IJ}^{H}(\omega) = \frac{1}{2}\left[\Pi_{IJ}(\omega) + \Pi_{JI}(-\omega)\right]$ where $\Pi_{IJ}(\omega)$ is given by Eq. 7.1. Such quantity can be also written in the form

$$\Pi_{IJ}^{H}(\omega) = 2 \sum_{\mathbf{k}i,\mathbf{k}'j}^{N_k} \frac{f_{\mathbf{k}i} - f_{\mathbf{k}'j}}{\epsilon_{\mathbf{k}i} - \epsilon_{\mathbf{k}'j}} \mathcal{W}_{\mathbf{k}i,\mathbf{k}'j}(\omega) \langle \psi_{\mathbf{k}'j} | \frac{\partial V_{\mathrm{KS}}}{\partial u_I} | \psi_{\mathbf{k}i} \rangle \langle \psi_{\mathbf{k}i} | \frac{\partial V_{\mathrm{KS}}}{\partial u_J} | \psi_{\mathbf{k}'j} \rangle \tag{7.5}$$

where the weighting function $\mathcal{W}$ is defined as

$$\mathcal{W}_{\mathbf{k}i,\mathbf{k}'j}(\omega) = -\frac{\omega(\epsilon_{\mathbf{k}i} - \epsilon_{\mathbf{k}'j} + \omega) + \eta^2}{(\epsilon_{\mathbf{k}i} - \epsilon_{\mathbf{k}'j} + \omega)^2 + \eta^2}. \tag{7.6}$$

This function is well behaved for any value of ω and $\eta \neq 0$. We can expand it in Taylor series around $\omega = 0$ as

$$\mathcal{W}_{\mathbf{k}i,\mathbf{k}'j}(\omega \approx 0) = \sum_n \frac{1}{n!} \mathcal{W}^{(n)}_{\mathbf{k}i,\mathbf{k}'j} \omega^n \tag{7.7}$$

where $\mathcal{W}^{(n)}_{\mathbf{k}i,\mathbf{k}'j}$ is the n-th derivative of $\mathcal{W}_{\mathbf{k}i,\mathbf{k}'j}(\omega)$ evaluated at $\omega = 0$. Note that here n runs from 0 to ∞ whereas in the series expansion of insulators the index ran from

1 to ∞. It can be shown that, under exchange of the band and momentum indexes $\mathbf{k}i \leftrightarrow \mathbf{k}'j$, the n-th derivative of $\mathcal{W}$ has the same parity of n, namely

$$\mathcal{W}^{(n)}_{\mathbf{k}i,\mathbf{k}'j} = (-1)^n \mathcal{W}^{(n)}_{\mathbf{k}'j,\mathbf{k}i}. \tag{7.8}$$

When expanding the self-energy Eq. 7.5 in Taylor series, we can separate the even and odd derivatives of $\mathcal{W}$. By doing so, the part containing the even derivatives is real and symmetric under exchange of the ionic indexes I and J, while the part containing the odd derivatives is imaginary and antisymmetric. The hermitian part of the self-energy $\Pi^H_{IJ}(\omega)$, in the zero frequency limit, reads

$$\begin{aligned}\Pi^H_{IJ}(\omega \approx 0) =& 4\mathrm{Re} \sum_{\mathbf{k}i,\mathbf{k}'j}^{N_k} \frac{f_{\mathbf{k}i}}{\epsilon_{\mathbf{k}i} - \epsilon_{\mathbf{k}'j}} \left[\mathcal{W}^{(0)}_{\mathbf{k}i,\mathbf{k}'j} + \frac{1}{2}\mathcal{W}^{(2)}_{\mathbf{k}i,\mathbf{k}'j}\omega^2 + \dots \right] \langle \psi_{\mathbf{k}'j} | \frac{\partial V_{\mathrm{KS}}}{\partial u_I} | \psi_{\mathbf{k}i} \rangle \langle \psi_{\mathbf{k}i} | \frac{\partial V_{\mathrm{KS}}}{\partial u_J} | \psi_{\mathbf{k}'j} \rangle \\ &+ 4i\mathrm{Im} \sum_{\mathbf{k}ij}^{N_k} \frac{f_{\mathbf{k}i}}{\epsilon_{\mathbf{k}i} - \epsilon_{\mathbf{k}'j}} \left[\mathcal{W}^{(1)}_{\mathbf{k}i,\mathbf{k}'j}\omega + \dots \right] \langle \psi_{\mathbf{k}'j} | \frac{\partial V_{\mathrm{KS}}}{\partial u_I} | \psi_{\mathbf{k}i} \rangle \langle \psi_{\mathbf{k}i} | \frac{\partial V_{\mathrm{KS}}}{\partial u_J} | \psi_{\mathbf{k}'j} \rangle .\end{aligned} \tag{7.9}$$

In the limit $\eta \to 0$, the coefficients in the square bracket are all the more divergent as the power of ω increases, but for the zero order term which vanishes. When $\eta \neq 0$, the zero order term of the expansion, being real and symmetric, can be incorporated in the adiabatic force constant matrix as a constant. The hermitian part of the approximate force constant matrix in the small frequency limit thus reads

$$\tilde{C}^H_{IJ}(\omega \approx 0) = C_{IJ}(0) + \Pi^H_{IJ}(0) - i\omega\Omega^{\mathrm{KS}}_{IJ} + \mathcal{O}(\omega^2) \tag{7.10}$$

where the coefficients of the linear term can be viewed as a generalized KS Berry curvature for metals defined in the same way as for insulators but for the small imaginary part η of the frequency ω, namely

$$\Omega^{\mathrm{KS}}_{IJ} = 2\sum_{\mathbf{k}i} f_{\mathbf{k}i}\Omega^{\mathrm{KS}}_{IJ,\mathbf{k}i} \tag{7.11}$$

$$\Omega^{\mathrm{KS}}_{IJ,\mathbf{k}i} = 2\mathrm{Im} \sum_{\mathbf{k}'j} \frac{\langle \psi_{\mathbf{k}'j} | \frac{\partial V_{\mathrm{KS}}}{\partial u_I} | \psi_{\mathbf{k}i} \rangle \langle \psi_{\mathbf{k}i} | \frac{\partial V_{\mathrm{KS}}}{\partial u_J} | \psi_{\mathbf{k}'j} \rangle}{(\epsilon_{\mathbf{k}i} - \epsilon_{\mathbf{k}'j} + i\eta)(\epsilon_{\mathbf{k}i} - \epsilon_{\mathbf{k}'j} - i\eta)} \tag{7.12}$$

where $\Omega^{\mathrm{KS}}_{IJ,\mathbf{k}i}$ is the Berry curvature associated with the KS eigenstate $|\psi_{\mathbf{k}i}\rangle$ and the phonon ionic displacements u_I and u_J. Note that, when defined as in Eq. 7.12, the Berry curvature includes the definition given for insulators as the limit $\eta = 0$. Such result can therefore be understood as the link between low-frequency non-adiabatic effects due to the electron-phonon coupling and topological effects in both insulating and metallic periodic systems.

7.2 The Kohn-Sham Berry curvature in reciprocal space

In order to relate the just seen result with the phonon eigenvalue problem in the screened Born-Oppenheimer approximation Eq. 3.34, we now aim at writing the phonon self-energy in reciprocal space as a function of the Fourier component of the Berry curvature.

For both metals and insulators, the phonon self-energy in reciprocal space can be written in density functional perturbation theory from Eq. 4.52 as

$$\Pi_{sr}(\mathbf{q},\omega) = \frac{2}{N_k}\sum_{\mathbf{k}ij}^{N_k}\left[\frac{f_{\mathbf{k+q}i}-f_{\mathbf{k}j}}{\epsilon_{\mathbf{k+q}i}-\epsilon_{\mathbf{k}j}+\omega+i\eta} - \frac{f_{\mathbf{k+q}i}-f_{\mathbf{k}j}}{\epsilon_{\mathbf{k+q}i}-\epsilon_{\mathbf{k}j}}\right] \times \langle u_{\mathbf{k}j}|\frac{\partial v_{\mathrm{KS}}}{\partial \mathbf{u}_{-\mathbf{q}s}}|u_{\mathbf{k+q}i}\rangle\langle u_{\mathbf{k+q}i}|\frac{\partial v_{\mathrm{KS}}}{\partial \mathbf{u}_{\mathbf{q}r}}|u_{\mathbf{k}j}\rangle \quad (7.13)$$

where $\mathbf{q}$ is the phonon quasimomentum, $u_{\mathbf{k}j}(\mathbf{r})$ is the lattice periodic part of the KS wavefunction and v_{KS} is the periodic part of the KS potential. Analogously to what we did for the self-energy in real space, we can consider the hermitian part of the self-energy and expand it in Taylor series around $\omega = 0$. Again, the expansion is legitimate in metals only if $\eta \neq 0$. In reciprocal space the coefficients of the expansion can be written in the form

$$\Pi^{H\,(n)}_{sr}(\mathbf{q},\omega) = \frac{2}{N_k}\sum_{\mathbf{k}i}^{N_k} f_{\mathbf{k}i}\left[\mathcal{Y}^{(n)}_{sr,\mathbf{k}i}(\mathbf{q}) + (-1)^n \mathcal{Y}^{(n)}_{rs,\mathbf{k}i}(-\mathbf{q})\right] \quad (7.14)$$

where the term in the square brackets is equal to the sum of some coefficients $\mathcal{Y}^{(n)}_{sr,\mathbf{k}i}(\mathbf{q})$ and its transpose (in the ionic indexes s and r) at $-\mathbf{q}$ for n even, to the difference for n odd. The sum/difference in the square bracket indeed corresponds to the real/imaginary part of the matrix elements in the real space self-energy Eq. 7.9. The functions $\mathcal{Y}^{(n)}$ are defined as

$$\mathcal{Y}^{(n)}_{sr,\mathbf{k}i}(\mathbf{q}) = \sum_j \frac{1}{\epsilon_{\mathbf{k}i}-\epsilon_{\mathbf{k+q}j}}\mathcal{W}^{(n)}_{\mathbf{k}i,\mathbf{k+q}j}\langle u_{\mathbf{k}i}|\frac{\partial v_{\mathrm{KS}}}{\partial \mathbf{u}_{-\mathbf{q}s}}|u_{\mathbf{k+q}j}\rangle\langle u_{\mathbf{k+q}j}|\frac{\partial v_{\mathrm{KS}}}{\partial \mathbf{u}_{\mathbf{q}r}}|u_{\mathbf{k}i}\rangle \quad (7.15)$$

where the real coefficients $\mathcal{W}^{(n)}_{\mathbf{k}i,\mathbf{k+q}j}$ have been defined in the previous section and have the same parity of n under exchange of the band and momentum indexes. For $n = 1$ the coefficients of the expansion can be expressed in terms of the Fourier transform of the KS Berry curvature Eq. 7.12 as

$$\Pi^{H\,(1)}_{sr}(\mathbf{q},\omega) = -i\Omega^{\mathrm{KS}}_{sr}(\mathbf{q}) \quad (7.16)$$

$$\Omega^{\mathrm{KS}}_{sr}(\mathbf{q}) = 2\sum_{\mathbf{k}i}^{N_k} f_{\mathbf{k}i}\Omega^{\mathrm{KS}}_{sr,\mathbf{k}i}(\mathbf{q}) = 2i\sum_{\mathbf{k}i}^{N_k} f_{\mathbf{k}i}\left[\mathcal{Y}^{(1)}_{sr,\mathbf{k}i}(\mathbf{q}) - \mathcal{Y}^{(1)}_{rs,\mathbf{k}i}(-\mathbf{q})\right] \quad (7.17)$$

$$\mathcal{Y}^{(1)}_{sr,\mathbf{k}i}(\mathbf{q}) = -\sum_j \frac{\langle u_{\mathbf{k}i}|\frac{\partial V_{\mathrm{KS}}}{\partial u_{-\mathbf{q}s}}|u_{\mathbf{k+q}j}\rangle\langle u_{\mathbf{k+q}j}|\frac{\partial v_{\mathrm{KS}}}{\partial u_{\mathbf{q}r}}|u_{\mathbf{k}i}\rangle}{(\epsilon_{\mathbf{k+q}j}-\epsilon_{\mathbf{k}i}+i\eta)(\epsilon_{\mathbf{k+q}j}-\epsilon_{\mathbf{k}i}-i\eta)}. \quad (7.18)$$

When written in this form, is can be easily verified that the KS Berry curvature in reciprocal space satisfies the following relations

$$\Omega^{KS}_{sr}(-\mathbf{q}) = \left[\Omega^{KS}_{sr}(\mathbf{q})\right]^* = -\Omega^{KS}_{rs}(\mathbf{q}), \quad (7.19)$$

namely the complex conjugate operation reverses the sign of $\mathbf{q}$ as it happens for any real function in direct space, and it is antihermitian since the coefficients $\mathcal{Y}^{(n)}$ are hermitian.

7.2.1 Nonlinear eigenvalue problem

In the low-frequency limit, by neglecting nonlinear order terms, the non-adiabatic dynamical matrix Eq. 4.53 can finally be written in the form

$$\tilde{D}_{sr}(\mathbf{q}, \omega \approx 0) \simeq \frac{1}{\sqrt{M_s M_r}} \left[C_{sr}(\mathbf{q}) - i\omega \Omega^{\mathrm{KS}}_{sr}(\mathbf{q}) \right] \tag{7.20}$$

where the zero order term of the expansion $\Pi^{H}_{sr}(\mathbf{q}, \omega = 0)$, which vanishes in insulators, is contained in the adiabatic force constant matrix $C_{sr}(\mathbf{q})$ and $\Omega^{\mathrm{KS}}_{sr}(\mathbf{q})$ is the Fourier transform of the generalized KS Berry curvature from Eq. 7.12. The nonlinear eigenvalue problem for the non-adiabatic dynamical matrix can therefore be written as

$$\sum_r \frac{1}{\sqrt{M_s M_r}} \left[C_{sr}(\mathbf{q}) - i\tilde{\omega}_{\mathbf{q}} \Omega^{\mathrm{KS}}_{sr}(\mathbf{q}) \right] \tilde{\boldsymbol{\varepsilon}}_r(\mathbf{q}) = \tilde{\omega}^2_{\mathbf{q}} \tilde{\boldsymbol{\varepsilon}}_s(\mathbf{q}). \tag{7.21}$$

This last equation, obtained from the non-adiabatic description of vibrational modes in the low-frequency limit, is equal to the eigenvalue problem Eq. 3.34 that we have encountered in the theory of harmonic lattice vibrations in the screened Born-Oppenheimer approximation. The nonlinear eigenvalue problem Eq. 7.21 can thus be solved by following the procedure detailed in section 3.2.2. Namely by defining an effective non-hermitian Hamiltonian for the coordinates and momenta polarization vectors and by introducing second quantization relations for the latter. In practice, we solve the nonlinear eigenvalue problem 7.21 numerically, with an iterative procedure, as discussed in section 4.4.3.

7.2.2 Phonon angular momentum

The solutions yield non-adiabatic phonon frequencies $\tilde{\omega}_{\mathbf{q}\nu}$ and polarization vectors $\tilde{\boldsymbol{\varepsilon}}_{\nu r}(\mathbf{q})$, labeled with a branch index ν. According to the properties of the curvature Eq. 7.19, it may seem that the non-adiabatic frequencies are odd functions of the momentum $\mathbf{q}$, namely $\tilde{\omega}_{\mathbf{q}} = -\tilde{\omega}_{-\mathbf{q}}$, and that the phonon polarization vectors obey the condition $\tilde{\boldsymbol{\varepsilon}}^*_s(\mathbf{q}) = \tilde{\boldsymbol{\varepsilon}}_s(-\mathbf{q})$.

Actually, the eigenvectors of the non-adiabatic dynamical matrix should be thought, strictly speaking, as a function of the frequency ω themselves, that is $\tilde{\boldsymbol{\varepsilon}}^*_s(\mathbf{q}, \omega)$. The fundamental relation $\tilde{D}^*(\mathbf{q}, \omega) = \tilde{D}(-\mathbf{q}, -\omega)$ holds for the non-adiabatic dynamical matrix (and for the hermitian part of the phonon self-energy). It follows that the eigenvectors obey the condition $\tilde{\boldsymbol{\varepsilon}}^*(\mathbf{q}, \omega) = \tilde{\boldsymbol{\varepsilon}}(-\mathbf{q}, -\omega)$. In this case, the phonon frequencies are even function of the momentum $\mathbf{q}$ and the complex conjugation on the phonon polarization vectors does not in general change the sign of $\mathbf{q}$, namely $\tilde{\boldsymbol{\varepsilon}}^*_{\nu s}(\mathbf{q}) \neq \tilde{\boldsymbol{\varepsilon}}_{\nu s}(-\mathbf{q})$. We summarize this result as

$$\tilde{\omega}_{\mathbf{q}\nu} = \tilde{\omega}_{-\mathbf{q}\nu} \tag{7.22}$$

$$\tilde{\boldsymbol{\varepsilon}}^*_{\nu s}(\mathbf{q}, \omega_{\mathbf{q}\nu}) = \tilde{\boldsymbol{\varepsilon}}_{\nu s}(-\mathbf{q}, -\omega_{\mathbf{q}\nu}). \tag{7.23}$$

Consequently, a finite phonon angular momentum can arise even for non-degenerate modes in the absence of external fields due to non-adiabatic effects. The phonon angular

momentum of the non-adiabatic mode ν with wavevector $\mathbf{q}$ can be calculated from the phonon polarization vectors as

$$\tilde{\boldsymbol{\ell}}_{\mathbf{q}\nu} = -i\hbar \sum_s \tilde{\boldsymbol{\varepsilon}}^*_{\nu s}(\mathbf{q}, \omega_{\mathbf{q}\nu}) \times \tilde{\boldsymbol{\varepsilon}}_{\nu s}(\mathbf{q}, \omega_{\mathbf{q}\nu}). \tag{7.24}$$

The expectation value of the total phonon angular momentum at zero temperature reads $\langle \mathbf{N}^{\mathrm{ph}} \rangle = \frac{1}{2} \sum_{\mathbf{q}\nu} \tilde{\boldsymbol{\ell}}_{\mathbf{q}\nu}$ (see Eq. 3.48). Since in this framework $\tilde{\boldsymbol{\varepsilon}}^*_{\nu s}(\mathbf{q}) \neq \tilde{\boldsymbol{\varepsilon}}_{\nu s}(-\mathbf{q})$, the angular momentum $\tilde{\boldsymbol{\ell}}_{\mathbf{q}\nu}$ is not an even function of $\mathbf{q}$ and the expectation value of the total angular momentum $\langle \mathbf{N}^{\mathrm{ph}} \rangle$ can be different from zero. Once again we stress that $\tilde{\boldsymbol{\ell}}_{\mathbf{q}\nu}$ is not the eigenvalue of the phonon angular momentum operator given that non-adiabatic effects act locally on each atom.

The important findings of this section can be summarized as follows. The phonon angular momentum and non-adiabatic effects are related to the electronic KS Berry curvature in the low-frequency limit. The KS Berry curvature in Eq. 7.21 breaks time-reversal symmetry of the phonon eigenvalue problem as a result of the electron-phonon interaction. When the curvature is nonzero, the non-adiabatic vibrational modes are nonlinearly polarized and carry a finite angular momentum.

7.2.3 Discussion

The limits of the present demonstration are the following. While the series expansion is fully justified in insulators with vibrational frequencies much smaller than the bandgap, in other materials the series expansion makes sense only if the parameter η is different from 0. The parameter represents the electron momentum-scattering rate due to all possible momentum-exchange scattering mechanisms. Its value slightly affects the phonon frequencies losing the adiabatic limit to the non-adiabatic spectrum. In the explicit calculation, the broadening η will also affect the phonon angular momentum but does not change the qualitative result.

Furthermore, given the series expansion for metals, we have unduly neglected higher order terms which are not related with the Berry curvature. In insulators, the linear approximation is justified if the vibrational frequencies are much smaller than the bandgap. When this is not the case and in metals, nonlinear ω-terms in the phonon self-energy are not necessarily small. However, non-adiabatic effects obtained by approximating the non-adiabatic dynamical matrix as in Eq. 7.21 are qualitatively the same as for the calculation with the full self-energy Eq. 7.13.

The derivation of the nonlinear eigenvalue problem Eq. 7.21 was intended to make evident the link between non-adiabatic effects due to the electron-phonon coupling and the Berry's formalism. When computing the force constant functional without series expansion, namely using the full self-energy Eq. 7.13, the phonon polarization vectors still comply with Eq. 7.23. Non-adiabatic vibrational modes thus can host nonzero angular momenta even if they are not related with the geometrical properties of the system. Nevertheless, the description of non-adiabatic effects via the KS Berry curvature provides the basis to determine in which systems phonons can host a sizeable angular momentum. Because the electronic wavefunctions can be taken in such a way that the deformation potential matrix elements are real in nonmagnetic and collinear

magnetic systems, we need to consider non-collinear magnetic systems in order to observe an intrinsic phonon angular momentum driven by non-adiabatic effects. In the next section we therefore extend the spin-dependent theory of non-adiabatic effects to the case of non-collinear magnetic periodic systems.

7.3 Spin-dependent non-adiabatic effects in solids

In spin density functional theory, the KS Hamiltonian $H_{\rm KS}^{[\mathbf{B}]}$ depends on the exchange-correlation magnetic field $\mathbf{B}$. Here $\mathbf{B}$ can also be an external magnetic field. When the time-reversal operator is applied to the Hamiltonian it changes the sign of the magnetic field, namely $\mathcal{T}H_{\rm KS}^{[\mathbf{B}]} = H_{\rm KS}^{[-\mathbf{B}]}\mathcal{T}$. We then consider two KS equations, one for $\mathbf{B}$ and one for $-\mathbf{B}$, and label the eigenvalues and eigenvectors with the superscript $[\mathbf{B}]$ and $[-\mathbf{B}]$ respectively. By comparing the solutions of the two equations, it can be shown that

$$\epsilon_{\mathbf{k}m}^{[-\mathbf{B}]} = \epsilon_{-\mathbf{k}m}^{[\mathbf{B}]} \tag{7.25}$$

$$|\psi_{\mathbf{k}m}^{[-\mathbf{B}]}\rangle = e^{i\varphi}|\mathcal{T}\psi_{-\mathbf{k}m}^{[\mathbf{B}]}\rangle \tag{7.26}$$

where $|\mathcal{T}\psi_{-\mathbf{k}m}^{[\mathbf{B}]}\rangle$ is the time-reversed eigenstate at $\mathbf{B}$ and φ is a $\mathbf{k}$-independent phase.

In the nonmagnetic case $\mathbf{B} = 0$, the Bloch wavefunction at $\mathbf{k}$ is related to the Bloch wavefunction at $-\mathbf{k}$ via time-reversal symmetry, namely $|\psi_{\mathbf{k}m}\rangle = e^{i\varphi}|\mathcal{T}\psi_{-\mathbf{k}m}\rangle$, and the pair is degenerate due to Kramers theorem, namely $\epsilon_{\mathbf{k}m} = \epsilon_{-\mathbf{k}m}$. In magnetic systems, the eigenfunction at k of the KS problem with magnetic field $\mathbf{B}$ can only be related to the time-reversed eigenfunction at $-\mathbf{k}$ of the KS problem with magnetic field $-\mathbf{B}$.

When it comes to the calculation of the phonon linear response in non-collinear magnetic solids, the calculation of the adiabatic or non-adiabatic dynamical matrix requires both the responses at $\mathbf{q}$ and $-\mathbf{q}$. In our implementation, we adopt the more convenient method proposed in reference [87] based on the usage of time-reversal operator to avoid calculation of the response at $-\mathbf{q}$. Before writing the phonon self-energy as the sum of a $\mathbf{B}$ and $-\mathbf{B}$ terms, in the next subsections we generalize the theory of non-adiabatic effects to non-collinear magnetic periodic systems for the $\mathbf{B}$ field only.

7.3.1 Time-dependent linear response

Here, we express the phonon response functions in the time-dependent spin density functional perturbation theory for solids. The derivative of the four-vector spin density in the frequency domain with respect to the phonon ionic displacement can be written for solids (insulators and metals) in the form

$$\frac{\partial\rho_\mu(\mathbf{r},\omega)}{\partial u_I} = \sum_{\mathbf{k}i,\mathbf{k}'j}^{N_k} \frac{f_{\mathbf{k}i} - f_{\mathbf{k}'j}}{\epsilon_{\mathbf{k}i} - \epsilon_{\mathbf{k}'j} + \omega + i\eta} \sum_{\sigma_1\sigma_2} \langle\psi_{\mathbf{k}'j}^{\sigma_1}| \frac{\partial V_{\rm KS}^{\sigma_1\sigma_2}(\mathbf{r},\omega)}{\partial u_I} |\psi_{\mathbf{k}i}^{\sigma_2}\rangle \sum_{\sigma\sigma'} \psi_{\mathbf{k}i\sigma}^*(\mathbf{r})\psi_{\mathbf{k}'j\sigma'}(\mathbf{r})\sigma_\mu^{\sigma\sigma'} \tag{7.27}$$

where, compared to Eq. 5.20 for molecules, the KS eigenvalues and eigenvectors as well as the Fermi occupation functions are labeled with the crystal momentum $\mathbf{k}$ in solids.

The phonon ionic displacement carries a cell index L in addition to the ionic index s, namely $I = \{L, s\}$. The Cartesian index is always omitted. We recall that, in Eq. 7.27 the index μ runs from 0 to 3 where $\mu = 0$ corresponds to the trace of the spin density matrix, namely $\rho_0(\mathbf{r}) = n(\mathbf{r})$, whereas the remaining three values of μ correspond to the Cartesian components of the magnetization density, namely $\rho_\alpha(\mathbf{r}) = m_\alpha(\mathbf{r})$.

In a similar fashion, the frequency dependent force constant matrix can be expressed for periodic systems as

$$C_{IJ}(\omega) = \sum_{\mathbf{k}i,\mathbf{k}'j}^{N_k} \frac{f_{\mathbf{k}i} - f_{\mathbf{k}'j}}{\epsilon_{\mathbf{k}i} - \epsilon_{\mathbf{k}'j} + \omega + i\eta} \sum_{\sigma_1\sigma_2} \langle \psi^{\sigma_1}_{\mathbf{k}'j} | \frac{\partial V^{\sigma_1\sigma_2}_{\mathrm{KS}}(\mathbf{r},\omega)}{\partial u_I} | \psi^{\sigma_2}_{\mathbf{k}i} \rangle \sum_{\sigma_3\sigma_4} \langle \psi^{\sigma_3}_{\mathbf{k}i} | \frac{\partial V^{\sigma_3\sigma_4}_{\mathrm{KS}}(\mathbf{r},\omega)}{\partial u_J} | \psi^{\sigma_4}_{\mathbf{k}'j} \rangle$$
$$+ \sum_\lambda \int d\mathbf{r} \frac{\partial^2 V_{\mathrm{ext},\lambda}(\mathbf{r})}{\partial u_I \partial u_J} \rho^0_\lambda(\mathbf{r}) - \sum_{\lambda\mu} \iint d\mathbf{r} d\mathbf{r}' \frac{\partial \rho_\lambda(\mathbf{r},\omega)}{\partial u_I} K_{\mathrm{Hxc},\lambda\mu}(\mathbf{r},\mathbf{r}') \frac{\partial \rho_\mu(\mathbf{r}',\omega)}{\partial u_J}, \tag{7.28}$$

where $\rho^0_\lambda(\mathbf{r})$ is the unperturbed spin density and $K_{\mathrm{Hxc},\lambda\mu}(\mathbf{r},\mathbf{r}')$ is the Hartree and exchange-correlation kernel defined by Eq. 5.19. The response function $C_{IJ}(\omega)$ is a complex function of the frequency ω. The hermitian part of the force constant matrix in real space, defined as

$$C^H_{IJ}(\omega) = \frac{1}{2}\left[C_{IJ}(\omega) + C_{JI}(-\omega)\right], \tag{7.29}$$

is related to the dynamical matrix in reciprocal space. Precisely, the dynamical matrix is equal to the Fourier transform of $C^H_{IJ}(\omega)$ divided by the square root of the masses, namely

$$D_{sr}(\mathbf{q},\omega) = \frac{1}{2\sqrt{M_s M_r}}\left[C_{sr}(\mathbf{q},\omega) + C_{rs}(-\mathbf{q},-\omega)\right], \tag{7.30}$$

where $C_{sr}(\mathbf{q},\omega)$ is the Fourier transform of $C_{IJ}(\omega)$ and $C_{rs}(-\mathbf{q},-\omega)$ is the Fourier transform of $C_{JI}(-\omega)$. We recall the relationships between complex conjugated force constant matrices in real and reciprocal space

$$C^*_{IJ}(\omega) = C_{IJ}(-\omega) \tag{7.31}$$
$$C^*_{sr}(\mathbf{q},\omega) = C_{sr}(-\mathbf{q},-\omega). \tag{7.32}$$

The non-adiabatic dynamical matrix is the quantity needed to calculate the non-adiabatic phonon frequencies and angular momenta.

7.3.2 First-principles scheme

Equations 7.27 and 7.28 constitute a frequency-dependent self-consistent scheme that allows the calculation of the non-adiabatic phonon response. The calculation is carried out using the first-principles scheme described in Sec. 4.4 where a stationary functional in the variation of the electronic charge density is used to avoid the self-consistent calculation of the derivative of the KS potential as a function of the frequency ω.

In this subsection we adapt the equations for the study of non-collinear magnetic solids. We take advantage of the properties of the time-reversal operator essentially following the same workflow as references [21, 87].

The approximate force constant matrix in frequency space reads

$$\tilde{C}_{IJ}(\omega) = \Pi_{IJ}(\omega) + C_{IJ}(0) \tag{7.33}$$

where $C_{IJ}(0)$ is the standard self-consistent force constant matrix and $\Pi_{IJ}(\omega)$ is the phonon self-energy. The latter represents the non-adiabatic effects due to the electron-phonon interaction. It can be expressed in the spin-dependent framework as

$$\begin{aligned}\Pi_{IJ}(\omega) = &\sum_{\mathbf{k}i,\mathbf{k}'j}^{N_k} \frac{f_{\mathbf{k}i} - f_{\mathbf{k}'j}}{\epsilon_{\mathbf{k}i} - \epsilon_{\mathbf{k}'j} + \omega + i\eta} \sum_{\sigma_1\sigma_2} \langle \psi^{\sigma_1}_{\mathbf{k}'j} | \frac{\partial V^{\sigma_1\sigma_2}_{\mathrm{KS}}}{\partial u_I} | \psi^{\sigma_2}_{\mathbf{k}i} \rangle \sum_{\sigma_3\sigma_4} \langle \psi^{\sigma_3}_{\mathbf{k}i} | \frac{\partial V^{\sigma_3\sigma_4}_{\mathrm{KS}}}{\partial u_J} | \psi^{\sigma_4}_{\mathbf{k}'j} \rangle \\ &- \sum_{\mathbf{k}i,\mathbf{k}'j}^{N_k} \frac{f_{\mathbf{k}i} - f_{\mathbf{k}'j}}{\epsilon_{\mathbf{k}i} - \epsilon_{\mathbf{k}'j}} \sum_{\sigma_1\sigma_2} \langle \psi^{\sigma_1}_{\mathbf{k}'j} | \frac{\partial V^{\sigma_1\sigma_2}_{\mathrm{KS}}}{\partial u_I} | \psi^{\sigma_2}_{\mathbf{k}i} \rangle \sum_{\sigma_3\sigma_4} \langle \psi^{\sigma_3}_{\mathbf{k}i} | \frac{\partial V^{\sigma_3\sigma_4}_{\mathrm{KS}}}{\partial u_J} | \psi^{\sigma_4}_{\mathbf{k}'j} \rangle \end{aligned} \tag{7.34}$$

where the static limit of the derivative of the spin density matrix has been considered at the cost of a negligible error.

Let us name $\Pi^{(+)}_{IJ}(\omega)$ the first term in the right hand side of Eq. 7.34, and $\Pi^{(-)}_{IJ}$ the second term (without minus) which is independent on the frequency ω and real (since it is hermitian and symmetric). The phonon self-energy then reads $\Pi_{IJ}(\omega) = \Pi^{(+)}_{IJ}(\omega) - \Pi^{(-)}_{IJ}$. When calculating the non-adiabatic force constant matrix, the second term $\Pi^{(-)}_{IJ}$ is subtracted from the adiabatic force constant matrix $C_{IJ}(0)$ and the first term $\Pi^{(+)}_{IJ}(\omega)$ is later added[17]. Note that $\Pi^{(+)}_{IJ}(\omega)$ is not hermitian due to the small imaginary part in the denominator but still satisfies the relation $\Pi^{(+)*}_{IJ}(\omega) = \Pi^{(+)}_{IJ}(-\omega)$. The hermitian part of the approximate force constant matrix can then be written as

$$\begin{aligned}\tilde{C}^{H}_{IJ}(\omega) &= \Pi^{(+)H}_{IJ}(\omega) - \Pi^{(-)}_{IJ} + C_{IJ}(0) \\ &= \frac{1}{2}\left[\Pi^{(+)}_{IJ}(\omega) + \Pi^{(+)}_{JI}(-\omega)\right] - \Pi^{(-)}_{IJ} + C_{IJ}(0)\end{aligned} \tag{7.35}$$

where only the frequency dependent term $\Pi^{(+)}_{IJ}(\omega)$ must be split into $+\omega$ and $-\omega$ contributions. The subtracting self-energy $\Pi^{(-)}_{IJ}$ and the adiabatic force constant matrix $C_{IJ}(0)$ are both real and symmetric under exchange of the ionic indexes. The function $\Pi^{(+)H}_{IJ}(\omega)$ is equal to the hermitian part of the adding self-energy $\Pi^{(+)}_{IJ}$, and it reads

$$\begin{aligned}\Pi^{(+)H}_{IJ}(\omega) = &\frac{1}{2}\sum_{\mathbf{k}i,\mathbf{k}'j}^{N_k} \frac{f_{\mathbf{k}i} - f_{\mathbf{k}'j}}{\epsilon_{\mathbf{k}i} - \epsilon_{\mathbf{k}'j} + \omega + i\eta} \sum_{\sigma_1\sigma_2} \langle \psi^{\sigma_1}_{\mathbf{k}'j} | \frac{\partial V^{\sigma_1\sigma_2}_{\mathrm{KS}}}{\partial u_I} | \psi^{\sigma_2}_{\mathbf{k}i} \rangle \sum_{\sigma_3\sigma_4} \langle \psi^{\sigma_3}_{\mathbf{k}i} | \frac{\partial V^{\sigma_3\sigma_4}_{\mathrm{KS}}}{\partial u_J} | \psi^{\sigma_4}_{\mathbf{k}'j} \rangle \\ &+ \frac{1}{2}\sum_{\mathbf{k}i,\mathbf{k}'j}^{N_k} \frac{f_{\mathbf{k}i} - f_{\mathbf{k}'j}}{\epsilon_{\mathbf{k}i} - \epsilon_{\mathbf{k}'j} - \omega + i\eta} \sum_{\sigma_1\sigma_2} \langle \psi^{\sigma_1}_{\mathbf{k}'j} | \frac{\partial V^{\sigma_1\sigma_2}_{\mathrm{KS}}}{\partial u_J} | \psi^{\sigma_2}_{\mathbf{k}i} \rangle \sum_{\sigma_3\sigma_4} \langle \psi^{\sigma_3}_{\mathbf{k}i} | \frac{\partial V^{\sigma_3\sigma_4}_{\mathrm{KS}}}{\partial u_I} | \psi^{\sigma_4}_{\mathbf{k}'j} \rangle\end{aligned} \tag{7.36}$$

with obvious meaning of the symbols.

[17] The two parts of the self-energy $\Pi^{(+)}_{IJ}(\omega)$ and $\Pi^{(-)}_{IJ}$ can be evaluated at different electronic temperatures and with different sampling of reciprocal space. The smearing and sampling of $\Pi^{(-)}_{IJ}$ must coincide with those used for the standard linear response calculation [20]

7.3.3 The magnetic field

So far we never made explicit the magnetic field $\mathbf{B}$ on KS occupations, eigenvalues, wavefunctions and potential because it was the same for all. Let us now insert in both matrix elements in the second term (on the left and right side of the derivative of the KS potential) the identity matrix $\mathcal{T}^\dagger\mathcal{T} = \mathbb{I}$ where $\mathcal{T} = i\sigma_y\mathcal{K}$ is the time-reversal operator for spin-1/2 particles. Then, by using the properties of antilinear operators and the relation $\mathcal{T}V_{\rm KS}^{[\mathbf{B}]}\mathcal{T}^\dagger = V_{\rm KS}^{[-\mathbf{B}]}$, the hermitian part of the adding self-energy can be written as (see appendix E)

$$\begin{aligned}\Pi_{IJ}^{(+)H}(\omega) =& \frac{1}{2}\sum_{\mathbf{k}i,\mathbf{k}'j}^{N_k}\frac{f_{\mathbf{k}i}^{[\mathbf{B}]} - f_{\mathbf{k}'j}^{[\mathbf{B}]}}{\epsilon_{\mathbf{k}i}^{[\mathbf{B}]} - \epsilon_{\mathbf{k}'j}^{[\mathbf{B}]} + \omega + i\eta}\sum_{\sigma_1\sigma_2}\langle\psi_{\mathbf{k}'j}^{[\mathbf{B}]\sigma_1}|\frac{\partial V_{\rm KS}^{[\mathbf{B}]\sigma_1\sigma_2}}{\partial u_I}|\psi_{\mathbf{k}i}^{[\mathbf{B}]\sigma_2}\rangle \\ &\times\sum_{\sigma_3\sigma_4}\langle\psi_{\mathbf{k}i}^{[\mathbf{B}]\sigma_3}|\frac{\partial V_{\rm KS}^{[\mathbf{B}]\sigma_3\sigma_4}}{\partial u_J}|\psi_{\mathbf{k}'j}^{[\mathbf{B}]\sigma_4}\rangle \\ &+\frac{1}{2}\sum_{\mathbf{k}i,\mathbf{k}'j}^{N_k}\frac{f_{-\mathbf{k}i}^{[-\mathbf{B}]} - f_{-\mathbf{k}'j}^{[-\mathbf{B}]}}{\epsilon_{-\mathbf{k}i}^{[-\mathbf{B}]} - \epsilon_{-\mathbf{k}'j}^{[-\mathbf{B}]} - \omega - i\eta}\sum_{\sigma_1\sigma_2}\langle\psi_{-\mathbf{k}i}^{[-\mathbf{B}]\sigma_1}|\frac{\partial V_{\rm KS}^{[-\mathbf{B}]\sigma_1\sigma_2}}{\partial u_J}|\psi_{-\mathbf{k}'j}^{[-\mathbf{B}]\sigma_2}\rangle \\ &\times\sum_{\sigma_3\sigma_4}\langle\psi_{-\mathbf{k}'j}^{[-\mathbf{B}]\sigma_3}|\frac{\partial V_{\rm KS}^{[-\mathbf{B}]\sigma_3\sigma_4}}{\partial u_I}|\psi_{-\mathbf{k}i}^{[-\mathbf{B}]\sigma_4}\rangle.\end{aligned} \tag{7.37}$$

The second part of the self-energy is now explicitly dependent on the KS occupations, eigenvalues, eigenfunctions and potential of the KS problem with magnetic field $-\mathbf{B}$. This expression allows to calculate the non-adiabatic force constant matrix in the first-principles scheme embodied by Eq. 7.33, in non-collinear magnetic solids.

In reciprocal space, the phonon self-energy can analogously be expressed as the sum of a $\mathbf{B}$ and $-\mathbf{B}$ terms. From Eq. 7.30, the approximate non-adiabatic dynamical matrix as a function of the frequency ω and of the phonon quasimomentum $\mathbf{q}$ can be written in the form

$$\tilde{D}_{sr}(\mathbf{q},\omega) = \frac{1}{\sqrt{M_s M_r}}\left[\Pi_{sr}^{(+)H}(\mathbf{q},\omega) - \Pi_{sr}^{(-)}(\mathbf{q}) + C_{sr}(\mathbf{q})\right] \tag{7.38}$$

where the hermitian matrices $\Pi_{sr}^{(-)}(\mathbf{q})$ and $C_{sr}(\mathbf{q})$ are the Fourier transforms of the subtracting self-energy and of the adiabatic force constant matrix, respectively. Using the properties of the time-reversal operator, the hermitian part of the adding self-energy in reciprocal space can be written as

$$\Pi_{sr}^{(+)H}(\mathbf{q},\omega) = \frac{1}{2}\left[\Pi_{sr}^{(+)}(\mathbf{q},\omega) + \Pi_{rs}^{(+)}(-\mathbf{q},-\omega)\right]. \tag{7.39}$$

In the above equation, the first term corresponds to the non-adiabatic phonon response with wavevector $\mathbf{q}$ and frequency ω related to the KS problem of magnetic field $\mathbf{B}$ while the second term corresponds to the non-adiabatic phonon response with wavevector $-\mathbf{q}$ and frequency $-\omega$ related to the KS problem of magnetic field $-\mathbf{B}$. The two terms are one the time-reversed of each other.

7.4 Summary

In this section we have shown how the non-adiabatic effects are related with the geometric properties of the system in both insulating and metallic solids. We demonstrated that the non-adiabatic dynamical matrix can be expressed as a Kohn-Sham Berry curvature that plays the role of an effective magnetic field and breaks time-reversal symmetry for the phonon eigenvalue problem. As a consequence, the non-adiabatic vibrational modes are nonlinearly polarized and carry a finite angular momentum. This description provides the ingredients to understand which systems can exhibit sizeable non-adiabatic effects and intrinsic phonon angular momentum.

The Kohn-Sham Berry curvature vanishes when time-reversal symmetry holds and in collinear magnetic systems. As a consequence, we must consider systems with non-collinear magnetic interactions in order to observe an intrinsic phonon angular momentum. To treat this case, we extended the spin-dependent theory of non-adiabatic effects to non-collinear magnetic periodic systems. The phonon self-energy thus obtained can be used to evaluate non-adiabatic phonons in both insulators and metals starting from the already existing linear response code.

In the next chapter we will study a metallic periodic system with non-collinear magnetic order and large spin-orbit coupling (Mn_3Pt) to show that non-adiabatic effects due to the electron-phonon coupling are time-reversal symmetry breaking interactions for the vibrational field and entail a nonzero angular momentum of phonons.

Chapter 8

Antiferromagnetic metallic manganese compound

Non-collinear magnetism in solids is often the result of competing relativistic effects and magnetic interactions or geometrical frustration. Manganese in particular, lying in the middle of the transition metals series, often exhibits antiferromagnetic exchange interactions. In compounds involving elements like Ge, Sn, Ir, Pt, the manganese atoms are often arranged in a triangular structure [102]. In these systems, the typical magnetic arrangements are triangular textures with magnetic moments oriented at 120° one to the other. The spin-orbit coupling of heavy atoms is transferred to the magnetic manganese ions through hybridisation [103]. In addition, these non-collinear magnetic manganese alloys can have a large anomalous Hall effect driven by nonzero Berry curvature in momentum space [23, 104, 105].

Here, we demonstrate the occurence of an intrinsic phonon angular momentum in the non-collinear antiferromagnetic manganese compound Mn_3Pt driven by non-adiabatic effects. Since this system is metallic, the theory on non-adiabatic effects for non-collinear magnetic systems described in chapter 7 is used. Our results prove that non-adiabatic effects lead to a finite angular momentum of phonons in non-collinear magnetic systems.

8.1 Structure and magnetic phase

The manganese platinum alloy Mn_3Pt is a cubic antiferromagnetic compound with Néel temperature $T_N \sim 475K$. It exhibits two antiferromagnetic phases [23]: a non-collinear phase below 360 K (D phase) and a collinear phase between 360 K and T_N (F phase). The transition between the two phases is accompanied by an abrupt $\sim 0.8\%$ lattice expansion [106, 107].

The anomalous Hall effect is strong in the low-temperature D phase but absent in the high-temperature collinear F phase [23]. The theoretical calculation of the anomalous Hall conductivity ($\sigma_{\mathrm{AHC}} = 98\ \Omega^{-1}\mathrm{cm}^{-1}$) [102] is in agreement with two different experimental results on epitaxial films of Mn_3Pt at room temperature [23–25].

In the D phase, the manganese and platinum atoms of Mn_3Pt are arranged in a

face-centered cubic cell with platinum atoms at the vertices and manganese atoms at face centers, as shown in the left side of Fig 8.1. The crystal space group is $Pm\bar{3}m$.

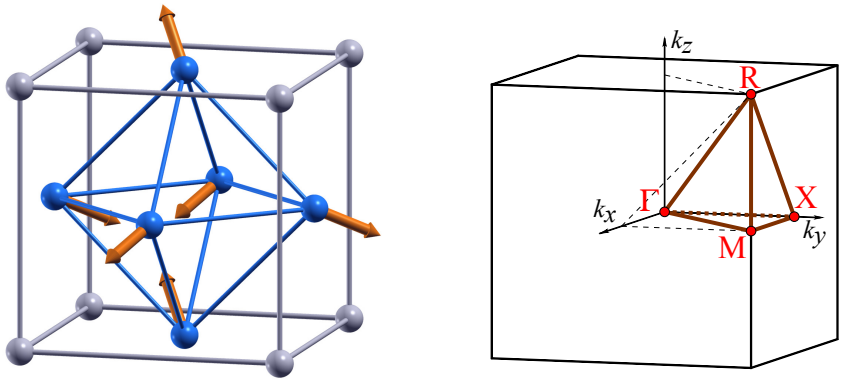

Figure 8.1: Non-collinear magnetic phase (left) and high symmetry points in the Brillouin zone (right) of Mn_3Pt. Blue atoms are manganese and grey atoms are platinum. The arrows on the manganese atoms represent its magnetic moments.

Within the (111) plane, the manganese sublattice forms a Kagome lattice with ABC-ABC stacking. In the Kagome plane, due to magneto-geometrical frustration, the manganese magnetic moments exhibit a non-collinear antiferromagnetic order, where the neighboring moments are aligned at a 120° angle (triangular spin texture) [102]. Magnetic moments of manganese atoms (3 μ_B/atom) all point towards or away from the center of the triangles (orange arrows in Fig 8.1). The total magnetization is zero while the absolute magnetization, defined as the integral of the absolute value of the magnetization density in the cell, is 9.6 μ_B/cell.

Mirror reflection with respect to the Kagome plane is a good symmetry of the manganese sublattice but it flips all the in-plane spin components. If combined with time-reversal operation $\mathcal{T}$, the mirror reflection preserves the kagome magnetic lattice. As a whole, Mn_3Pt is invariant under inversion symmetry but lacks (111) plane mirror symmetry due to the fcc stacking of the kagome sublattices. Heavy platinum atoms with sizeable spin-orbit coupling, hybridize with magnetic manganese atoms and break the mirror symmetry. As a consequence, the non-collinear antiferromagnetic compound exhibits an anomalous Hall effects even without external magnetic field. This topic has been investigated in Ref. [103] for the closely related material Mn_3Ir.

8.1.1 Computational details

We perform fully relativistic *ab-initio* calculations using version 6.7.0 of the QUANTUM-ESPRESSO suite [88,89]. We use norm-conserving ONCV pseudopotentials [90,91] with Perdew-Burke-Ernzerhof exchange-correlation functional [92] and a kinetic energy cut-off of 90 Ry. For the electronic structure calculation, we start with a simple cubic Bravais lattice with experimental lattice parameter [107,108]. Then we allow the structure to relax with a cell-volume relaxation. The resulting lattice parameter is $a = 3.76$ Å. The platinum atom is positioned at the origin while manganese atoms are located at

$(\frac{1}{2}, \frac{1}{2}, 0)$, $(\frac{1}{2}, 0, \frac{1}{2})$ and $(0, \frac{1}{2}, \frac{1}{2})$ in crystal units (see Fig. 8.1). The energy of the non-collinear antiferromagnetic configuration is converged with respect to k-points mesh and electronic temperature. We use a $10 \times 10 \times 10$ Monkhorst–Pack k-points grid [109] and 0.05 Ry degauss with Methfessel-Paxton smearing [110]. The convergence threshold for the total energy is 5×10^{-9} Ry.

8.1.2 Band structure

The calculated band structure of Mn_3Pt is represented in Fig. 8.2 in an energy window of 1.2 eV around the Fermi energy. The material is metallic with several crossings of the Fermi level (red line) along the high symmetry directions. The band structure is in agreement with results obtained in references [102] and [23] from fully relativistic calculations.

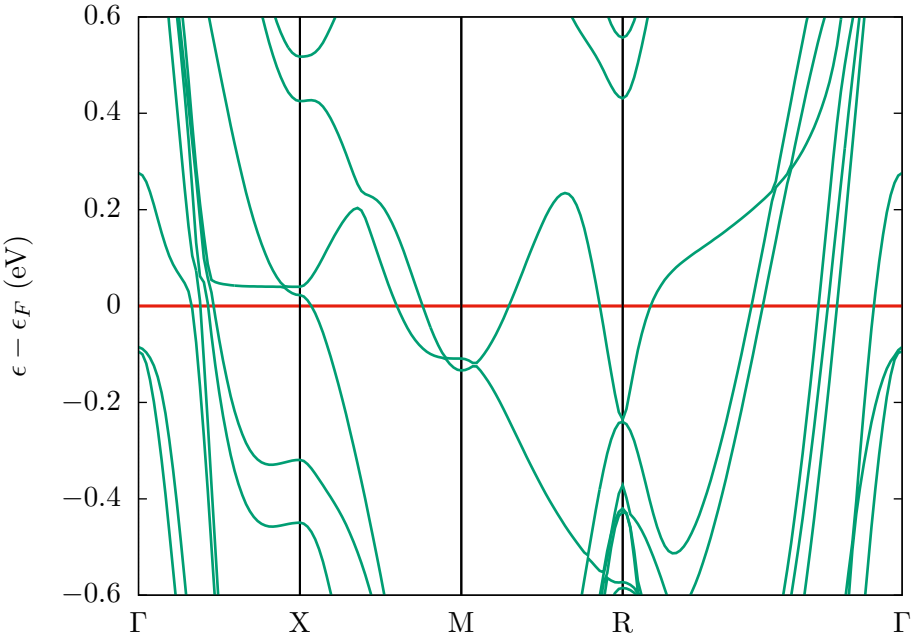

Figure 8.2: Band structure of Mn_3Pt, plotted along the high-symmetry path Γ-X-M-R-Γ. The Fermi level corresponds to the red line.

It is interesting to distinguish the contribution to the band structure from each atomic kind. This can be done by calculating the projected density of states resolved in k-space. In fig. 8.3 the band structure of Mn_3Pt is represented together with the atomic type character of the associated wave functions. The main contribution to the band structure close to the Fermi level is due to the d-type orbitals of manganese atoms.

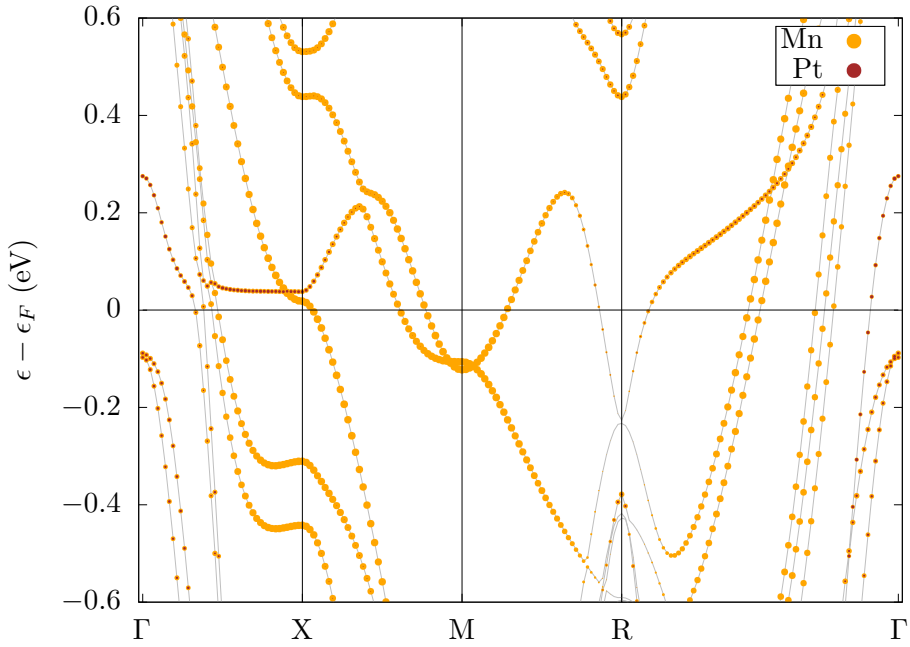

Figure 8.3: Atomic type contribution to the band structure of Mn_3Pt, plotted along the high-symmetry path Γ-X-M-R-Γ. The bands close to the Fermi level are mainly related to the *d* orbitals of manganese atoms.

8.2 Adiabatic phonon response

Mn_3Pt has 12 vibrational modes of which 3 acoustic and 9 optical. The adiabatic phonon dispersion curves of Mn_3Pt were obtained performing a linear response calculation with the PHonon package. We used a 2×2×2 q-point grid, a convergence threshold of 10^{-17} and the acoustic sum rule for interpolation. The phonon bands are shown in Fig. 8.4 along the high symmetry path Γ-X-M-R-Γ in the Brillouin zone (see the right hand side of Fig 8.1). In the right hand side panel of Fig. 8.4, the phonon density of states is also reported.

As a result of the non-equivalence between manganese atoms in the crystal basis due to the non-collinear magnetic configuration, the phonon branches are not degenerate anywhere in the Brillouin zone even if some modes exhibit very close energies at the high symmetry points. The adiabatic phonon frequencies of Mn_3Pt obtained from self-consistent linear response calculation at the high symmetry points of the Brillouin zone are listed in Table 8.1. To our knowledge there exists no other experimental or theoretical study on vibrational properties of non-collinear antiferromagnetic Mn_3Pt in literature.

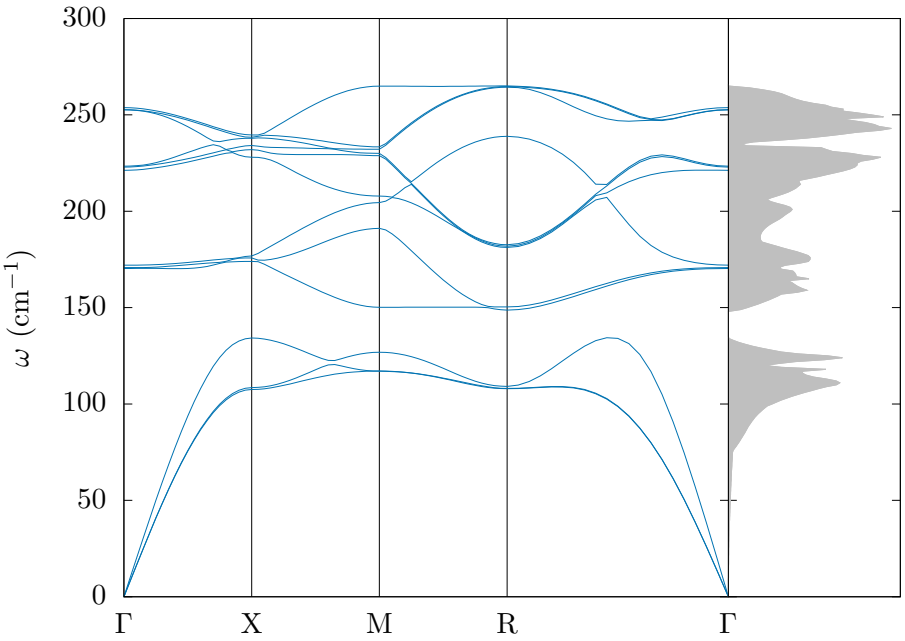

Figure 8.4: Phonon dispersion curves and phonon density of states (in grey) of Mn_3Pt along the high symmetry path Γ-X-M-R-Γ in the Brillouin zone.

Table 8.1: Adiabatic phonon frequencies at the high symmetry points Γ, X, M, R of the Brillouin zone in Mn_3Pt from self-consistent linear response calculation.

ν	ω_Γ (cm^{-1})	ω_X (cm^{-1})	ω_M (cm^{-1})	ω_R (cm^{-1})
1	0	107.4	117.5	107.9
2	0	108.4	117.6	108.1
3	0	134.2	126.9	109.1
4	173.9	175.1	148.8	148.7
5	174.7	175.6	193.3	150.4
6	175.8	176.2	203.5	181.2
7	221.3	228.4	206.9	181.9
8	222.9	231.4	230.6	182.6
9	223.4	233.6	231.4	238.9
10	252.6	238.2	231.7	264.4
11	252.8	238.8	232.1	264.7
12	253.9	239.8	264.2	265.0

8.3 Non-adiabatic phonon response

Non-adiabatic effects due to the electron-phonon coupling are now taken into consideration. Using the first-principles method of section 7.3.2, we calculate the non-adiabatic dynamical matrix in non-collinear antiferromagnetic Mn_3Pt at the high symmetry points Γ, X, M, R of the Brillouin zone. We implement Eq. 7.37 in our code to calculate the phonon self-energy in reciprocal space as a function of the frequency ω and momentum $\mathbf{q}$. Since the material is metallic, we use a finite parameter $\eta = 8 \times 10^{-4}$ Ry $\simeq 11$ meV. The non-adiabatic dynamical matrix is then given by Eq. 7.38. The non-adiabatic phonon frequencies and polarization vectors are obtained by solving the nonlinear eigenvalue problem for each mode separately. The non-adiabatic phonon frequencies at the high symmetry points of the Brillouin zone are listed in Tab. 8.2.

Table 8.2: Non-adiabatic phonon frequencies at the high symmetry points Γ, X, M, R of the Brillouin zone in the non-collinear antiferromagnetic phase of Mn_3Pt from non-self-consistent linear response calculation.

ν	$\tilde{\omega}_\Gamma$ (cm^{-1})	$\tilde{\omega}_X$ (cm^{-1})	$\tilde{\omega}_M$ (cm^{-1})	$\tilde{\omega}_R$ (cm^{-1})
1	0.0	106.3	115.9	106.8
2	0.0	106.5	116.9	106.9
3	0.0	134.5	126.5	107.1
4	169.5	169.0	141.3	141.4
5	170.4	169.7	187.6	143.1
6	171.9	170.0	198.5	175.5
7	218.1	224.6	202.4	176.2
8	218.9	229.0	227.4	178.8
9	219.2	229.3	227.5	234.3
10	249.0	234.6	228.1	260.9
11	250.1	234.9	228.3	262.0
12	250.3	236.2	261.7	262.4

As in the case of platinum clusters, non-adiabatic effects do not significantly modify the vibrational spectrum. As a general behavior, we observe that non-adiabatic effects tend to decrease the phonon frequencies. The difference between adiabatic and non-adiabatic frequencies is however, no greater than 7 cm^{-1} (5% of the adiabatic frequency) for all the modes and q-points studied. Moreover, the phonon frequencies in Tab. 8.2 were obtained with a finite parameter η which further sets apart adiabatic and non-adiabatic frequencies.

Compared to the case of platinum clusters, here we do not present the vibrational frequencies obtained from the low-frequency expansion of the phonon self-energy as in Mn_3Pt they are equal to the adiabatic frequencies even though $\eta \neq 0$. The non-adiabatic evaluation of the phonon dispersion curves as in Fig. 8.4 has not been done yet. It requires adapting the Wannier interpolation technique of Ref. [20] to non-collinear magnetic solids.

8.3.1 Interpolation technique

In metals, the k-points grid used for the adiabatic phonon response usually is not dense enough to converge the summation in the phonon self-energy Eq. 7.37. We therefore need to run a non-self-consistent calculation of the deformation potential on a more dense k-points grid and generate the Kohn-Sham wavefunctions and eigenvalues on the latter. By doing so, the ω-dependent part of the self-energy can be obtained. The ω-independent part instead must be calculated using the same k-points grid of the adiabatic phonon calculation.

For Mn_3Pt, we employ about 12000 k-points for the calculation of the ω-dependent part of the self-energy. The $10 \times 10 \times 10$ mesh, used for adiabatic phonon response, is not sufficient. However, the non-self-consistent calculation of the deformation potential matrix elements on the dense k-points grid resulted to be unfeasible because of memory shortage, already above the $15 \times 15 \times 15$ mesh. We needed therefore to break up the summation into separate contributions. We used a $12 \times 12 \times 12$ k-points grid as a base and shifted the grid in 6 directions identified by the labels (100), (010), (001), (110), (101), (011) in the space of the reciprocal lattice vectors. In these labels, the 1s are associated to a displacement by half a grid step in the corresponding direction. For example, (010) labels the grid shifted by half a grid step in the y direction. Similarly the others.

We evaluate the ω-dependent part of the self-energy on each grid, including the original one, and sum the results divided by the number of grids. The matrix is subsequently symmetrized according to the magnetic crystal group determined by the initial magnetic configuration. Finally, the ω-independent part of the phonon self-energy is subtracted from the adiabatic dynamical matrix and the ω-dependent part is added. The non-adiabatic phonon frequencies are then obtained as the square root of the eigenvalues of the dynamical matrix. The symmetrization of the dynamical matrix according to the magnetic space group is done in a separate program, adapting the already existing code.

It should be pointed out that the ω-dependent part of the self-energy can also be calculated with a different electronic temperature than the one used for the adiabatic phonon calculation. This is useful to converge the phonon frequencies in metals. In Mn_3Pt, however, we did not change the smearing when evaluating the phonon self-energy and always used the initial value of 0.05 Ry.

8.4 Phonon angular momentum

We calculate the non-adiabatic phonon polarization vectors by diagonalizing the non-adiabatic dynamical matrix. In Mn_3Pt, the adiabatic phonon polarization vectors are real everywhere in the Brillouin zone and the angular momentum of the static modes vanishes. When we consider non-adiabatic effects, the phonon polarization vectors become nontrivially complex and phonons can host a finite angular momentum. The phonon polarization vectors determine the trajectory of the ions around the equilibrium positions. Phonon with nontrivially complex polarization vectors can be understood as collective modes in which the ions spin around the equilibrium positions giving rise to

an orbital angular momentum perpendicular to the plane of the trajectory.

8.4.1 Two zone-corner optical modes

As an illustrative example, we show in Fig. 8.5 the phonon polarization vectors of two optical modes of Mn_3Pt at $\mathbf{q} = \mathrm{M} = (0, -\frac{1}{2}, -\frac{1}{2})$, namely $\nu = 6$ and $\nu = 7$. Because zone-corner phonons do not have the same periodicity of the crystal lattice, to represent the eigendisplacements we use a 2×2 supercell in the y and z directions, according to the coordinates of the selected $\mathbf{q}$ point. From left to right, in Fig. 8.5, the adiabatic (static) polarization vectors, the real and imaginary parts of the non-adiabatic (dynamical) polarization vectors (green arrows) and the angular momentum of the two modes are represented (red arrows). Since the real and imaginary parts of the non-adiabatic modes lie in the y-z plane, the angular momentum is parallel to the x direction in both vibrational modes. The adiabatic and non-adiabatic vibrational frequencies of these modes are respectively $\omega_{\mathrm{M6}} = 203.5$ cm^{-1}, $\tilde{\omega}_{\mathrm{M6}} = 198.5$ cm^{-1}, $\omega_{\mathrm{M7}} = 206.9$ cm^{-1} and $\tilde{\omega}_{\mathrm{M7}} = 202.4$ cm^{-1}.

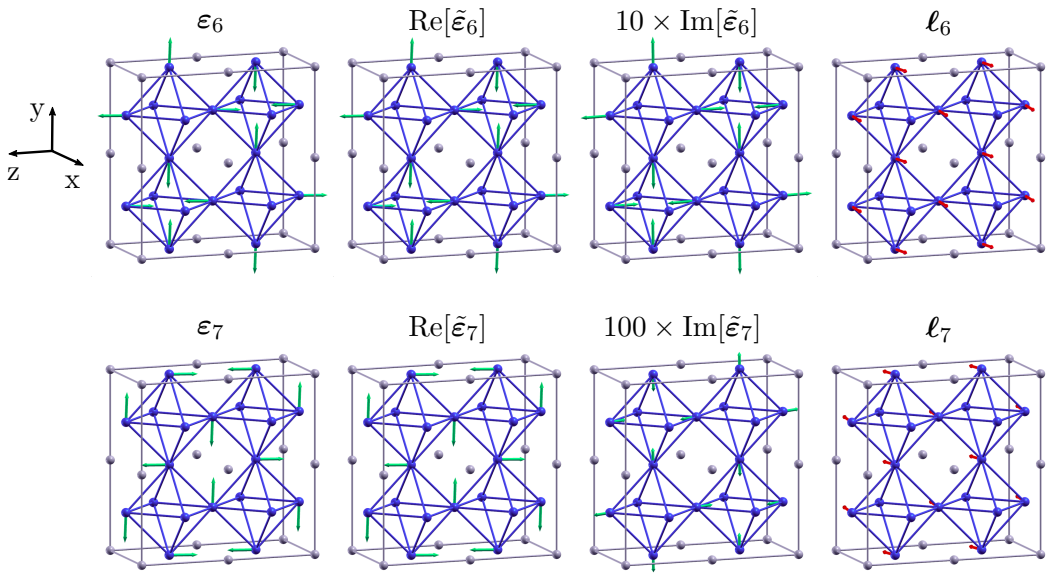

Figure 8.5: From left to right, representation in a 2×2 supercell in the y and z directions of the adiabatic (static) phonon polarization vectors $\boldsymbol{\varepsilon}_{\mathbf{q}\nu}$, of the real and imaginary parts of the non-adiabatic (dynamical) phonon polarization vectors $\tilde{\boldsymbol{\varepsilon}}_{\mathbf{q}\nu}$ and of the phonon angular momentum $\boldsymbol{\ell}_{\mathbf{q}\nu}$ for two optical modes $\nu = 6, 7$ in the non-collinear antiferromagnetic phase of Mn_3Pt at $\mathbf{q} = \mathrm{M} = (0, -\frac{1}{2}, -\frac{1}{2})$. The adiabatic and non-adiabatic frequencies are respectively $\omega_{\mathrm{M6}} = 203.5$ cm^{-1}, $\tilde{\omega}_{\mathrm{M6}} = 198.5$ cm^{-1}, $\omega_{\mathrm{M7}} = 206.9$ cm^{-1} and $\tilde{\omega}_{\mathrm{M7}} = 202.4$ cm^{-1}.

In the absence of magnetic interactions, these two modes would be degenerate and a linear combination of the eigenvectors could be used to generate a phonon angular momentum for each mode with opposite sign. In presence of magnetic interactions

instead, the degeneracy is broken due to the sizeable spin-orbit coupling of platinum atoms. When non-adiabatic effects are taken into consideration, the phonon angular momenta of the two modes $\nu = 6, 7$ are actually equal and opposite on each ion (see Fig. 8.5) but there is a gap of about 4 cm^{-1} between the phonon frequencies. This result demonstrates that non-adiabatic effects due to the electron-phonon interaction can be used to generate intrinsic angular momenta of phonons in materials with non-collinear magnetism and sizeable spin-orbit coupling.

The imaginary parts of the phonon eigendisplacements in the non-adiabatic framework are magnified in Fig. 8.5. One can object that the imaginary parts for mode $\nu = 7$ have smaller size than the imaginary parts for mode $\nu = 6$ while the angular momentum is of the same magnitude. This is due to the fact that the imaginary parts of the phonon polarization vectors $\tilde{\boldsymbol{\varepsilon}}_{\text{M6}}$ are almost parallel to the real parts, while the imaginary parts of the polarization vectors $\tilde{\boldsymbol{\varepsilon}}_{\text{M7}}$ are perpendicular to the real parts on each site. Given the definition of the angular momentum Eq. 7.24, even if the imaginary parts for mode $\nu = 7$ are smaller, their contribution to the cross product is larger. For the two selected modes, the x component of the phonon angular momentum is equal to $\ell_{\text{M6},x} = -\ell_{\text{M7},x} = 0.011\ \hbar$, which is the same order of magnitude of orbital angular momenta of electrons in itinerant ferromagnets [26], namely few percents of $\hbar$.

8.4.2 High symmetry points of the Brillouin zone

The non-adiabatic phonon polarization vectors and phonon angular momenta have been calculated for each mode at the high symmetry $\mathbf{q}$-points Γ, $\text{X} = (0, 0, -\frac{1}{2})$, $\text{M} = (0, -\frac{1}{2}, -\frac{1}{2})$, $\text{R} = (-\frac{1}{2}, -\frac{1}{2}, -\frac{1}{2})$. The Cartesian components of $\boldsymbol{\ell}_{\mathbf{q}\nu}$ are listed in Tab. 8.3 in units of $\hbar$ together with the corresponding non-adiabatic phonon frequencies. Some modes exhibit a huge angular momentum but are quasi-degenerate with other modes that have the same angular momentum with opposite sign (see for example $\nu = 1$, $\nu' = 2$ at X and $\nu = 9$, $\nu' = 11$ at M). This can make it difficult to detect them.

The most interesting result concerns those modes that are far apart enough in energy to be distinguishable, and, at the same time, have sizeable angular momentum. This is the case of optical modes $\nu = 6$ and $\nu' = 7$ at M, described previously. The phonon frequencies are about 4 cm^{-1} far apart in energy and the angular momentum is equal to few percent of $\hbar$. In this case, the two modes can be distinguished and the angular momentum of each can be observed.

Another interesting result from our analysis is that angular momentum is large particularly for vibrational modes that involve manganese atoms. This must be related to the fact that manganese atoms determine the magnetic configuration of the system. Therefore, the sizeable angular momentum is probably the consequence of the variation of the magnetic moments of the ions due to the phonon ionic displacement.

When non-adiabatic effects are evaluated using the low-frequency expansion of the self-energy, Eq. 7.21, the phonon angular momentum is nonzero. Indeed, the phonon polarization vectors and the phonon angular momentum are affected by non-adiabatic effects at the very first order in the low-frequency expansion. The vibrational frequencies instead are modified only at second order. The finite angular momentum of phonons in non-collinear antiferromagnetic Mn_3Pt is therefore mainly due to the Kohn-

Table 8.3: Non-adiabatic phonon frequencies $\tilde{\omega}_{\mathbf{q}}$ (in cm^{-1}) and phonon angular momentum (in units of $\hbar$) in the non-collinear antiferromagnetic phase of Mn_3Pt at the high symmetry points of the Brillouin zone Γ, X $= (0, 0, -\frac{1}{2})$, M $= (0, -\frac{1}{2}, -\frac{1}{2})$, R $= (-\frac{1}{2}, -\frac{1}{2}, -\frac{1}{2})$ (a, b, c, d sub-tables respectively).

$\tilde{\omega}_\Gamma(\mathrm{cm}^{-1})$	$\ell_x(\hbar)$	$\ell_y(\hbar)$	$\ell_z(\hbar)$
0.0	−0.004	−0.005	−0.004
0.0	0.003	0.005	0.004
0.0	0.000	0.000	0.000
169.5	−0.005	−0.004	−0.002
170.4	0.005	0.004	0.001
171.9	−0.001	0.000	0.000
218.1	0.002	0.019	0.024
218.9	0.033	−0.014	−0.027
219.2	−0.032	−0.002	0.006
249.0	−0.002	−0.002	−0.002
250.1	−0.027	−0.026	−0.029
250.3	0.027	0.026	0.029

(a)

$\tilde{\omega}_X(\mathrm{cm}^{-1})$	$\ell_x(\hbar)$	$\ell_y(\hbar)$	$\ell_z(\hbar)$
106.3	−0.011	−0.010	−0.319
106.5	0.009	0.008	0.319
134.5	0.002	0.002	0.000
169.0	0.000	0.000	0.020
169.7	0.001	0.000	0.000
170.0	0.000	0.000	−0.020
224.6	0.000	0.000	0.000
229.0	−0.003	−0.002	0.109
229.3	0.003	0.002	−0.111
234.6	−0.015	−0.045	0.007
234.9	0.004	0.045	−0.028
236.2	0.010	0.001	0.021

(b)

$\tilde{\omega}_M(\mathrm{cm}^{-1})$	$\ell_x(\hbar)$	$\ell_y(\hbar)$	$\ell_z(\hbar)$
115.9	−0.027	−0.004	−0.004
116.9	0.028	0.002	0.002
126.5	0.000	0.003	0.003
141.3	0.000	0.000	0.000
187.6	0.000	−0.001	−0.001
198.5	0.011	0.000	0.000
202.4	−0.011	0.000	0.000
227.4	0.000	−0.001	0.000
227.5	−0.122	0.004	0.003
228.1	0.000	0.001	0.000
228.3	0.121	−0.003	−0.001
261.7	0.001	0.000	0.000

(c)

$\tilde{\omega}_R(\mathrm{cm}^{-1})$	$\ell_x(\hbar)$	$\ell_y(\hbar)$	$\ell_z(\hbar)$
106.8	−0.015	−0.025	−0.035
106.9	0.007	0.023	0.039
107.1	0.007	0.002	−0.004
141.4	0.001	0.001	0.001
143.1	0.000	0.000	0.000
175.5	0.019	0.026	0.030
176.2	−0.018	−0.027	−0.032
178.8	−0.002	0.000	0.000
234.3	0.001	0.001	0.001
260.9	−0.002	0.000	0.002
262.0	0.043	0.030	0.023
262.4	−0.042	−0.031	−0.025

(d)

Sham Berry curvature Eq. 7.17 which breaks time-reversal symmetry for the phonon eigenvalue equation. Our study on Mn_3Pt in the D phase shows that non-adiabatic effects due to the electron-phonon coupling are time-reversal symmetry breaking interactions for the vibrational field. Consequently, non-degenerate phonon modes host an intrinsic angular momentum driven by the non-adiabatic effects.

8.5 Summary

In this chapter we presented the results obtained in the framework of the theory discussed in chapter 7 for a metallic manganese compound in the non-collinear magnetic phase. We performed fully relativistic *ab-initio* calculations of electronic properties, of the magnetic structure and of vibrational properties in antiferromagnetic Mn_3Pt. This system is particularly attractive because recent studies have demonstrated the existence of the anomalous Hall effect in epitaxial films of Mn_3Pt at room temperature [23–25].

The calculated results showed that this material is stable in a non-collinear antiferromagnetic (D) phase with a triangular spin texture on the manganese atoms and that *d*-type orbitals of manganese atoms provide the main contribution to the band structure close to the Fermi level determining the metallic character of the system.

As for what concerns the vibrational properties, we firstly obtained the phonon dispersion curves with a static linear response calculation. Then, we used our code and the self-consistent deformation potentials to calculate the non-adiabatic effects of phonons at the high symmetry points of the Brillouin zone with a finite broadening. We obtained the non-adiabatic phonon frequencies and polarization vectors as solutions of the nonlinear eigenvalue problem of the dynamical matrix Eq. 4.54. As a last step, we calculated the phonon angular momentum from the phonon polarization vectors using Eq. 7.24.

We find that some phonon modes host a sizeable angular momentum driven by the non-adiabatic effects. Interestingly, the Cartesian components of the phonon angular momentum are equal and opposite for non-degenerate modes. The intrinsic nonlinear phonon polarization can hence be detected via spin-polarized Raman spectroscopy.

Conclusions

Non-adiabatic effects due to the electron-phonon interaction are usually investigated in the Raman spectrum, particularly at zone center, in metallic systems. Though, they have never been related neither to the geometric properties of materials such as the Berry curvature nor to the angular momentum of phonons. In this thesis, we demonstrate that non-adiabatic effects due to the coupling between electrons and vibrational modes are time-reversal symmetry breaking interactions for the vibrational field in non-collinear magnetic molecules and non-collinear magnetic periodic systems. As in these systems the deformation potential matrix elements cannot be real valued, a nonzero synthetic field (Kohn-Sham Berry curvature) arises. As a result, an intrinsic nonzero phonon angular momentum occurs even for non-degenerate modes and in the absence of external time-reversal symmetry breaking probes.

We outlined the theoretical and experimental background in which our research has been carried on as well as the methodological framework on which we relied to develop our own theories. The interaction between vibrational modes and external magnetic fields is demonstrated by the phonon Hall effect, in which a transverse thermal current is measured, and by the phonon contribution to the gyromagnetic ratio in the Einstein-de Haas effect, where a variation of the electronic magnetization induces a mechanical rotation of the system. When the external time-reversal symmetry breaking mechanism is accompanied with an internal spin-phonon interaction, phonons carry an elliptical polarization and a finite (pseudo) angular momentum. In the absence of external probes instead, phonons are linearly polarized and a nonzero angular momentum can arise in twofold degenerate modes through a linear combination of the phonon eigenvectors.

As a third option, we identified an intrinsic mechanism to generate nonzero phonon angular momentum in the absence of external probes, for non-degenerate modes. In the Born-Oppenheimer approximation, we showed that the nuclear dynamics along the potential energy surface is governed by an effective Hamiltonian which includes the back-interaction of electrons under the form of a *synthetic* gauge field, namely the Berry curvature defined in the space of the ionic displacements. In the harmonic approximation, the screening of electrons therefore affects the phonon eigenvalue problem resulting in a linear term in the vibrational frequency ω. In the same way as the equations of motion are handled for an ionic crystal lattice into an external magnetic field, we separated the polarization vectors of the coordinates and momenta and diagonalized the curvature-dependent effective Hamiltonian. The screening of electrons acts on the nuclear dynamics as an effective magnetic field that breaks time-reversal symmetry for

the phonon field. As a consequence, the phonons are allowed to host a finite angular momentum which we call *intrinsic* because it arises from the Berry connection of electrons in the absence of external probes.

Then, we demonstrated, both at the theoretical and the numerical stage, that non-adiabatic effects due to the electron-phonon coupling result in the aforementioned non-linear eigenvalue problem of lattice dynamics and hence entail an intrinsic angular momentum of phonons.

In the Kohn-Sham formulation of density functional perturbation theory, non-adiabatic effects can be taken into account via time-dependent linear response. This way of proceeding is usually referred to as the *dynamical* Born-Oppenheimer approximation, opposed to the more common *static* one. Following the approach of reference [20], we evaluated the non-adiabatic phonon response with a non-self-consistent procedure involving the k-point grid interpolation of the adiabatic deformation potential. We generalized this first-principles method to study non-adiabatic effects, first in insulating molecular systems, and then in periodic extended insulating and metallic systems with non-collinear magnetic phases.

In insulators with vibrational frequencies much smaller than the electronic gap, the phonon self-energy can be expanded in power series of the frequency ω, the linear order coefficients being proportional to the Berry curvature of the Kohn-Sham wavefunctions defined in the space of the phonon ionic displacements. Since the Berry curvature vanishes in nonmagnetic and collinear magnetic systems, because the deformation potential matrix elements are real valued, we perform a first-principles calculation of adiabatic and non-adiabatic vibrational modes in two non-collinear magnetic platinum clusters. The large spin-orbit coupling, together with the magnetic interaction, leads to a time-reversal symmetry breaking for the optical modes in these nanoparticles. Therefore, a sizeable angular momentum arises, especially in those modes that would have been degenerate in the absence of the symmetry breaking, even though the non-adiabatic correction of the vibrational frequency is negligible.

In metals, the series expansion can be carried out only by retaining the finite broadening η. The parameter represents the electron momentum-scattering rate and, even if small, it cannot be neglected when the self-energy is singular. With this precuation, the non-adiabatic force constant matrix can still be related with a generalized Kohn-Sham Berry curvature in the low-frequency limit. Even if the higher order terms should not in principle be neglected, in practical calculations, we show that the results obtained in the linear approximation are qualitatively correct. The theory of non-adiabatic effects for insulators is recovered by setting $\eta = 0$. The demonstration highlights the link between low-frequency non-adiabatic effects, due to the coupling between electrons and vibrational modes, and geometric properties of the system such as the Kohn-Sham Berry curvature, in materials ranging from insulating molecular systems to metallic solids.

Finally, the theoretical prediction is tested against numerical simulations in bulk manganese alloy Mn_3Pt with non-collinear antiferromagnetic order. The system is not only suitable for our purpose, as the platinum atoms transfer the spin-orbit coupling via hybridization to the magnetic manganese ions, but also it is known to exhibit topo-

logical anomalous Hall currents in its two-dimensional form [23–25]. On Mn_3Pt, we perform fully relativistic *ab-initio* calculations of the electronic properties, of the magnetic structure and of the phonon response. The material stabilizes in a non-collinear Néel phase with the magnetic manganese atoms arranged in a Kagome sublattice with triangular spin texture. The main contribution to the band structure close to the Fermi level, and hence the metallic character of the compound, is determined by the $3d$ orbitals of the manganese atoms. Non-adiabatic effects and the angular momentum of phonons are then obtained from the nonlinear eigenvalue problem of the dynamical matrix, with a selected value of the parameter η, at the high symmetry points Γ, M, X, R, with and without the low-frequency linear expansion. A k-points interpolation technique is employed to calculate the frequency-dependent part of the phonon self-energy.

In Mn_3Pt, several non-degenerate phonon modes (up to 4 cm^{-1} far apart) host a sizeable angular momentum driven by the non-adiabatic effects, the magnitude being of the same order of electron orbital momenta in itinerant ferromagnets, namely few percents of $\hbar$. Moreover, our analysis shows that the angular momentum is finite for vibrational modes that involve primarily the magnetic manganese atoms. The effect is probably the consequence of the variation of the magnetic moments of the ions due to the phonon ionic displacement. The numerical simulations in Mn_3Pt prove that non-adiabatic effects due to the electron-phonon coupling are time-reversal symmetry breaking interactions for the phonon field. As a result, non-degenerate phonon modes host an intrinsic angular momentum driven by the non-adiabatic effects.

The angular momentum of non-degenerate phonons can be measured via polarization-resolved Raman spectroscopy, as the scattering intensities are different for different phonon polarizations. The phonon angular momentum that we obtained is qualitatively different from any other study because it arises intrinsically from the non-adiabatic interaction between phonons and electrons.

Hopefully, our work will foster new experiments in the field aimed at measuring and discovering new physical effects due to the occurence of a finite angular momentum of phonons.

Appendix A

Time-reversal symmetry

Time-reversal (TR) is the operation that reverses the time, namely $\mathcal{T} : t \to -t$. The TR symmetry is the property of physical laws and phenomena of being invariant under the TR transformation. In classical mechanics, TR is equivalent to motion reversal as typically the Lagrangian of the system is quadratic in the velocities. If the trajectory $r(t)$ is a solution of the Lagrangian equations, also $r(-t)$ will be so. In quantum mechanics the TR operator $\mathcal{T}$ transforms the coordinates and momenta according to

$$\mathcal{T}\mathbf{r}\mathcal{T}^{-1} = \mathbf{r} \tag{A.1}$$

$$\mathcal{T}\mathbf{p}\mathcal{T}^{-1} = -\mathbf{p} \tag{A.2}$$

Since the commutation relation $[r_i, p_j] = i\hbar\delta_{ij}$ holds, the TR operator is antilinear, namely it includes the action of the complex conjugation operator $\mathcal{K}$. But how does the TR operator transform the wavefunction $\psi(r,t)$? We must distinguish between spinless particles, for which the wavefunction is scalar, and spinfull particles, for which the wavefunction is a spinor.

A.1 Spinless particles

For spinless particles the time-reversed Schrödinger equation reads

$$-i\hbar\frac{\partial\psi(r,-t)}{\partial t} = H\psi(r,-t), \tag{A.3}$$

which is equal to the ordinary Schrödinger equation for the complex conjugated wavefunction due to the reality of the hamiltonian. In the spinless case therefore the TR operator is equal to the complex conjugation operator, namely $\mathcal{T} = \mathcal{K}$, and its action on the wavefunction is simply given by $\mathcal{T}\psi(r,t) = \psi^*(r,-t)$.

A.2 Spinfull particles

More in general it can be shown that the TR operator must be an antiunitary operator namely $\mathcal{T} = U\mathcal{K}$ where U is a unitary operator. Notice that, even if $\mathcal{T}$ commutes with

the Hamiltonian, there is no conserved quantity associated with it because it does not commute with the evolution operator $e^{-iHt/\hbar}$. In order to derive an expression for $\mathcal{T}$, we consider the action of the TR operator on the angular momentum. Stemming from equations A.1, the orbital angular momentum defined as $\mathbf{L} = \mathbf{r} \times \mathbf{p}$, transforms as

$$\mathcal{T}\mathbf{L}\mathcal{T}^{-1} = -\mathbf{L}. \tag{A.4}$$

As for the spin angular momentum, we require that it also changes sign under time-reversal transformation, namely

$$\mathcal{T}\mathbf{S}\mathcal{T}^{-1} = -\mathbf{S}. \tag{A.5}$$

By considering the action of a antiunitary operator on the components of the spin angular momentum, we get

$$-S_x = U\mathcal{K}S_x\mathcal{K}U = US_xU \tag{A.6}$$
$$-S_y = U\mathcal{K}S_y\mathcal{K}U = -US_yU \tag{A.7}$$
$$-S_z = U\mathcal{K}S_z\mathcal{K}U = US_zU. \tag{A.8}$$

The unitary operator U must therefore be equal to a $-\pi$ spin rotation about the y axis, namely $U = e^{iS_y\pi/\hbar}$. For half-integer spin particles (fermions), the TR operator satisfies $\mathcal{T}^2 = -1$ while for an integer spin particle (bosons) the TR operator satisfies $\mathcal{T}^2 = 1$. For spin-1/2 particles (like electrons) the unitary operator can be written as $U = e^{i\sigma_y\pi/2}$ where σ_y is the Pauli matrix. Then, by writing the exponential in power series and using the property of the Pauli matrix $\sigma_y^2 = \mathbb{I}$, the unitary operator reads $U = i\sigma_y$. Finally, the time-reversal operator for spin-1/2 particles can be written as

$$\mathcal{T} = i\sigma_y\mathcal{K}. \tag{A.9}$$

A crucial property of TR symmetry when applied to spinfull[18] electrons is the Kramers degeneracy theorem which states that for every energy eigenstate of a TR symmetric system there is at least one more eigenstate with the same energy. When the spin-orbit coupling (SOC) is weak, the two degenerate states (Kramers doublet) can be seen as *spin-up* and *spin-down* partners but when SOC is strong[19] they can only be thought of as time-reversed partners.

In magnetic materials, the TR symmetry is *spontaneously* broken which means that the system finds energetically favourable a configuration in which the spin $\uparrow$ and $\downarrow$ states (or the time-reversal paired states) are not equally populated. In this case then, the Hamiltonian is TR invariant but the ground state is not. Typically, the magnetic moments arrange in a well defined magnetic order so as to minimize the energy of exchange interactions between them. The most common magnetic orders (ferro-, antiferro-, ferri- magnetism) fall within the family of *collinear magnetism* in which all the spins are aligned along a preferencial direction. But there exist also some stable configurations of *noncollinear magnetic order*, mostly due to geometric frustration, as for example the Néel 120° structure in which the magnetic moments are aligned with an angle of 120° between neighbouring magnetic moments.

[18] Sometimes electrons are treated as spinless particles.

[19] In the Hamiltonian SOC is invariant under TR.

A.3 Bloch states

In solids, the electrons wavefunction complies with the Bloch's theorem

$$\psi_{\mathbf{k}}(\mathbf{r}) = e^{i\mathbf{k}\cdot\mathbf{r}} u_{\mathbf{k}}(\mathbf{r}) \tag{A.10}$$

where $\mathbf{k}$ is the crystal momentum of the electron and $u_{\mathbf{k}}(\mathbf{r})$ is the periodic part of the wavefunction which satisfies $u_{\mathbf{k}}(\mathbf{r}) = u_{\mathbf{k}}(\mathbf{r}+\mathbf{R})$ with $\mathbf{R}$ lattice translational vector. The time-independent Shrödinger equation reads

$$H_{\mathbf{k}} u_{\mathbf{k}}(\mathbf{r}) = \epsilon_{\mathbf{k}} u_{\mathbf{k}}(\mathbf{r}) \tag{A.11}$$

where $H_{\mathbf{k}} = e^{-i\mathbf{k}\cdot\mathbf{r}} H e^{i\mathbf{k}\cdot\mathbf{r}}$ is a $\mathbf{k}$-dependent effective Hamiltonian. Time-reversal transforms $\mathbf{k}$ to $-\mathbf{k}$ in Bloch wavefunctions and Hamiltonian, namely

$$\mathcal{T}\psi_{\mathbf{k}}(\mathbf{r}) = \psi_{-\mathbf{k}}(\mathbf{r}) \tag{A.12}$$

$$\mathcal{T} H_{\mathbf{k}} \mathcal{T}^{-1} = H_{\text{-}\mathbf{k}}. \tag{A.13}$$

When $\mathbf{k} = -\mathbf{k} + \mathbf{G}$, where $\mathbf{G}$ is a reciprocal lattice vector, the effective Hamiltonian $H_{\mathbf{k}}$ commutes with time-reversal operator and the Bloch state is doubly degenerate owing to Kramers theorem. These special wavevectors are called *time reversal invariant momenta*. When inversion symmetry is also present, the combined operator $\mathcal{I} * \mathcal{T}$ maps $\mathbf{k}$ to itself at all $\mathbf{k}$ and the bands are doubly degenerate everywhere in the Brillouin zone.

The spinor Bloch wavefunction transforms as

$$\mathcal{T}\begin{pmatrix}\psi_{\mathbf{k}\uparrow}\\ \psi_{\mathbf{k}\downarrow}\end{pmatrix} = \begin{pmatrix}\psi_{-\mathbf{k}\downarrow}\\ -\psi_{-\mathbf{k}\uparrow}\end{pmatrix}. \tag{A.14}$$

Applying the time-reversal transformation twice gives $\mathcal{T}^2 = -1$. When time-reversal symmetry holds, the two time-reversed states are degenerate (Kramers theorem), namely $\epsilon_{\mathbf{k}\uparrow} = \epsilon_{-\mathbf{k}\downarrow}$. If also inversion symmetry holds or in the absence of spin-orbit interaction, then $\epsilon_{\mathbf{k}\sigma} = \epsilon_{-\mathbf{k}\sigma}$ where $\sigma = \{\uparrow, \downarrow\}$.

Appendix B

Berry connection in the harmonic approximation

In the harmonic approximation, the Hamiltonian of the ionic vibrations include only quadratic terms in the phonon displacement $\mathbf{u}$ and its conjugate momentum $\mathbf{p}$. This is why the Berry connection in 3.30 must be linear with $\mathbf{u}$. To this end, we take inspiration from electromagnetism. In fact, we remind that the vector potential $\mathbf{A}$, in the symmetric gauge, can be expressed in terms of the constant magnetic field $\mathbf{B}$ and of the spacial coordinate as

$$\mathbf{A} = \frac{1}{2}\mathbf{B} \times \mathbf{r} \tag{B.1}$$

Analogously we may write the geometric vector potential in a proper gauge as

$$\boldsymbol{\mathcal{X}} = \frac{1}{2}\boldsymbol{\mathcal{Y}} \times \mathbf{u} \tag{B.2}$$

where $\boldsymbol{\mathcal{Y}}$ is a constant vector to be determined. Again by analogy with the magnetic field, $\boldsymbol{\mathcal{Y}}$ is equal to the curl of the Berry connection and therefore it is related to the Berry curvature Ω in the following way

$$\boldsymbol{\mathcal{Y}} = \boldsymbol{\nabla} \times \boldsymbol{\mathcal{X}} = \begin{pmatrix} \Omega_{yz} \\ \Omega_{zx} \\ \Omega_{xy} \end{pmatrix} \tag{B.3}$$

Then by replacing Eq. B.3 into Eq. B.2 we obtain the linearized Cartesian components of the Berry connection as

$$\mathcal{X}_\alpha = -\frac{1}{2}\sum_\beta \Omega_{\alpha\beta} u_\beta. \tag{B.4}$$

Appendix C

Phonon angular momentum

Let us rewrite here the second quantization relation of the phonon ionic displacement

$$\mathbf{u}_{Ls} = \sqrt{\frac{\hbar}{2N}} \sum_k \boldsymbol{\varepsilon}_{ks} \frac{1}{\sqrt{M_s \omega_k}} \left(a_k e^{-i\omega_k t} + a^\dagger_{-k} e^{i\omega_k t} \right) e^{i\mathbf{q}\cdot\mathbf{R}_L}. \tag{C.1}$$

Its time derivative is

$$\dot{\mathbf{u}}_{Ls} = \sqrt{\frac{\hbar}{2N}} \sum_k \boldsymbol{\varepsilon}_{ks} \frac{1}{\sqrt{M_s \omega_k}} \left(-i\omega_k a_k e^{-i\omega_k t} + i\omega_k a^\dagger_{-k} e^{i\omega_k t} \right) e^{i\mathbf{q}\cdot\mathbf{R}_L}. \tag{C.2}$$

The z component of the phonon angular momentum reads

$$N_z^{ph} = \frac{\hbar}{2N} \sum_{Ls} \sum_{kk'} (\varepsilon_{ksx}\varepsilon_{k'sy} - \varepsilon_{ksy}\varepsilon_{k'sx}) \frac{1}{\sqrt{\omega_k}} \left(a_k e^{-i\omega_k t} + a^\dagger_{-k} e^{i\omega_k t} \right) i\sqrt{\omega_{k'}} \left(-a_{k'} e^{-i\omega_{k'} t} + a^\dagger_{-k'} e^{i\omega_{k'} t} \right) e^{i(\mathbf{q}+\mathbf{q}')\cdot\mathbf{R}_L}. \tag{C.3}$$

We then use the relation $\sum_L e^{i(\mathbf{q}+\mathbf{q}')\cdot\mathbf{R}_L} = N\delta_{\mathbf{q},-\mathbf{q}'}$ to rewrite it as

$$N_z^{ph} = \frac{\hbar}{2} \sum_{s} \sum_{k\nu'} (\varepsilon_{ksx}\varepsilon^*_{\mathbf{q}\nu' sy} - \varepsilon_{ksy}\varepsilon^*_{\mathbf{q}\nu' sx}) \frac{1}{\sqrt{\omega_k}} \left(a_k e^{-i\omega_k t} + a^\dagger_{-k} e^{i\omega_k t} \right) i\sqrt{\omega_{\mathbf{q}\nu'}} \left(-a_{-\mathbf{q}\nu'} e^{-i\omega_{\mathbf{q}\nu'} t} + a^\dagger_{\mathbf{q}\nu'} e^{i\omega_{\mathbf{q}\nu'} t} \right). \tag{C.4}$$

We consider only $aa^\dagger$ and $a^\dagger a$ terms because the others vanish at equilibrium. The z-component of the phonon angular momentum can be written as

$$N_z^{ph} = \frac{\hbar}{2} \sum_{s} \sum_{k\nu'} (\varepsilon_{ksx}\varepsilon^*_{\mathbf{q}\nu' sy} - \varepsilon_{ksy}\varepsilon^*_{\mathbf{q}\nu' sx}) i\sqrt{\frac{\omega_{\mathbf{q}\nu'}}{\omega_k}} \times \left(a_k a^\dagger_{\mathbf{q}\nu'} e^{i(\omega_{\mathbf{q}\nu'} - \omega_k)t} - a^\dagger_{-k} a_{-\mathbf{q}\nu'} e^{-i(\omega_{\mathbf{q}\nu'} - \omega_k)t} \right). \tag{C.5}$$

Using the commutation relation $[a_k, a^\dagger_{k'}] = \delta_{kk'}$ and changing $k \to -k$ in the last term we obtain

$$N_z^{ph} = \frac{1}{2} \sum_{kk'} \ell_{kk',z} \left(\sqrt{\frac{\omega_k}{\omega_{k'}}} + \sqrt{\frac{\omega_{k'}}{\omega_k}} \right) \delta_{\mathbf{q},\mathbf{q}'} a^\dagger_{k'} a_k e^{i(\omega_{k'} - \omega_k)t} + \frac{1}{2} \sum_k \ell_{kk,z}. \tag{C.6}$$

which is Eq. 3.47 in the main text, where $k = (\mathbf{q}, \nu)$ and $\ell_{kk',z} = \hbar \sum_s i(\varepsilon_{ksx}\varepsilon^*_{k'sy} - \varepsilon_{ksy}\varepsilon^*_{k'sx})$. The expectation value of the phonon angular momentum is then given by

$$\langle N_z^{ph} \rangle = \sum_{\mathbf{q}\nu} \ell_{\mathbf{q}\nu,z} \left[b(\omega_{\mathbf{q}\nu}) + \frac{1}{2} \right]. \tag{C.7}$$

Appendix D

Methodological framework

Some methods and techniques that are commonly used in first-principles calculations are rapidly reviewed. From a computational point of view, the KS equations are implemented with an iterative procedure known as *self-consistent field* (SCF) method. The starting guess charge density $n(\mathbf{r})$, obtained from atomic orbitals, is used to calculate the Hartree and exchange-correlation functional.Then we replace the potentials into Eq. 4.1 and diagonalize the KS Hamiltonian to obtain the eigenstates $|\psi_i\rangle$. Finally, the new charge density is calculated from the eigenstates, using Eq. 4.5. The procedure is then iterated until the difference between the input and the output charge density is smaller than a given threshold.

D.1 Plane waves basis set

Bloch's theorem states that the solutions of the Schrödinger equation in a periodic potential take the form of a plane wave modulated by a periodic function, namely $\psi_{\mathbf{k}i}(\mathbf{r}) = e^{i\mathbf{k}\cdot\mathbf{r}}u_{\mathbf{k}i}(\mathbf{r})$ where $u_{\mathbf{k}i}(\mathbf{r})$ has the same periodicity of the crystal, namely $u_{\mathbf{k}i}(\mathbf{r}) = u_{\mathbf{k}i}(\mathbf{r}+\mathbf{R})$, and $\mathbf{k}$ is the crystal momentum vector. In practical calculations the wavefunction is usually expanded in a plane waves basis set as [111]

$$\psi_{\mathbf{k}i}(\mathbf{r}) = \frac{1}{\sqrt{V}}\sum_{\mathbf{G}} c_{\mathbf{k}+\mathbf{G}}e^{i(\mathbf{k}+\mathbf{G})\cdot\mathbf{r}} \tag{D.1}$$

where the reciprocal lattice vectors $\mathbf{G}$ are defined by $e^{i\mathbf{G}\cdot\mathbf{R}} = 1$ where $\mathbf{R}$ is any vector of the Bravais lattice. The plane waves expansion of Eq. D.1 is formally exact but it requires an infinite number of plane waves. The summation thus needs to be truncated to include only the plane waves that have a kinetic energy smaller than a given cutoff, namely $\frac{1}{2}|\mathbf{k}+\mathbf{G}|^2 < E_{\text{cut}}$. This approximation affects the accuracy of the results.

D.2 Pseudopotential approximation

The core electrons do not take part in the chemical bonds as the latter is entirely determined by the outermost peak of the valence electrons wavefunction. The external potential of the nuclei Eq. 4.2 is therefore replaced, in practical calculations, by an effective potential acting on the valence electrons [112]. As the wavefunctions of the

valence electrons are orthogonal to the core electrons wavefunctions, they rapidly oscillate in the core region ($r < r_c$, where r_c is the core radius). When expanding the wavefunctions on a plane wave basis set it is therefore extremely time-consuming to reproduce such a behavior, as too many plane waves would be necessary.

In the pseudopotential approximation instead, we replace the core electrons and the strong Coulomb potential with a weaker *pseudopotential* (PP) that acts on a set of smooth pseudo-wavefunctions. These pseudo-wavefunctions are smooth in the core region and they reproduce the behavior of the all-electron (AE) wavefunctions outwards. So that the pseudo and all-electron wavefunctions coincide beyond the core radius, the integrals of squared amplitudes of the two functions must be the same [113], namely

$$\int_0^{r_c} |\psi^{\mathrm{PP}}(r)|^2 dr = \int_0^{r_c} |\psi^{\mathrm{AE}}(r)|^2 dr. \tag{D.2}$$

The PPs that fulfil Eq. D.2 are called norm-conserving (NC) PPs because the norm of the wavefunction is conserved. This property also ensures the charge conservation in the core region. The PP is built one and for all for each atom starting from the AE wavefunctions. Then a parametrized form for the ionic PP is chosen and adjusted so that the pseudo-wavefunctions match the AE wavefunctions outside the core radius and the pseudo-eigenvalues are equal to the AE ones. The PPs thus built can then be used reliably for any other atomic or periodic configuration. Such transferability is one of the main benefit of the pseudopotential technique over all electron density functional theory implementations.

Alternative approaches to the NC scheme have been later proposed. The ultrasoft (US) pseudopotential scheme [114] allows to relax the norm conservation condition on the wavefunction and it introduces some localized augmentation charges (the charge density difference between AE and pseudo wavefunction) to make up for the charge deficit. The projector augmented wave (PAW) method [115] instead is an all-electron technique in which some auxiliary wavefunctions are used to construct the true wavefunctions and the total energy functional is evaluated from the latter. A more complete description of PPs techniques can be found in reference [75].

D.3 Electronic temperature

The electronic temperature is a computational artifact that improves convergence with respect to Brillouin zone sampling in metals. At zero temperature, the occupation function drops abruptly from 1 to 0 as the corresponding eigenvalue becomes larger than the Fermi energy. Since key physical quantities like the charge density and the total energy are obtained as a sum over all the occupied states, in a metal at zero temperature we end up integrating functions that drop abruptly to zero when the corresponding band crosses the Fermi energy. As the integration of a discontinuous function requires a very fine mesh, we use an electronic temperature to smear the occupation function and reduce the computational cost. The price to pay is that we are adding an electronic entropical term to the energy. We thus have to converge the electronic temperature with respect to k-points. Nowadays, there exist many different kind of smearing techniques (occupation functions). An overview of the most relevant ones together with advantages and drawbacks of each can be found in Ref. [116].

Appendix E

Properties of the approximated force constant matrix

Let us take a closer look at the product of the deformation potential matrix elements in real space used in the approximated force constant functional with explicit spin, namely

$$d^{\lambda}_{k'k} d^{\eta}_{kk'} = \sum_{\sigma_1\sigma_2} \langle \psi_{k'\sigma_1} | \frac{\partial V^{\sigma_1\sigma_2}_{\mathrm{KS}}}{\partial u_\lambda} | \psi_{k\sigma_2} \rangle \sum_{\sigma_3\sigma_4} \langle \psi_{k\sigma_3} | \frac{\partial V^{\sigma_3\sigma_4}_{\mathrm{KS}}}{\partial u_\eta} | \psi_{k'\sigma_4} \rangle. \tag{E.1}$$

Here the index k includes both the wavevector $\mathbf{k}$ and the band index i (same for k') and the index λ includes the ionic index I and the Cartesian index α (same for η). We then consider a function of the kind

$$F_{\lambda\eta} = \sum_{kk'} W(k,k') \sum_{\sigma_1\sigma_2} \langle \psi_{k'\sigma_1} | \frac{\partial V^{\sigma_1\sigma_2}_{\mathrm{KS}}}{\partial u_\lambda} | \psi_{k\sigma_2} \rangle \sum_{\sigma_3\sigma_4} \langle \psi_{k\sigma_3} | \frac{\partial V^{\sigma_3\sigma_4}_{\mathrm{KS}}}{\partial u_\eta} | \psi_{k'\sigma_4} \rangle \tag{E.2}$$

where $W(k,k')$ is some real weighting function that only depends on the indexes k and k'. It easy to show that the matrix elements, and hence F itself, are hermitian under exchange of the indexes λ and η, namely

$$F_{\lambda\eta} = F^*_{\eta\lambda}. \tag{E.3}$$

Moreover, we can relate the symmetry properties of the matrix F to the symmetry properties of the weighting function W. Indeed, if we exchange the summation indexes $k \leftrightarrow k'$, $\sigma_1 \leftrightarrow \sigma_2$, $\sigma_3 \leftrightarrow \sigma_4$, we get

$$F_{\lambda\eta} = F_{\eta\lambda} \quad \Longleftrightarrow \quad W(k,k') = W(k',k) \tag{E.4}$$

$$F_{\lambda\eta} = -F_{\eta\lambda} \quad \Longleftrightarrow \quad W(k,k') = -W(k',k) \tag{E.5}$$

Together with the hermiticity condition Eq. E.3, this implies that F is real if W is symmetric and imaginary if W is antisymmetric.

E.1 Fourier transformation

In this section we make explicit all the indexes but omit the spin as the latter case is straightforward. The Fourier transform of the derivative of some potential $V(\mathbf{r})$ with

respect to the ionic displacement $\mathbf{u}_I$ is given by

$$\frac{\partial V(\mathbf{r})}{\partial \mathbf{u}_I} = \frac{1}{N}\sum_{\mathbf{q}} e^{-i\mathbf{q}\cdot\mathbf{R}_L}\frac{\partial V(\mathbf{r})}{\partial \mathbf{u}_{\mathbf{q}s}}. \tag{E.6}$$

The Fourier transform of the matrix elements given in Eq. E.1 can therefore be calculated as follows. First we rewrite the matrix element as

$$\mathbf{d}^I_{\mathbf{k}i,\mathbf{k}'j} = \langle\psi_{\mathbf{k}i}|\frac{\partial V_{\mathrm{KS}}(\mathbf{r})}{\partial \mathbf{u}_I}|\psi_{\mathbf{k}'j}\rangle = \frac{1}{N}\sum_{\mathbf{q}}\langle\psi_{\mathbf{k}i}|\frac{\partial v_{\mathrm{KS}}(\mathbf{r})}{\partial \mathbf{u}_{\mathbf{q}s}}e^{i\mathbf{q}\cdot(\mathbf{r}-\mathbf{R}_L)}|\psi_{\mathbf{k}'j}\rangle \tag{E.7}$$

where $v_{\mathrm{KS}}(\mathbf{r})$ is the periodic part of the KS potential, namely $V_{\mathrm{KS}}(\mathbf{r}) = v_{\mathrm{KS}}(\mathbf{r})e^{i\mathbf{q}\cdot\mathbf{r}}$. Then we use the Bloch theorem for solids

$$\psi_{\mathbf{k}i}(\mathbf{r}) = \frac{1}{\sqrt{N}}e^{i\mathbf{k}\cdot\mathbf{r}}u_{\mathbf{k}i}(\mathbf{r}) \tag{E.8}$$

to express the matrix element through the periodic part of the wavefunction as

$$\mathbf{d}^I_{\mathbf{k}i,\mathbf{k}'j} = \frac{1}{N}\sum_{\mathbf{q}} e^{-i\mathbf{q}\cdot\mathbf{R}_L}\frac{1}{N}\sum_{\mathbf{R}}\int_{\substack{unit\\cell}} d\mathbf{r}\; e^{i(\mathbf{k}'-\mathbf{k}+\mathbf{q})\cdot\mathbf{r}}\; u^*_{\mathbf{k}i}(\mathbf{r})\frac{\partial v_{\mathrm{KS}}(\mathbf{r})}{\partial \mathbf{u}_{\mathbf{q}s}}u_{\mathbf{k}'j}(\mathbf{r}) \tag{E.9}$$

where we made explicit the sum over lattice vectors and the integral over the unit cell. Then we change variables $\mathbf{r} = \mathbf{r}' + \mathbf{R}$, exploit the periodicity of the product $u^*\frac{\delta v}{\delta \mathbf{u}}u$ and use the relation $\frac{1}{N}\sum_{\mathbf{R}} e^{i\mathbf{k}\cdot\mathbf{R}} = \delta_{\mathbf{k}}$ to write

$$\mathbf{d}^I_{\mathbf{k}i,\mathbf{k}'j} = \frac{1}{N}\sum_{\mathbf{q}} e^{-i\mathbf{q}\cdot\mathbf{R}_L}\;\delta_{\mathbf{k},\mathbf{k}'+\mathbf{q}}\;\langle u_{\mathbf{k}'+\mathbf{q}i}|\frac{\partial v_{\mathrm{KS}}(\mathbf{r})}{\partial \mathbf{u}_{\mathbf{q}s}}|u_{\mathbf{k}'j}\rangle \tag{E.10}$$

where integration in equation E.10 is understood to be on the unit cell.
The other matrix element, when multiplied by $\delta_{\mathbf{k},\mathbf{k}'+\mathbf{q}}$, following the same procedure as for the former, can be written as

$$\delta_{\mathbf{k},\mathbf{k}'+\mathbf{q}}\mathbf{d}^J_{\mathbf{k}'j,\mathbf{k}i} = \delta_{\mathbf{k},\mathbf{k}'+\mathbf{q}}\frac{1}{N}e^{i\mathbf{q}\cdot\mathbf{R}_M}\langle u_{\mathbf{k}'j}|\frac{\partial v_{\mathrm{KS}}(\mathbf{r})}{\partial \mathbf{u}^*_{\mathbf{q}r}}|u_{\mathbf{k}'+\mathbf{q}i}\rangle \tag{E.11}$$

Therefore the product $\mathbf{d}^I_{\mathbf{k}i,\mathbf{k}'j}\mathbf{d}^J_{\mathbf{k}'j,\mathbf{k}i}$ reads

$$\mathbf{d}^I_{\mathbf{k}i,\mathbf{k}'j}\mathbf{d}^J_{\mathbf{k}'j,\mathbf{k}i} = \frac{1}{N^2}\sum_{\mathbf{q}} e^{-i\mathbf{q}\cdot(\mathbf{R}_L-\mathbf{R}_M)}\delta_{\mathbf{k},\mathbf{k}'+\mathbf{q}}\langle u_{\mathbf{k}'+\mathbf{q}i}|\frac{\partial v_{\mathrm{KS}}}{\partial \mathbf{u}_{\mathbf{q}s}}|u_{\mathbf{k}'j}\rangle\langle u_{\mathbf{k}'j}|\frac{\partial v_{\mathrm{KS}}}{\partial \mathbf{u}^*_{\mathbf{q}r}}|u_{\mathbf{k}'+\mathbf{q}i}\rangle \tag{E.12}$$

and the Fourier transform can be defined as

$$\mathbf{d}^I_{\mathbf{k}i,\mathbf{k}'j}\mathbf{d}^J_{\mathbf{k}'j,\mathbf{k}i} \quad \overset{\mathrm{FT}}{\longleftrightarrow} \quad \delta_{\mathbf{k},\mathbf{k}'+\mathbf{q}}\tilde{\mathbf{d}}^s_{\mathbf{k}'+\mathbf{q}i,\mathbf{k}'j}(\tilde{\mathbf{d}}^r_{\mathbf{k}'+\mathbf{q}i,\mathbf{k}'j})^* \tag{E.13}$$

where the Fourier transformed deformation potential matrix element is given by $\tilde{\mathbf{d}}^s_{\mathbf{k}'+\mathbf{q}i,\mathbf{k}'j} = \langle u_{\mathbf{k}'+\mathbf{q}i}|\frac{\partial v_{\mathrm{KS}}}{\partial \mathbf{u}_{\mathbf{q}s}}|u_{\mathbf{k}'j}\rangle$. The function F in real space defined in Eq. E.2 can be written in this context as

$$F_{IJ} = \sum_{\mathbf{k}i}\sum_{\mathbf{k}'j} W(\mathbf{k}i,\mathbf{k}'j)\mathbf{d}^I_{\mathbf{k}i,\mathbf{k}'j}\mathbf{d}^J_{\mathbf{k}'j,\mathbf{k}i} \tag{E.14}$$

where the weighting function W is independent on the cell coordinates. Its Fourier transform is therefore given by

$$\tilde{F}_{sr}(\mathbf{q}) = \sum_{\mathbf{k}ij} W(\mathbf{k}+\mathbf{q}i, \mathbf{k}j)\tilde{\mathbf{d}}^{s}_{\mathbf{k}+\mathbf{q}i,\mathbf{k}j}(\tilde{\mathbf{d}}^{r}_{\mathbf{k}+\mathbf{q}i,\mathbf{k}j})^{*}. \tag{E.15}$$

Following the symmetry properties of F_{IJ}, also the Fourier transform is hermitian, namely $\tilde{F}_{sr}(\mathbf{q}) = \tilde{F}^{*}_{rs}(\mathbf{q})$ and satisfies the following relations:

$$\tilde{F}^{*}_{sr}(\mathbf{q}) = \tilde{F}_{sr}(-\mathbf{q}) \quad \Longleftrightarrow \quad W(k,k') = W(k',k) \tag{E.16}$$

$$\tilde{F}^{*}_{sr}(\mathbf{q}) = -\tilde{F}_{sr}(-\mathbf{q}) \quad \Longleftrightarrow \quad W(k,k') = -W(k',k). \tag{E.17}$$

E.2 Deformation potentials and time-reversal symmetry

Let us consider only the matrix element in real space $d^{I[\mathbf{B}]}_{k'k}$ with magnetic field $\mathbf{B}$ and see what happens if we enforce time-reversal symmetry. We recall that $\mathcal{T} = i\sigma_y\mathcal{K}$ for spin systems. By multiplying for the identity $\mathbb{I} = \mathcal{T}^{\dagger}\mathcal{T}$ on both sides of the deformation potential, one obtains

$$d^{I[\mathbf{B}]}_{\mathbf{k}i,\mathbf{k}'j} = \langle\psi^{[\mathbf{B}]}_{\mathbf{k}i}| \left(\mathcal{T}^{\dagger}\mathcal{T}\frac{\partial V^{[\mathbf{B}]}_{\mathrm{KS}}}{\partial u_I}\mathcal{T}^{\dagger}\mathcal{T}|\psi^{[\mathbf{B}]}_{\mathbf{k}'j}\rangle \right) \tag{E.18}$$

where the bracket are necessary to make clear that operators act on the right and summation over spin indexes is included in the spinor product. We then use the property of antilinear operators $\langle\phi|(\mathcal{A}|\psi\rangle) = [(\langle\psi|\mathcal{A}^{\dagger})|\phi\rangle]^{*} = \langle\psi|(\mathcal{A}^{\dagger}|\phi\rangle)$ to rewrite the matrix element as

$$d^{I[\mathbf{B}]}_{\mathbf{k}i,\mathbf{k}'j} = \langle\psi^{[-\mathbf{B}]}_{-\mathbf{k}'j}|\mathcal{T}\frac{\partial V^{[\mathbf{B}]}_{\mathrm{KS}}}{\partial u_I}\mathcal{T}^{\dagger}|\psi^{[-\mathbf{B}]}_{-\mathbf{k}i}\rangle \tag{E.19}$$

where hermiticity of V_{KS} has been used and $|\psi^{[-\mathbf{B}]}_{-\mathbf{k}i}\rangle$ is the time-reversed of $|\psi^{[\mathbf{B}]}_{\mathbf{k}i}\rangle$ intended as a spinor. For magnetic systems, the KS potential is such that $\mathcal{T}V^{[\mathbf{B}]}_{\mathrm{KS}}\mathcal{T}^{\dagger} = V^{[-\mathbf{B}]}_{\mathrm{KS}}$. Therefore the matrix element at $\mathbf{B}$ can be related to the time-reversed matrix element as

$$d^{I[\mathbf{B}]}_{\mathbf{k}i,\mathbf{k}'j} = \langle\psi^{[-\mathbf{B}]}_{-\mathbf{k}'j}|\frac{\partial V^{[-\mathbf{B}]}_{\mathrm{KS}}}{\partial u_I}|\psi^{[-\mathbf{B}]}_{-\mathbf{k}i}\rangle. \tag{E.20}$$

If the system is not invariant under time-reversal, as for example magnetic materials, the Kramers degeneracy is broken and the two time-reversal pair states have different energies.

Bibliography

[1] C. Strohm, G. L. J. A. Rikken, and P. Wyder. Phenomenological Evidence for the Phonon Hall Effect. *Phys. Rev. Lett.*, 95:155901, Oct 2005.

[2] A. V. Inyushkin and A. N. Taldenkov. On the phonon Hall effect in a paramagnetic dielectric. *JETP Letters*, 86(6):379–382, 2007.

[3] A. Einstein and W. J. de Haas. Experimenteller Nachweis der Ampereschen Molekularströme. *Verh. Dtsch. Phys. Ges.*, 17:152, 1915.

[4] Lifa Zhang and Qian Niu. Angular Momentum of Phonons and the Einstein–de Haas Effect. *Phys. Rev. Lett.*, 112:085503, Feb 2014.

[5] Hanyu Zhu, Jun Yi, Ming-Yang Li, Jun Xiao, Lifa Zhang, Chih-Wen Yang, Robert A. Kaindl, Lain-Jong Li, Yuan Wang, and Xiang Zhang. Observation of chiral phonons. *Science*, 359(6375):579–582, 2018.

[6] Lifa Zhang and Qian Niu. Chiral Phonons at High-Symmetry Points in Monolayer Hexagonal Lattices. *Phys. Rev. Lett.*, 115:115502, Sep 2015.

[7] Yizhou Liu, Chao-Sheng Lian, Yang Li, Yong Xu, and Wenhui Duan. Pseudospins and Topological Effects of Phonons in a Kekulé Lattice. *Phys. Rev. Lett.*, 119:255901, Dec 2017.

[8] Xifang Xu, Wei Zhang, Jiaojiao Wang, and Lifa Zhang. Topological chiral phonons in center-stacked bilayer triangle lattices. *Journal of Physics: Condensed Matter*, 30(22):225401, may 2018.

[9] Xifang Xu, Hao Chen, and Lifa Zhang. Nondegenerate chiral phonons in the Brillouin-zone center of $\sqrt{3} \times \sqrt{3}$ honeycomb superlattices. *Phys. Rev. B*, 98:134304, Oct 2018.

[10] Hao Chen, Weikang Wu, Shengyuan A. Yang, Xiao Li, and Lifa Zhang. Chiral phonons in kagome lattices. *Phys. Rev. B*, 100:094303, Sep 2019.

[11] M. Born and R. Oppenheimer. Zur Quantentheorie der Molekeln. *Annalen der Physik*, 389(20):457–484, 1927.

[12] Stefano Baroni, Stefano de Gironcoli, Andrea Dal Corso, and Paolo Giannozzi. Phonons and related crystal properties from density-functional perturbation theory. *Rev. Mod. Phys.*, 73:515–562, Jul 2001.

[13] S. Engelsberg and J. R. Schrieffer. Coupled electron-phonon system. *Phys. Rev.*, 131:993–1008, Aug 1963.

[14] A. Marco Saitta, Michele Lazzeri, Matteo Calandra, and Francesco Mauri. Giant Nonadiabatic Effects in Layer Metals: Raman Spectra of Intercalated Graphite Explained. *Phys. Rev. Lett.*, 100:226401, Jun 2008.

[15] W. Kohn. Image of the fermi surface in the vibration spectrum of a metal. *Phys. Rev. Lett.*, 2:393–394, May 1959.

[16] S. Piscanec, M. Lazzeri, Francesco Mauri, A. C. Ferrari, and J. Robertson. Kohn anomalies and electron-phonon interactions in graphite. *Phys. Rev. Lett.*, 93:185503, Oct 2004.

[17] Michele Lazzeri and Francesco Mauri. Nonadiabatic Kohn Anomaly in a Doped Graphene Monolayer. *Phys. Rev. Lett.*, 97:266407, Dec 2006.

[18] Raffaele Resta. Manifestations of Berry's phase in molecules and condensed matter. *Journal of Physics: Condensed Matter*, 12(9):R107–R143, 2000.

[19] P. Schmelcher, L. S. Cederbaum, and H.-D. Meyer. Electronic and nuclear motion and their couplings in the presence of a magnetic field. *Phys. Rev. A*, 38:6066–6079, Dec 1988.

[20] Matteo Calandra, Gianni Profeta, and Francesco Mauri. Adiabatic and nonadiabatic phonon dispersion in a Wannier function approach. *Phys. Rev. B*, 82:165111, Oct 2010.

[21] Andrea Urru and Andrea Dal Corso. Density functional perturbation theory for lattice dynamics with fully relativistic ultrasoft pseudopotentials: The magnetic case. *Phys. Rev. B*, 100:045115, Jul 2019.

[22] Oliviero Bistoni, Francesco Mauri, and Matteo Calandra. Intrinsic vibrational angular momentum from nonadiabatic effects in noncollinear magnetic molecules. *Phys. Rev. Lett.*, 126:225703, Jun 2021.

[23] Z. Q. Liu, H. Chen, J. M. Wang, J. H. Liu, K. Wang, Z. X. Feng, H. Yan, X. R. Wang, C. B. Jiang, J. M. D. Coey, and A. H. MacDonald. Electrical switching of the topological anomalous Hall effect in a non-collinear antiferromagnet above room temperature. *Nature Electronics*, 1(3):172–177, Mar 2018.

[24] Ning An, Meng Tang, Shuai Hu, HuangLin Yang, WeiJia Fan, ShiMing Zhou, and XuePeng Qiu. Structure and strain tunings of topological anomalous Hall effect in cubic noncollinear antiferromagnet Mn3Pt epitaxial films. *Science China Physics, Mechanics & Astronomy*, 63(9):297511, May 2020.

[25] Joynarayan Mukherjee, T. S. Suraj, Himalaya Basumatary, K. Sethupathi, and Karthik V. Raman. Sign reversal of anomalous Hall conductivity and magnetoresistance in cubic noncollinear antiferromagnet Mn_3Pt thin films. *Phys. Rev. Materials*, 5:014201, Jan 2021.

[26] R. A. Reck and D. L. Fry. Orbital and spin magnetization in fe-co, fe-ni, and ni-co. *Phys. Rev.*, 184:492–495, Aug 1969.

[27] Hualing Zeng, Junfeng Dai, Wang Yao, Di Xiao, and Xiaodong Cui. Valley polarization in MoS2 monolayers by optical pumping. *Nature Nanotechnology*, 7(8):490–493, Aug 2012.

[28] Bruno R. Carvalho, Yuanxi Wang, Sandro Mignuzzi, Debdulal Roy, Mauricio Terrones, Cristiano Fantini, Vincent H. Crespi, Leandro M. Malard, and Marcos A. Pimenta. Intervalley scattering by acoustic phonons in two-dimensional MoS2 revealed by double-resonance Raman spectroscopy. *Nature Communications*, 8(1):14670, Mar 2017.

[29] Matteo Rini, Ra'anan Tobey, Nicky Dean, Jiro Itatani, Yasuhide Tomioka, Yoshinori Tokura, Robert W. Schoenlein, and Andrea Cavalleri. Control of the electronic phase of a manganite by mode-selective vibrational excitation. *Nature*, 449(7158):72–74, Sep 2007.

[30] M. Först, R. Mankowsky, and A. Cavalleri. Mode-Selective Control of the Crystal Lattice. *Accounts of Chemical Research*, 48(2):380–387, Feb 2015.

[31] V. L. Korenev, M. Salewski, I. A. Akimov, V. F. Sapega, L. Langer, I. V. Kalitukha, J. Debus, R. I. Dzhioev, D. R. Yakovlev, D. Müller, C. Schröder, H. Hövel, G. Karczewski, M. Wiater, T. Wojtowicz, Yu. G. Kusrayev, and M. Bayer. Long-range p–d exchange interaction in a ferromagnet–semiconductor hybrid structure. *Nature Physics*, 12(1):85–91, Jan 2016.

[32] Dominik M. Juraschek, Michael Fechner, Alexander V. Balatsky, and Nicola A. Spaldin. Dynamical multiferroicity. *Phys. Rev. Materials*, 1:014401, Jun 2017.

[33] Masato Hamada and Shuichi Murakami. Phonon rotoelectric effect. *Phys. Rev. B*, 101:144306, Apr 2020.

[34] T. Nomura, X.-X. Zhang, S. Zherlitsyn, J. Wosnitza, Y. Tokura, N. Nagaosa, and S. Seki. Phonon Magnetochiral Effect. *Phys. Rev. Lett.*, 122:145901, Apr 2019.

[35] Ron Naaman and David H. Waldeck. Spintronics and Chirality: Spin Selectivity in Electron Transport Through Chiral Molecules. *Annual Review of Physical Chemistry*, 66(1):263–281, 2015. PMID: 25622190.

[36] Nianbei Li, Jie Ren, Lei Wang, Gang Zhang, Peter Hänggi, and Baowen Li. Colloquium: Phononics: Manipulating heat flow with electronic analogs and beyond. *Rev. Mod. Phys.*, 84:1045–1066, Jul 2012.

[37] Wei Fu, Zhen Shen, Yuntao Xu, Chang-Ling Zou, Risheng Cheng, Xu Han, and Hong X. Tang. Phononic integrated circuitry and spin–orbit interaction of phonons. *Nature Communications*, 10(1):2743, Jun 2019.

[38] Lifa Zhang. Berry curvature and various thermal hall effects. *New Journal of Physics*, 18(10):103039, oct 2016.

[39] A. Einstein and W. J. de Haas. Experimental proof of the existence of Ampère's molecular currents. *Verh. Dtsch. Phys. Ges.*, 18:173, 1916.

[40] L. Sheng, D. N. Sheng, and C. S. Ting. Theory of the Phonon Hall Effect in Paramagnetic Dielectrics. *Phys. Rev. Lett.*, 96:155901, Apr 2006.

[41] Yu. Kagan and L. A. Maksimov. Anomalous Hall Effect for the Phonon Heat Conductivity in Paramagnetic Dielectrics. *Phys. Rev. Lett.*, 100:145902, Apr 2008.

[42] Jian-Sheng Wang and Lifa Zhang. Phonon Hall thermal conductivity from the Green-Kubo formula. *Phys. Rev. B*, 80:012301, Jul 2009.

[43] Lifa Zhang, Jie Ren, Jian-Sheng Wang, and Baowen Li. Topological Nature of the Phonon Hall Effect. *Phys. Rev. Lett.*, 105:225901, Nov 2010.

[44] Lifa Zhang, Jie Ren, Jian-Sheng Wang, and Baowen Li. The phonon Hall effect: theory and application. *Journal of Physics: Condensed Matter*, 23(30):305402, jul 2011.

[45] Tao Qin, Jianhui Zhou, and Junren Shi. Berry curvature and the phonon Hall effect. *Phys. Rev. B*, 86:104305, Sep 2012.

[46] A. Holz. Phonons in a strong static magnetic field. *Il Nuovo Cimento B (1971-1996)*, 9(1):83–95, May 1972.

[47] K. N. Shrivastava. Theory of Spin–Lattice Relaxation. *physica status solidi (b)*, 117(2):437–458, 1983.

[48] D.A Torchia and Attila Szabo. Spin-lattice relaxation in solids. *Journal of Magnetic Resonance (1969)*, 49(1):107–121, 1982.

[49] F. W. Sheard. *Phonon Scattering in Solids*, pages 154–162. Springer US, Boston, MA, 1976.

[50] R.L. Melcher. Spin-Phonon Interactions in Solids. In *1970 Ultrasonics Symposium*, pages 35–47, 1970.

[51] Michael Victor Berry. Quantal phase factors accompanying adiabatic changes. *Proceedings of the Royal Society of London. A. Mathematical and Physical Sciences*, 392(1802):45–57, 1984.

[52] Gerd Bergmann. The anomalous Hall effect. *Physics Today*, 32(8):25–30, 1979.

[53] Ming-Che Chang and Qian Niu. Berry phase, hyperorbits, and the Hofstadter spectrum: Semiclassical dynamics in magnetic Bloch bands. *Phys. Rev. B*, 53:7010–7023, Mar 1996.

[54] Ming-Che Chang and Qian Niu. Berry Phase, Hyperorbits, and the Hofstadter Spectrum. *Phys. Rev. Lett.*, 75:1348–1351, Aug 1995.

[55] Lifa Zhang. *Phonon Hall Effect in Two-Dimensional Lattices*. PhD thesis, Department of Physics, Nanjing Normal University, China, 2011.

[56] Dazhi Hou, Zhiyong Qiu, R. Iguchi, K. Sato, E. K. Vehstedt, K. Uchida, G. E. W. Bauer, and E. Saitoh. Observation of temperature-gradient-induced magnetization. *Nature Communications*, 7(1):12265, Jul 2016.

[57] Masato Hamada, Emi Minamitani, Motoaki Hirayama, and Shuichi Murakami. Phonon Angular Momentum Induced by the Temperature Gradient. *Phys. Rev. Lett.*, 121:175301, Oct 2018.

[58] David Vanderbilt. *Berry Phases in Electronic Structure Theory: Electric Polarization, Orbital Magnetization and Topological Insulators*, chapter 3. Cambridge University Press, 2018.

[59] Jeeva Anandan, Joy Christian, and Kazimir Wanelik. Resource Letter GPP-1: Geometric Phases in Physics. *American Journal of Physics*, 65(3):180–185, 1997.

[60] Y. Aharonov and D. Bohm. Significance of Electromagnetic Potentials in the Quantum Theory. *Phys. Rev.*, 115:485–491, Aug 1959.

[61] Murray Peshkin and Akira Tonomura. *The Aharonov-Bohm Effect*, volume 340. Springer, 1989.

[62] Michael V. Berry. The quantum phase, five years after. *Geometric phases in physics*, pages 7–28, 1989.

[63] C. Alden Mead. The geometric phase in molecular systems. *Rev. Mod. Phys.*, 64:51–85, Jan 1992.

[64] Ph. Dugourd, J. Chevaleyre, R. Antoine, M. Broyer, J.P. Wolf, and L. Wöste. Isotopic effects in pseudo-rotating homonuclear triatomic molecules. application to li3. *Chemical Physics Letters*, 225(1):28–36, 1994.

[65] Jisoon Ihm. Broken time-reversal symmetry and Berry's phase. *International Journal of Modern Physics B*, 7(11):2109–2146, 1993.

[66] W. Kohn and L. J. Sham. Self-Consistent Equations Including Exchange and Correlation Effects. *Phys. Rev.*, 140:A1133–A1138, Nov 1965.

[67] D. M. Ceperley and B. J. Alder. Ground State of the Electron Gas by a Stochastic Method. *Phys. Rev. Lett.*, 45:566–569, Aug 1980.

[68] O. Gunnarsson and B. I. Lundqvist. Exchange and correlation in atoms, molecules, and solids by the spin-density-functional formalism. *Phys. Rev. B*, 13:4274–4298, May 1976.

[69] John P. Perdew, J. A. Chevary, S. H. Vosko, Koblar A. Jackson, Mark R. Pederson, D. J. Singh, and Carlos Fiolhais. Atoms, molecules, solids, and surfaces: Applications of the generalized gradient approximation for exchange and correlation. *Phys. Rev. B*, 46:6671–6687, Sep 1992.

[70] A. D. Becke. Density-functional exchange-energy approximation with correct asymptotic behavior. *Phys. Rev. A*, 38:3098–3100, Sep 1988.

[71] David C. Langreth and M. J. Mehl. Beyond the local-density approximation in calculations of ground-state electronic properties. *Phys. Rev. B*, 28:1809–1834, Aug 1983.

[72] Axel D. Becke. A new mixing of Hartree–Fock and local density-functional theories. *The Journal of Chemical Physics*, 98(2):1372–1377, 1993.

[73] Douglas Rayner Hartree and W. Hartree. Self-consistent field, with exchange, for beryllium. *Proceedings of the Royal Society of London. Series A - Mathematical and Physical Sciences*, 150(869):9–33, 1935.

[74] V. Fock. Näherungsmethode zur Lösung des quantenmechanischen Mehrkörperproblems. *Zeitschrift für Physik*, 61(1):126–148, Jan 1930.

[75] Richard M. Martin. *Electronic Structure: Basic Theory and Practical Methods*. Cambridge University Press, 2004.

[76] A K Rajagopal. Inhomogeneous relativistic electron gas. *Journal of Physics C: Solid State Physics*, 11(24):L943–L948, dec 1978.

[77] A H MacDonald and S H Vosko. A relativistic density functional formalism. *Journal of Physics C: Solid State Physics*, 12(15):2977–2990, aug 1979.

[78] Leonard Kleinman. Relativistic norm-conserving pseudopotential. *Phys. Rev. B*, 21:2630–2631, Mar 1980.

[79] D D Koelling and B N Harmon. A technique for relativistic spin-polarised calculations. *Journal of Physics C: Solid State Physics*, 10(16):3107–3114, aug 1977.

[80] Hans Hellmann. *Hans Hellmann: Einführung in Die Quantenchemie: Mit Biografischen Notizen von Hans Hellmann Jr.* Springer-Verlag, 2015.

[81] R. P. Feynman. Forces in Molecules. *Phys. Rev.*, 56:340–343, Aug 1939.

[82] Massimiliano Di Ventra and Sokrates T. Pantelides. Hellmann-Feynman theorem and the definition of forces in quantum time-dependent and transport problems. *Phys. Rev. B*, 61:16207–16212, Jun 2000.

[83] G.D. Mahan. *Many-Particle Physics*. Physics of Solids and Liquids. Springer US, 2010.

[84] E.G Maksimov and S.V Shulga. Nonadiabatic effects in optical phonon self-energy. *Solid State Communications*, 97(7):553–560, 1996.

[85] David R. Yarkony. Nonadiabatic quantum chemistry—past, present, and future. *Chemical Reviews*, 112(1):481–498, 2012. PMID: 22050109.

[86] Sungjoon Park and Bohm-Jung Yang. Phonon angular momentum hall effect. *Nano Letters*, 20(10):7694–7699, Oct 2020.

[87] Andrea Urru. *Lattice dynamics with Fully Relativistic Pseudopotentials for magnetic systems, with selected applications*. PhD thesis, Scuola Internazionale Superiore di Studi Avanzati, Trieste, Italy, 2020.

[88] Paolo Giannozzi, Stefano Baroni, Nicola Bonini, Matteo Calandra, Roberto Car, Carlo Cavazzoni, Davide Ceresoli, Guido L. Chiarotti, Matteo Cococcioni, Ismaila Dabo, Andrea Dal Corso, Stefano de Gironcoli, Stefano Fabris, Guido Fratesi, Ralph Gebauer, Uwe Gerstmann, Christos Gougoussis, Anton Kokalj, Michele Lazzeri, Layla Martin-Samos, Nicola Marzari, Francesco Mauri, Riccardo Mazzarello, Stefano Paolini, Alfredo Pasquarello, Lorenzo Paulatto, Carlo Sbraccia, Sandro Scandolo, Gabriele Sclauzero, Ari P. Seitsonen, Alexander Smogunov, Paolo Umari, and Renata M. Wentzcovitch. QUANTUM ESPRESSO: a modular and open-source software project for quantum simulations of materials. *Journal of Physics: Condensed Matter*, 21(39):395502, 2009.

[89] P. Giannozzi, O. Andreussi, T. Brumme, O. Bunau, M. Buongiorno Nardelli, M. Calandra, R. Car, C. Cavazzoni, D. Ceresoli, M. Cococcioni, N. Colonna, I. Carnimeo, A. Dal Corso, S. de Gironcoli, P. Delugas, R. A. DiStasio, A. Ferretti, A. Floris, G. Fratesi, G. Fugallo, R. Gebauer, U. Gerstmann, F. Giustino, T. Gorni, J. Jia, M. Kawamura, H.-Y. Ko, A. Kokalj, E. Küçükbenli, M. Lazzeri, M. Marsili, N. Marzari, F. Mauri, N. L. Nguyen, H.-V. Nguyen, A. Otero de-la Roza, L. Paulatto, S. Poncé, D. Rocca, R. Sabatini, B. Santra, M. Schlipf, A. P. Seitsonen, A. Smogunov, I. Timrov, T. Thonhauser, P. Umari, N. Vast, X. Wu, and S. Baroni. Advanced capabilities for materials modelling with Quantum ESPRESSO. *Journal of physics: Condensed matter*, 29(46):465901, oct 2017.

[90] D. R. Hamann. Optimized norm-conserving Vanderbilt pseudopotentials. *Phys. Rev. B*, 88:085117, Aug 2013.

[91] M.J. van Setten, M. Giantomassi, E. Bousquet, M.J. Verstraete, D.R. Hamann, X. Gonze, and G.-M. Rignanese. The pseudodojo: Training and grading a 85 element optimized norm-conserving pseudopotential table. *Computer Physics Communications*, 226:39 – 54, 2018.

[92] John P. Perdew, Kieron Burke, and Matthias Ernzerhof. Generalized Gradient Approximation Made Simple. *Phys. Rev. Lett.*, 77:3865–3868, Oct 1996.

[93] H.K. Yuan, H. Chen, A.L. Kuang, and B. Wu. Spin–orbit effect and magnetic anisotropy in pt clusters. *Journal of Magnetism and Magnetic Materials*, 331:7 – 16, 2013.

[94] Piotr Błoński, Samuel Dennler, and Jürgen Hafner. Strong spin–orbit effects in small Pt clusters: Geometric structure, magnetic isomers and anisotropy. *The Journal of Chemical Physics*, 134(3):034107, 2011.

[95] M. N. Huda, Manish K. Niranjan, B. R. Sahu, and Leonard Kleinman. Effect of spin-orbit coupling on small platinum nanoclusters. *Phys. Rev. A*, 73:053201, May 2006.

[96] Ngangbam Bedamani Singh and Utpal Sarkar. Structure, vibrational, and optical properties of platinum cluster: a density functional theory approach. *Journal of Molecular Modeling*, 20(12):2537, 2014.

[97] Kaustava Bhattacharyya and Chiranjib Majumder. Growth pattern and bonding trends in ptn (n=2–13) clusters: Theoretical investigation based on first principle calculations. *Chemical Physics Letters*, 446(4):374 – 379, 2007.

[98] T Futschek, J Hafner, and M Marsman. Stable structural and magnetic isomers of small transition-metal clusters from the Ni group: anab initiodensity-functional study. *Journal of Physics: Condensed Matter*, 18(42):9703–9748, oct 2006.

[99] Li Xiao and Lichang Wang. Structures of Platinum Clusters: Planar or Spherical? *The Journal of Physical Chemistry A*, 108(41):8605–8614, 2004.

[100] Sang H Yang, David A Drabold, James B Adams, Pablo Ordejón, and Keith Glassford. Density functional studies of small platinum clusters. *Journal of Physics: Condensed Matter*, 9(5):L39–L45, feb 1997.

[101] Kent M. Ervin, Joe Ho, and W. C. Lineberger. Electronic and vibrational structure of transition metal trimers: Photoelectron spectra of Ni_3^-, Pd_3^-, and Pt_3^-. *The Journal of Chemical Physics*, 89(8):4514–4521, 1988.

[102] Yang Zhang, Yan Sun, Hao Yang, Jakub Železný, Stuart P. P. Parkin, Claudia Felser, and Binghai Yan. Strong anisotropic anomalous Hall effect and spin Hall effect in the chiral antiferromagnetic compounds Mn_3X (X = Ge, Sn, Ga, Ir, Rh, and Pt). *Phys. Rev. B*, 95:075128, Feb 2017.

[103] Hua Chen, Qian Niu, and A. H. MacDonald. Anomalous Hall Effect Arising from Noncollinear Antiferromagnetism. *Phys. Rev. Lett.*, 112:017205, Jan 2014.

[104] Ajaya K. Nayak, Julia Erika Fischer, Yan Sun, Binghai Yan, Julie Karel, Alexander C. Komarek, Chandra Shekhar, Nitesh Kumar, Walter Schnelle, Jürgen Kübler, Claudia Felser, and Stuart S. P. Parkin. Large anomalous Hall effect driven by a nonvanishing Berry curvature in the noncolinear antiferromagnet Mn₃Ge. *Science Advances*, 2(4):e1501870, 2016.

[105] Satoru Nakatsuji, Naoki Kiyohara, and Tomoya Higo. Large anomalous Hall effect in a non-collinear antiferromagnet at room temperature. *Nature*, 527(7577):212–215, Nov 2015.

[106] E. Krén, G. Kádár, L. Pál, and P. Szabó. Investigation of the First-Order Magnetic Transformation in Mn3Pt. *Journal of Applied Physics*, 38(3):1265–1266, 1967.

[107] E. Krén, G. Kádár, L. Pál, J. Sólyom, P. Szabó, and T. Tarnóczi. Magnetic Structures and Exchange Interactions in the Mn-Pt System. *Phys. Rev.*, 171:574–585, Jul 1968.

[108] E. Krén, G. Kádár, L. Pál, J. Sólyom, and P. Szabó. Magnetic structures and magnetic transformations in ordered Mn3(Rh, Pt) alloys. *Physics Letters*, 20(4):331–332, 1966.

[109] Hendrik J. Monkhorst and James D. Pack. Special points for brillouin-zone integrations. *Phys. Rev. B*, 13:5188–5192, Jun 1976.

[110] M. Methfessel and A. T. Paxton. High-precision sampling for Brillouin-zone integration in metals. *Phys. Rev. B*, 40:3616–3621, Aug 1989.

[111] M. C. Payne, M. P. Teter, D. C. Allan, T. A. Arias, and J. D. Joannopoulos. Iterative minimization techniques for ab initio total-energy calculations: molecular dynamics and conjugate gradients. *Rev. Mod. Phys.*, 64:1045–1097, Oct 1992.

[112] H. Hellmann. A New Approximation Method in the Problem of Many Electrons. *The Journal of Chemical Physics*, 3(1):61–61, 1935.

[113] D. R. Hamann, M. Schlüter, and C. Chiang. Norm-Conserving Pseudopotentials. *Phys. Rev. Lett.*, 43:1494–1497, Nov 1979.

[114] David Vanderbilt. Soft self-consistent pseudopotentials in a generalized eigenvalue formalism. *Phys. Rev. B*, 41:7892–7895, Apr 1990.

[115] P. E. Blöchl. Projector augmented-wave method. *Phys. Rev. B*, 50:17953–17979, Dec 1994.

[116] Nicola marzari. THEOS Electronic Temperature. `http://theossrv1.epfl.ch/Main/ElectronicTemperature`.